

AN ABSTRACT OF THE THESIS OF

Johanna Chevallier for the degree of Master of Science in Geophysics presented on February 18, 2004.

Title: Seismic Sequence Stratigraphy and Tectonic Evolution of Southern Hydrate Ridge.

Redacted for privacy

Abstract approved _____

Anne M. Tréhu

A 3D seismic volume was acquired summer 2000 over the southern end of Hydrate Ridge (HR), an anomalously shallow ridge 100 km offshore Newport, Oregon. The survey followed a succession of scientific expeditions aimed at studying the gas hydrates present in the shallow subsurface that gave the name to the ridge. This thesis consists of a seismic sequence analysis of the high-resolution (125 Hz) 3D survey. Identification of seismic units and interpretation of depositional sequences observed on the seismic sections is presented. The sequence analysis is compared with the results from nine sites cored during ODP Leg 204 during summer 2002. The first objective is to document in detail the stratigraphy of the ridge so that we can compare it with the gas hydrate distribution. The second is to reconstruct the structural evolution through time of this complex anticline as inferred from the depositional history. The result is a time series of structural evolutionary cross-sections as well as a series of paleo-bathymetric maps revealing the development of and interplay between the structures now buried in the subsurface of southern HR. The structural evolutionary diagrams show the existence of three anticlines, interpreted as thrust-related folds. They formed at the deformation front and controlled the distribution and deformation of the sediments

during the Pleistocene. The current southern HR started its uplift less than 0.5 Ma. A seismic relict in the form of a double BSR is a witness to the evolution of the gas hydrate system of HR. It confirms the recent uplift of the ridge and consequent shallowing of the base of the gas hydrate stability zone (GHSZ). Further detailed studies of the stratigraphy reveal stratigraphic controls on the fluid flow, which in turn control the distribution of gas hydrates. Analysis of the amplitude map of the bottom-simulating reflector (BSR), which is a proxy for the free gas distribution, shows a relationship between anticlinal features within the older strata (older than 1.6 Ma) and strong amplitude anomalies of the BSR, which confirm previous observations suggesting a very low permeability for the young slope-basin sediments and an accumulation of gas within the older sediments underneath.

©Copyright by Johanna Chevallier
February 18, 2004
All Rights Reserved

Seismic Sequence Stratigraphy and Tectonic Evolution of Southern Hydrate Ridge.

by
Johanna Chevallier

A THESIS

Submitted to
Oregon State University

in partial fulfillment of
the requirements for the
degree of

Master of Science

Presented February 18, 2004
Commencement June, 2004

Master of Science thesis of Johanna Chevallier presented on February 18, 2004.

APPROVED:

Redacted for privacy

Major Professor, representing Geophysics

Redacted for privacy

Dean of the College of Oceanic and Atmospheric Sciences

Redacted for privacy

Dean of the Graduate School

I understand that my thesis will become part of the permanent collection of Oregon State University libraries. My signature below authorizes release of my thesis to any reader upon request.

Redacted for privacy

Johanna Chevallier, Author

ACKNOWLEDGEMENTS

I am extremely thankful to my advisor, Anne Tréhu, for taking me as her student and for making the writing of this thesis possible. I appreciated her support as much as the great independence she gave me throughout the research process. The thoughtful revisions, comments, and direction Jack Meyer offered were greatly appreciated as well as his help in my becoming proficient with Kingdom Suite. I also would like to thank my other committee members, Bob Lillie for his time and valuable comments and Joe Hendricks for his support. I wish to thank Joel Johnson, Nathan Bangs, Ingo Pecher, and Achim Kopf for the time they took to discuss my ideas, as well as all professors and researchers at the College of Oceanic and Atmospheric Sciences, the OSU Geosciences department, and the Geological Institute of Tuebingen University, who helped to extend my knowledge in the field. And I thank the Ocean Drilling Program to make this data available for this work.

I also would like to thank the College of Oceanic and Atmospheric Science faculty and the Research Computing Staff Tom Leach, Chuck Sears, Bruce Marler, Dave Reinert and Curt Vandetta, as well as Dave Gosset from Seismic Micro Tech, Inc. always helpful in panicked times.

A special thank you to my only fellow grad student Sue Potter who has been a fine homework teammate (and climbing partner) and to Matt Arsenault for his help in solving the various Unix, GMT etc... computer issues and for keeping the lab an enjoyable place to be working over the past two years. I also thank Kush Tandon for his valuable input and his great help particularly in the final phase of my thesis.

I am thankful for the constant energy and support I received from my friends in Corvallis and my friends overseas in Germany and in France. They helped me keep

my physical strength as much through their moral support as through shared bike-rides in the forest, runs, climbing trips, etc...

This work was made possible through the National Science Foundation grants # 0002 410-OCE and # 9906990-OCE.

TABLE OF CONTENTS

	<u>Page</u>
1 INTRODUCTION	1
2 GEOLOGICAL SETTING OF HYDRATE RIDGE	6
3 DATA COLLECTION	11
3.1 3D/2D seismic	11
3.1.1 Seismic volume (June –July 2000)	11
3.1.2 2D lines (June – July 2000)	15
3.2 ODP Leg 204	15
4 SEISMIC SEQUENCE STRATIGRAPHY	19
4.1 Use of Sequence stratigraphy in a tectonic active environment	19
4.2 Establishing seismostratigraphic units for southern Hydrate Ridge	22
4.3 description of the seismic units	31
4.3.1 Unit S.VII (>1.6my)	31
4.3.2 Unit S.VI (1my – 0.3my)	32
4.3.3 Unit S.V (>1.6my – 1.0my)	37
4.3.4 Unit S.IV (>1.6my – 1.15my)	37
4.3.5 Unit S.III (1.15my – 1.0my)	50
4.3.6 Unit S.II (1.0my – 0.3my)	54
4.3.7 Unit S.IB (0.3 – 0.2my)	58

TABLE OF CONTENTS (continued)

	<u>Page</u>
4.3.8 Unit S.IA (0.2my to present)	67
5 BIOSTRATIGRAPHY	70
6 STRUCTURAL GEOLOGY	74
6.1 Regional structures	74
6.2 Structures on southern HR	74
6.2.1 Anticline B	75
6.2.2 Dome	76
6.2.3 Fold F	77
6.2.4 Syn- and post deformation within S.II strata; uplift of southern HR	78
6.2.5 Fault system E	78
7 TECTONIC HISTORY OF SHR	86
7.1 Early Pleistocene 1.6 - 1.15 Ma	87
7.2 Early to mid Pleistocene 1.15 - 0.3.	88
7.3 Mid-Pleistocene 0.3-0.2 or 0.1	91
7.4 Late Pleistocene - Holocene 0.2 – present	92
7.5 Summary	92
8 IMPACT OF THE STRATIGRAPHY ON THE GAS HYDRATES	94
8.1 Effects of uplift on gas hydrates	94

TABLE OF CONTENTS (continued)

	<u>Page</u>
8.2 Double BSR as a relict of the tectonic uplift	97
8.3 Gas hydrate distribution and faulting	100
8.4 Stratigraphy of horizon A	100
8.5 Relation between BSR amplitude anomalies and stratigraphy	101
9 CONCLUSION	105
BIBLIOGRAPHY	107
APPENDIX A	113
APPENDIX B	114
APPENDIX C	117

LIST OF FIGURES

<u>Figure</u>	<u>Page</u>
1. Maps of the Cascadia subduction zone and of Hydrate Ridge region ...	2
2. 2D MCS EW profiles across the deformation front and the outer edge of the accretionary complex	7
3. Frequency range spectrum from the seismic volume.....	14
4. Diagram showing the lithologic units out of the ODP Leg 204 initial report overlain by the seismic-stratigraphic units	17
5. Sketch showing the principal depositional features used for the reconstruction of the depositional history of the sediments.....	21
6. Four EW sections extracted from the seismic volume, with AGC	24
7. NS 2D MCS section	29
8. Time maps of Horizon K and bathymetry of southern HR.....	34
9. Time map of Horizon U	36
10. Sequential structural diagram showing the evolution of fold F	39
11. Time maps of horizons A and A'	41

LIST OF FIGURES (continued)

<u>Figure</u>	<u>Page</u>
12. EW sections of the summit region extracted from the seismic volume with AGC	45
13. NS section of the summit region extracted from the seismic volume, with AGC	47
14. EW section close to Site 1247 extracted from the seismic volume, with AGC	49
15. Time isopach maps of Units S.III, S.II, S.IB, S.IA	51
16. Time map of horizon B	55
17. EW section showing Unit S.II strata extracted from the seismic volume, with AGC	57
18. EW section showing Unit S.IB strata extracted from the seismic volume, with AGC	60
19. Close ups on sequence boundary details, examples extracted from the seismic volume, presented with AGC	62
20. Seismic sequence stratigraphic analysis of S.IB strata	64

LIST OF FIGURES (continued)

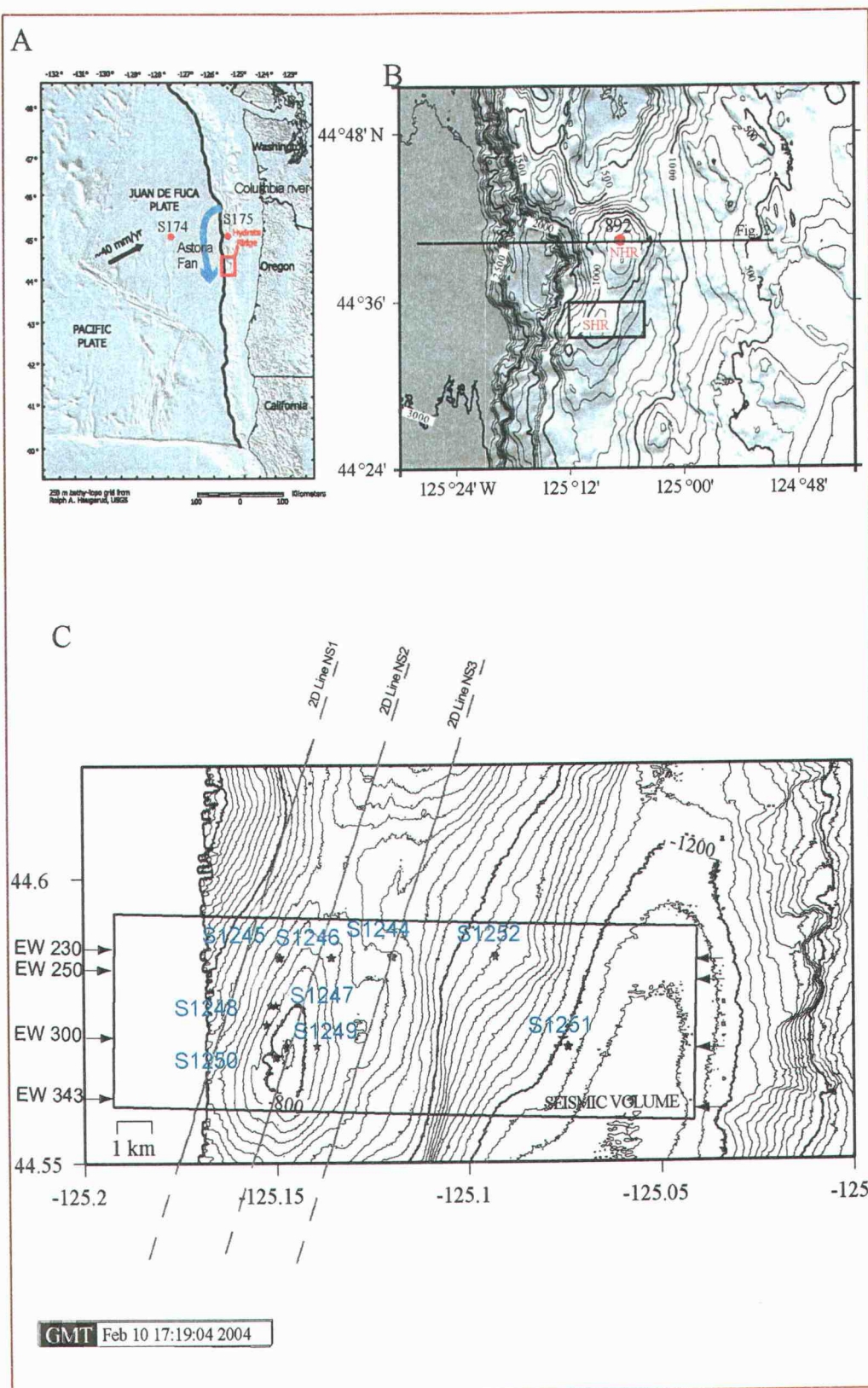
<u>Figure</u>	<u>Page</u>
21. NS sections of the basin region extracted from the seismic volume, with AGC	69
22. Structural evolutionary cross-sections of EW 230.....	80
23. Structural evolutionary cross-sections of EW 300.....	82
24. Sequence of paleo-bathymetric maps.....	84
25. Diagrams showing the stabilization and destabilization condition of gas hydrates.....	96
26. EW section of the transition region between the basin and the ridge showing the double-BSR	99
27. Amplitude map of the BSR overlain by the units hosting the BSR .	103

Seismic Sequence Stratigraphy and Tectonic Evolution of Southern Hydrate Ridge

1 INTRODUCTION

Hydrate Ridge (HR) is an anomalously wide peanut shape thrust anticline (MacKay, 1995, Trehu et al., 1999, Suess et al., 2000) located 100km offshore Newport (Oregon) at 1200 - 600m depth within the accretionary prism, which built part of the Oregon continental rise (Fig. 1). Pliocene strata are exposed at the seafloor at the northern summit while younger sediments cover correlative strata beneath the southern summit. This ridge is bearing gas hydrates and has been the target of multiple international, interdisciplinary investigations aimed at understanding fluid flow in accretionary prisms (e.g. Bohrmann et al., 1998, Trehu et al., 1999, Suess et al., 2001, Suess, 2002, Torres et al., 2002, Tryon et al., 2002, Johnson et al., 2003). The common goal of these projects is to improve our general understanding of subsurface fluid activity on convergent margins and on the processes that form gas hydrates in this environment. Gas hydrates (clathrates) are a solid form of water and gas (mostly methane) that is stable at sufficiently high pressure and low temperature (Kvenvolden, 1993). The gas hydrates may represent a future fuel source as they represent an important natural methane reservoir (Kvenvolden and Lorenson, 2001). However many questions still are to be resolved, for example the role of gas hydrates systems on climate changes during Earth history. At HR, a strong bottom simulating reflector (BSR), commonly used as a proxy for the base of the gas hydrate layer, is observed to cross the stratigraphy at around 120 mbsf. This reflection results from the relatively high-velocity zone due to gas hydrates filling the pore space over a zone containing free gas.

Figure 1: A) the tectonic setting of HR (marked with a red square) Also shown is the path of the deep-sea fan sediments coming from the Columbia River. Location of DSDP sites 174 and 175 are marked with red dots The continuous black line represents the deformation front of the subduction zone. B) Bathymetric map of the HR region. (SHR = southern HR). ODP site 892 is marked with a red dot. A black square shows the emplacement of the seismic volume run on SHR. C) Close-up on southern Hydrate Ridge, shows the boundaries of the seismic volume with inline numbers corresponding to the sections shown on Figure 6, the three NS 2D-MCS lines are also shown. Stars and blue digits name and locate the nine ODP Leg 204 sites.



Multiple studies of dewatering processes of accretionary complexes suggest that lithologic variations and fault surfaces lead to permeability, heterogeneity and can act as major gas/fluid conduits (e.g. Rowe and Gettrust, 1993, Mann and Kukowski, 1999, Taylor et al. 2000, Trehu and Flemings, 2003). Geologic factors thus represent indirect geologic controls on gas hydrate nucleation and growth. Furthermore, tectonic uplift and subsidence of the seafloor influences subsurface pressure and temperature within the sediments (e.g. Grevemeyer et al., 2000, Pecher et al., 2001, Trehu et al., 2003c) and hence affects the gas solubility and gas hydrate stability. Subsurface pressure, temperature and the amount of gas available are three important parameters controlling gas hydrate nucleation and stability (Kvenvolden, 1993). An improved understanding of the geologic and tectonic history of HR is therefore valuable for understanding gas hydrate distribution within the gas hydrate stability zone (GHSZ) and its temporal evolution.

The objective of this thesis is to map the subsurface geology of southern Hydrate Ridge and to construct a model for the structural evolution of the region during the Pleistocene and Holocene. To do this we integrated stratigraphic and structural information from the 3D seismic volume acquired from southern HR in summer 2000 with the ODP Leg 204 coring results (Shipboard Scientific Party, 2003, Trehu et al. 2003a). Leg 204 was designed to determine the distribution and concentration of gas hydrates in the thrust anticline and its adjacent slope basin as well as to investigate the mechanisms that transport methane and other gases into the GHSZ. Seismic sequence stratigraphy (Mitchum, 1977) is the tool used to interpret the pre-, syn- and post-deposition deformation patterns of each of the depositional sequence distinguished within the volume. This work focuses on the sedimentary sequences that mantle the older sediments, which form the seismically incoherent core. While seismic stratigraphy provides an understanding of the nature of the tectonic activity and the relative age of events, biostratigraphic data

provide absolute ages for the strata within each basin. This gives the information needed for the sequential structural reconstruction of two chosen seismic sections. The result is a tectonic model showing the thrust and fold deformation that deformed the abyssal plain sediment at the deformation front, and the following deformations ongoing during the accretion as recorded in the strata.

2. GEOLOGIC SETTING OF HYDRATE RIDGE

The geology of the Cascadia convergent margin of Oregon and Washington is controlled by the subduction of the Juan de Fuca plate beneath the North American plate (Fig. 1 and 2). Sediments from the Astoria fan system fill the trench region as it is growing such that no topographic trench exists offshore Oregon. Instead, a large accretionary prism exists west of the outer shelf of Oregon, which is composed of thick sedimentary units scrapped off of the oceanic plate onto the continental plate (Fig. 2). The accretionary prism is characterized by NS-striking folded thrust slices of Pliocene and Pleistocene accreted abyssal plain strata (Seely et al. 1974, Snavely, 1987, Mac Kay et al., 1992, MacKay, 1995). Hydrate Ridge is a particularly prominent NS-striking bathymetric-high located 17.5 km east of the Cascadia deformation front offshore Oregon (Fig. 1B, Fig. 2) (44.5° latitude; 125.15° longitude). Westbrook (1994) computed that the sediments building the ridge were at the deformation front between 1.0 – 2.0 Ma based on the prism configuration and assuming a constant accretion rate.

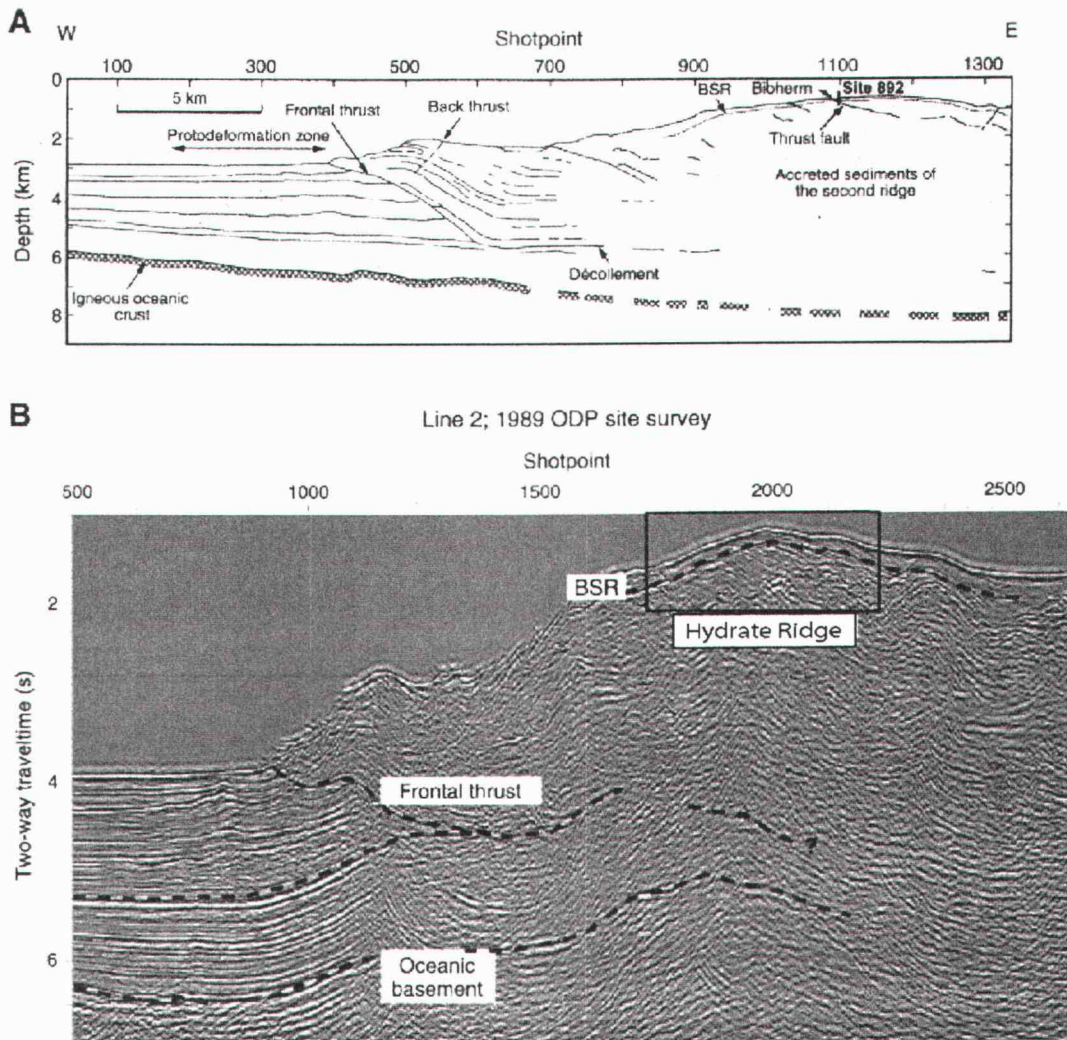


Figure 2: EW profile across the subduction zone. A. Schematic line drawing of the crustal structure across Hydrate Ridge based on depth-converted migrated seismic reflection data (from Westbrook, 1994). Interpretation is based on Line 9 from a 1989 ODP site survey (MacKay et al., 1992), along which ODP Site 892 was located. On the scale shown here, primary structural features are the same as those along Line 2, which is shown in B. B. Line 2 from the 1989 ODP site survey showing primary structural features of the deformation front.

In the abyssal plain, west of the deformation front, an angular unconformity coincident with a change in heavy mineralogy at DSDP Site 174 (Fig. 1A) separates the Astoria fan sediments that originated at the Columbia River from the older abyssal plain sediments sourced from the Klamath Mountains and from the Vancouver Island (Kulm et Fowler, 1974). The Columbia River represents the main, if not only, submarine canyon on the central Cascadia slope connecting the shelf to the abyssal plain. Hence the submarine Astoria fan represents the only major accumulation of terrigenous material from the Cascade Range on the abyssal plain. Early Pliocene subsidence of the Oregon shelf basin occurred concomitant to the uplift of the Cascadia outer arc high (McNeil et al, 2000). As a result, the basin filled and retained the clastic debris shed from the Cascades and from the Coast Range during the Pliocene. McNeil et al. (2000) proposed that the appearance of Astoria fan deposits at Site 174 correlates with out-breaching of the outer-arc-high, which previously retained the shelf deposits. This event resulted in the extension of the Astoria fan from a trench-confined fan to a much broader fan that reaches Site 174 as modeled by Schweller and Kulm (1978). Timing for the expansion of the fan is uncertain. Late Pleistocene (1.8 Ma) Astoria fan turbidity sequences found on the continental rise at Site 175 imply the existence of the submarine fan with Columbia River input offshore Oregon at 1.8 Ma. Results from Site 174 revealed that the deposition of Astoria fan sediments occurred only 1.4 Ma (Fig. 1A for the location of the sites). The difference in ages for the onset of the Astoria fan sediments suggests an expansion to the west of the Astoria fan with time. The expansion can be explained by the delay between an increase in sediment input at the head of the Astoria Canyon. Alternatively, Nelson (1976) suggested that the older fan deposits may have been located northwest of Site 174, implying a migration of the channels during fan history.

In summary, the abyssal plain strata uplifted onto the accretionary complex since 1.4 Ma are from the Astoria fan, while material older than 2 Ma originated in the Klamath Mountains and/or Vancouver Island. Sediments with an age between 2 and 1.4 Ma could have originated from either region, depending on the propagation of the submarine fan and its position relative to the depocenters.

The deep-sea deposits are scrapped-off as the deformation front migrates to the west and uplifted onto the continental plate to build the accretionary prism (e.g. Seely et al, 1974). This model is confirmed by the presence of typical abyssal plain deposits found in dredge samples and cored at Site 175 on the continental slope (Fig. 1) (Kulm et Fowler, 1974). These units can also be correlated with the lithologic units at Site 174 (abyssal plain) (Fig. 1) (Kulm et Fowler, 1974). The sediments at ODP Site 892 can also be correlated with the interlayered distal turbidites and hemipelagic clay cored at Site 174. They are interpreted as Pliocene abyssal plain deposits (Shipboard Scientific Party, 1994).

The upper stratigraphy at Site 175 differ from the deep-sea sediments. These sediments were interpreted as late Pleistocene and Holocene deposits covering the accreted abyssal plain sediments (Kulm et Fowler, 1974). These slope-basin sediments are themselves deformed by the active subsurface thrust-fault systems and some folds rise above the general level of the basins. Hence, depositional sequences within these basins were controlled by the formation and evolution (growth and migration) of the subsurface thrusts and folds. The sediment sources available in this geological setting are pelagic sediment raining out of the water column and reworked accreted material, (Seely et al., 1974; Kulm et Fowler, 1974, Snavelly, 1987).

In summary, data from earlier DSDP and ODP legs indicate that HR is a late Pliocene - early Pleistocene structure (Westbrook, 1994) that resulted from the

uplift and shortening of abyssal plain sediments during their accretion onto the continental plate (Fig. 2). Continuing deformation of the prism is recorded by Pleistocene and Holocene sediments that filled the depocenters formed on the ridge during the ongoing accretion. The ridge is hence built by deep-sea fan deposits accreted onto the accretionary wedge and by younger pelagic sediments interlayered with reworked accreted material. The objective of this thesis is to refine this interpretation and discuss implications for the evolution of the gas hydrate system hosted by Hydrate Ridge.

3. DATA COLLECTION

3.1 3D/ 2D seismic data

3.1.1 Seismic volume (June –July 2000)

Multi-channel seismic data were collected during summer 2000 on the R/V Thomas Thompson to produce a 3D high-resolution volume (Trehu and Bangs, 2000). The survey covers a 4 km x 9 km region that includes southern summit of Hydrate Ridge and an adjacent slope basin.

The ship was navigated by a GPS system provided by RACAL (including DGPS correction from a weighted average of 4 RACAL base stations). These raw fixes were recorded at 1Hz. They were smoothed to remove the rolling and pitching of the ship for derivation of the location and velocity of the ship at each update and were corrected to compensate for the offset of the source from the GPS antenna.

The streamer's geometry was determined by four bird compasses positioned at 150m intervals. These records were used to reposition each single receiver channel. There was no tail buoy for independent determination of the location of the end of the streamer. The depths and the wing angles of the birds were not logged, but were monitored by the watch-stander using a graphical display.

Shots were fired at 15m intervals based on the smoothed velocity estimate from the differential GPS fixes. The source was two GI guns (45/45 cu in.) towed at a depth of 2.5 m and fired simultaneously. They proved to be a good broadband source, producing useable energy from 10-240Hz. The signal was recorded on the Lamont portable, 600m long, 48-channel-streamer, which was towed at a depth of 2.5m.

The bridge used the Nav99 program written by Mark Weidenspahn (UTIG) to steer the source location down the selected line. Nav99 also provided a minimum radius turn path between lines, which were always shot heading east in the northern half of the grid (line numbers 100 to 139) and west in the southern half (line numbers 140 to 180). Shotpoints were numbered to increase from 100 on the west edge of the survey to 833 on the east edge. Recorded trace length was 6s.

The 3-D survey grid consisted of 81 11 km-long EW sections that were shot 50 m apart in a racetrack pattern. The grid was laid out in a UTM projection with a central meridian of 123W. During the cruise, 3-D fold was monitored based on streamer reconstructions to identify locations where additional data were needed in order to obtain adequate fold in each bin. This resulted in reshooting 18 lines because of variable degrees of streamer feathering or navigational problems resulting from strong currents.

On board of the R/V Thomas Thompson, the raw SEG-D field data were copied from 3480 tapes to SEG-Y disk files using Sioseis. The SEG-Y disk files were then converted to Paradigm Geophysical's FOCUS internal format. Seven bad traces had to be killed at this stage. Data were processed as 2D lines for quality control and a first look at the data, assuming a velocity of 1500ms for normal moveout and frequency wavenumber migration.

Source navigation and streamer location data for the 3D grid were converted to UTM coordinates and written in UKOOA90 format. These navigation data were converted into FOCUS format 3D navigation traces and binned using the FOCUS 3D QC/binning package. Fold maps were generated and optimized for 50m x 25m and 25m x 12.5m bin sizes. In both cases, the optimum grid azimuth was 348.5 degrees.

On land, the 3D processing was done by Bangs at UTIG with a binning of 12.5 x 25 m. Lines were renumbered from 200 – 360 to accommodate interpolated lines (Fig. 1B). The traces were sorted into common depth point (CDP) gathers. A velocity analysis was done for every 10th line and every 100th cmp. A high-pass filter with a ramp from 15 to 25Hz was applied to the traces to remove noise done to seastate. The data were then corrected for normal moveout (NMO), the inner trace was muted (to attenuate the seafloor multiple) and the data were stacked. A poststack Kirchhoff migration using stacking velocities was applied. This yields the 3D volume, which is 4km wide 9km long and contains a frequency range of: 20 to 180 Hz (Fig. 3) and dominant frequency at 125 Hz, which suggests a vertical resolution of 3m. The presence of reflections of multiple origins (sediments bedding, onlapping surfaces and gas hydrate related reflections such as the base of the gas hydrate layer or BSR) interfering with each other; lower the effective vertical resolution for the stratigraphic analysis, which is estimated at 15m.

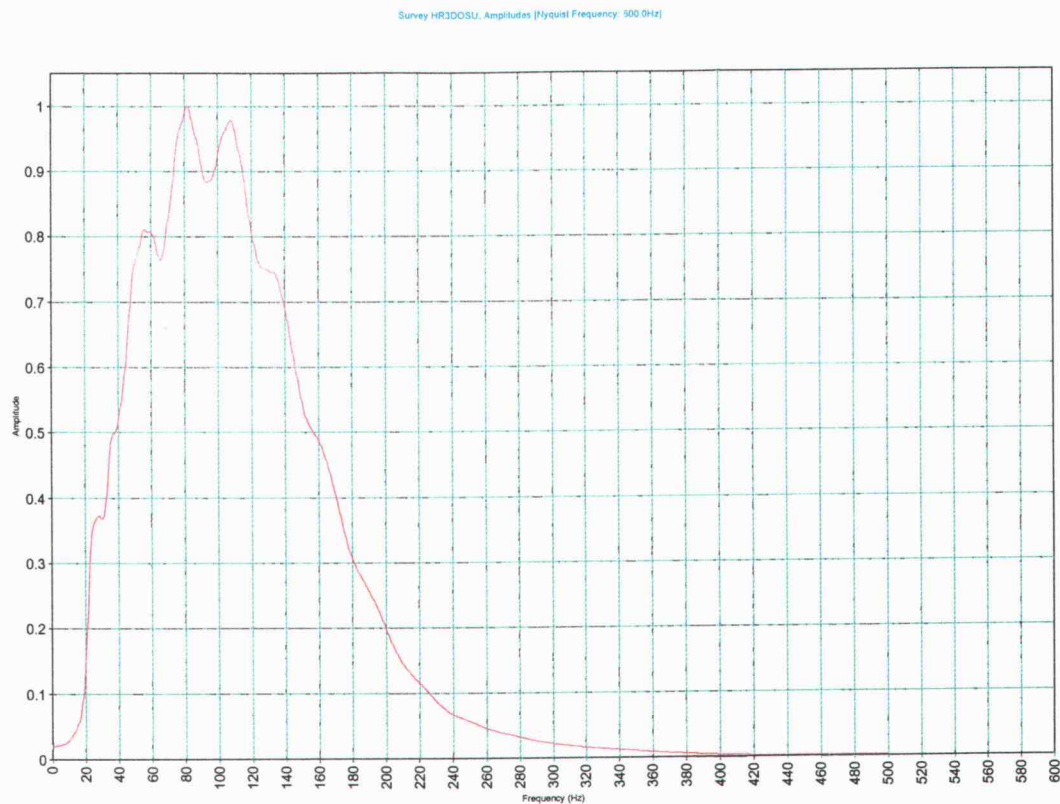


Figure 3: Frequency spectrum of the seismic volume extracted with TracePak (Kingdom Suite software); shows a nominal frequency range between 40 and 240Hz.

3.1.2 2D lines (June – July 2000)

Six regional 2D lines were recorded on the same multichannel streamer. The three NS-lines used during this study are shown on Fig. 1B. The shot interval for these lines was 37.5m. These lines were processed onboard. Data were sorted into 12.5m bins, resulting in 16-24 fold data. A high pass filter was applied with a ramp from 25 to 35Hz. The data were corrected for NMO, stretch mute was done with a 35% maximum stretch and the data were stacked assuming a constant velocity of 1500m/s. A velocity of 1500m/s was also used for f/k migration of the data.

3.2 ODP LEG 204

Nine sites were drilled during ODP Leg 204. The maximum coring depth ranged from 90 to 540 mbsf. Sediment classification was recorded based on visual description and smear slide analysis (Trehu et al, 2003a). The results were stored in core description profiles. A complete record of each core is in the lithology chapter of the initial report. Minor lithology and biogenic content were also logged on board, and an initial interpretation was done of the environment of deposition. This thesis relied on the initial report for control on lithology as well as the depositional environment

Mudstones and siltstones of turbidite origin, as well as debris-flow deposits and hemipelagic clays dominate the lithologies observed during ODP Leg 204. Definition of the lithologic units by the Leg 204 shipboard sedimentologists as shown on Figure 4 was based on the examination and combination of several sedimentological and physical property datasets (i.e. changes in the biogenic content, the minor lithology composition, and variability in the turbidity occurrence). Appendix 2 shows the correlation between the lithologic units and the seismic units distinguished within the survey at S1244, S1245 and S1251 as well

as the characteristic lithologies for each of them. Deeper stratigraphy was interpreted as part of the accretionary wedge (Fig. 4) (Shipboard Scientific Party, 2003, Site 1244 and Site 1251). Absolute ages of strata were determined based on the bioevents distinguished in the cores and presented in the Initial Report. The biostratigraphic zones were inferred from the first and last occurrence of diatoms and of calcareous nannofossils. All given ages are based on the biostratigraphic results unless otherwise specified.

Figure 4: Diagram showing the lithologic units out of the ODP Leg204 initial report, overlain by the seismostratigraphic units defined in this thesis based on the 3D survey. An overall good fit between both sets of units (lithology and seismostratigraphy) is observed. Exceptions are: 1-Unit IB is not distinguished in the lithologic data. 2- Unit IA in the west is not distinguished from Unit II on the seismic sections. The diagram also includes the seismic horizons distinguished prior to the Leg204 (Trehu et al, 2002). Colors legend for the units and the horizons are consistent throughout the thesis (Appendix A).

4. SEISMIC SEQUENCE STRATIGRAPHY

4.1 Use of sequence stratigraphy in a tectonic active environment

Sequence stratigraphic analysis is based on the identification of depositional sequences, which are stratigraphic units composed of a relatively conformable succession of genetically related strata bounded by two major angular unconformities (Mitchum, 1977). This method generally aims to reconstruct effects of sea-level rise and fall on the basin sedimentation. Seismic stratigraphic analysis of southern HR differs from traditional sequence stratigraphy in that the stratal succession was not significantly influenced by sea-level changes. Southern HR is located on the continental slope at 800 m depths (Fig. 1) and the sediments composing the core of the ridge originated from the abyssal plain (2600 m depth). The depositional environment is controlled by the formation and evolution of a thrust-fold-belt system. Different types of angular unconformities can be distinguished based on the geometry of the strata and their termination; onlap, offlap, overlap (Fig. 5). The unconformities bound sets of relatively concordant strata. Each of these sets represents one depositional sequence. Each seismic stratigraphic unit is subdivided into a few depositional sequences. Characteristics of the sequences are controlled by syn- and post deposition tectonic activity. The primary tectonic activity observed on southern HR is the thrust-related folding of the strata and the migration of the thrust system, which controls the location and growth of the depocenters. Both result in the tilting the strata on the limbs of the folds and/or along the flank of a subsiding depocenter (Fig. 5).

Chronological and geometrical sequence analysis of the mapped sequences was used to reconstruct the sedimentary and tectonic evolution of the thrust and fold system of southern HR and the concomitant active basins. The seismic sequence

stratigraphic analysis included evaluating the relationship between the syn-sedimentary thrust and fold systems responsible for the formation of the ridge and the migration of the foreland-basins. Since no relevant impact of the sea-level changes can be expected at this depth, a direct link can be assumed between the tectonic crestal uplift and/or basin subsidence and the variation of the accommodation space available for the sediments. The sediment aggradation rate depends on the sediment supply and on the tectonic activity. Erosion is expected to be very limited in these deep-sea settings, such that the depositional sequences can be assumed to be mostly preserved in direct juxtaposition with the structures that controlled their geometrical and sedimentological character. In other words, erosion events are unlikely to bias the uplift and subsidence computed from the depositional sequences; sedimentation rates inferred from the biostratigraphy can in almost all instances be used to directly reconstruct phases of aggradation versus phases of non-deposition. However, local erosion surfaces, tentatively assigned to slope failure events, are inferred. Hence the reference lines need to be chosen with care away from the erosion surface, for computation of relative movements of the sediments.

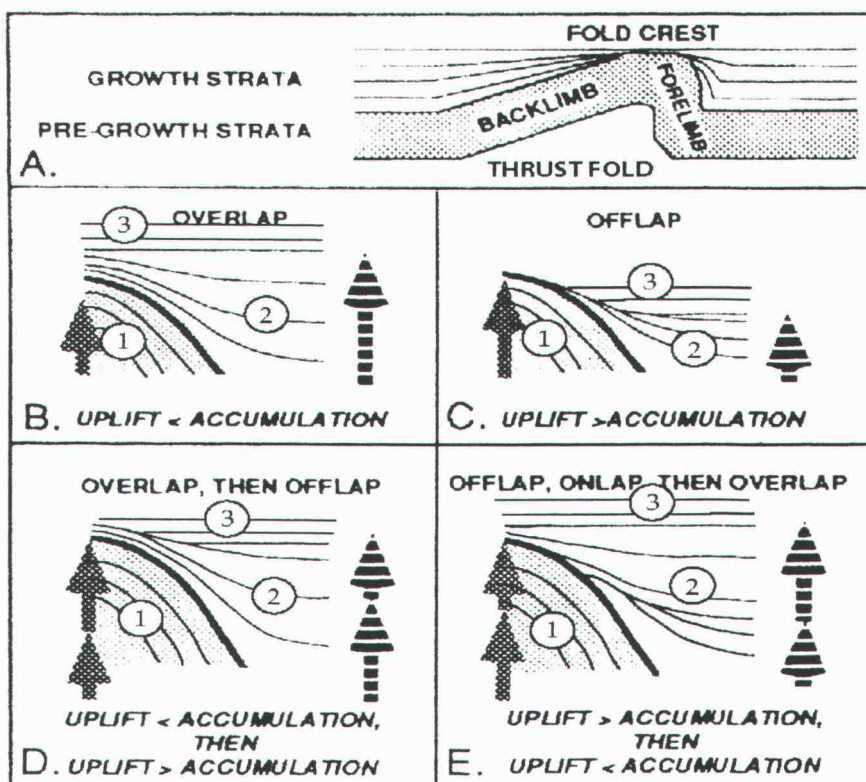


Figure 5: A) Nomenclature for a thrust fold and growth strata deposited during folding. B-E) Show four models of overlap, offlap and onlap. Predictable geometries of syntectonic strata result from different ratio between the relative rates of crestal uplift and coeval sedimentation rates. Crestal uplift is measured with respect of either the base of the syntectonic strata adjacent to the fold or the position of the correlative marker beds found in both the anticline and the adjacent syncline. When rates of accumulation are consistently greater than the rate of crestal uplift, overlap will occur (Figure 5b, Fig. 18), whereas lower rates of accumulation versus uplift lead to offlap (Figure 5C). Reversals in the relative magnitude of these rates cause a switch in the bedding geometry (Figure 5D).

Onlap (Figure 5E) occurs following offlap and a change to more rapid accumulation rates. Encircled number indicate (1) pre-tectonic depositional sequences characterized by parallel bedding; (2) syn-tectonic sequences characterized by the divergence of the strata and the stratigraphic features discussed above; (3) post-tectonic sequences characterized by onlapping against pre-depositional relief. (modified from Burbank and Verges, 1994). Examples out of the seismic volume are shown on Figure 18C, D and E.

Figure 5 sketches the relationship between an evolving bathymetry (the syn-sedimentary growth and activity of thrust-and-fold systems) and the depositional sequences (onlap-offlap geometries of the syntectonic sedimentary bed) (model modified from Burbank and Verges, 1994). The relationships are expressed in the context of the relative rate of sediment accumulation versus the rate of uplift of the crest of the folds. Significance of internal facies patterns such as divergency versus parallel bedding also can be extracted from the model. On the other hand, chaotic reflections will often reflect intense post-sedimentary deformations that destroyed the original depositional strata.

4.2 Establishing seismic stratigraphic units for southern HR

Seismic stratigraphy is the study of stratigraphy and depositional facies as interpreted from seismic data (Mitchum, 1977). The terminations of the reflections along surfaces of seismic unconformity are interpreted as strata termination along unconformable sequence boundaries and the configuration of the reflections are interpreted as the expression of the sequence internal strata geometry/stratification patterns. Seismic units (S.) were defined based on termination of the reflections and their seismic facies. They were correlated with the lithologic units (L.) inferred from the coring results (Trehu et al. 2003a) (Fig. 4, Appendix B). Well information were tied to the seismic volume by correcting depth to two-way-travel-time (TWTT) assuming 1550m/s for the upper few hundreds of meters based on a 3D tomographic inversion of first arrivals recorded on ocean bottom seismometers (Arsenault et al., 2001). The value was confirmed by the coincidence of the pronounced reflections A, B, B', Y and U (Fig. 6) with lithologic anomalies such as ash layers or erosion surfaces when juxtaposing seismic and lithologic 2D profiles (Appendix B). These five reflections were named and described by Trehu et al. (2002) prior to the ODP cruise Leg 204. Reflections A, Y and U were used as unit boundaries, and the stratigraphic

surfaces coinciding with the reflections were interpreted and extended across the survey to obtain complete seismic horizons.

The horizons used for the sequence stratigraphy were mapped on arbitrary seismic sections spaced 20 to 50 m apart. The picks were then interpolated using the Kingdom-Suite 3D-Hunt tool to create a smooth time map of the horizon that becomes useable to visualize the three-dimensional geometry of the units composing southern HR. In addition to the five reflections referred to by Trehu et al, (2002), multiple seismic horizons were defined based on changes in seismic facies and on the onlap-offlap geometries (horizons A', A'', K, C, D, Fig. 6). Two striking mudflow deposits in the eastern basin namely: DBF1 and DBF2 (Fig. 6) could also be traced across the volume and used for the 3D stratigraphic interpretation. Figure 6 and 7 illustrate all relevant horizons on EW and NS sections respectively.

A good overall match is observed between the seismic units (S.) and the lithologic units (L.) from the ODP leg 204 Preliminary Report (Fig. 4). It is presented in Appendix B. Each seismic stratigraphic unit corresponds to a distinct tectonic phase and has a distinct depositional environment controlled by inherited relief and the sediment supply. The objective of this thesis is the interpretation of the inherited relief and the syn- and the post deposition deformations based on the strata patterns and the unit geometry. Nine units were distinguished and analyzed based on the seismic and lithology data (Fig. 4, 6, 7). Some of these units are coeval. Disrupted synchronous surfaces had to be reconstructed based on the biostratigraphy ages to create restored cross-sections and paleo-maps.

Figure.6: Four EW lines extracted from the 3D migrated seismic volume. Each couple of sections shows the un-interpreted and the interpreted version of the same section. The figure summarizes the observations discussed in the text that is: The seismic units and the seismic horizons described in seismic sequence stratigraphy chapter 4 (see appendix A for the legend). The ODP sites presented in Figure 4 (blue vertical lines). The ODP biostratigraphic results are marked along the wells (in Ma). They are discussed in the biostratigraphy chapter 5. Finally the structural features inferred from the cross-sections as well as from the depositional history of the sediments. They are presented in more details in the structural chapter 6. Two orange-red lines mark two unconformities interpreted as local slumping surface, which were since tectonically deformed. Also shown are the location of Figures 12, 17, 18 and 26. (The location of each section is shown in the plan view of the seismic volume, upper right corner of each page).

A time-depth chart for S1245 and S1251 are drawn of Fig. 6A and 6C respectively. Lithologic events, which coincide with density and velocity anomalies, were tight to outstanding reflections from the MCS data. The resulting time-depth charts at sites S1245 and S1251 were completed with the sonic log data achieved during ODP Leg 204 at both sites and with tomography results for the deeper parts of the seismic volume (Arsenault et al, 2001). The seismic horizons corresponding to the stratigraphic event used are placed on the time-depth charts. Time-depth chart for site 1245 encompasses slope-basin sediments and un-lithified material. It is, applicable, with decent accuracy to units S.V, S.IV, S.III, S.II, S.IB and S.IA over the whole survey. The time-depth chart at site 1251 can be used as reference for the deeper stratigraphy (S.VII, S.VI), as it encompasses, in its deeper part, lithified and partly lithified accreted material from the abyssal plain.

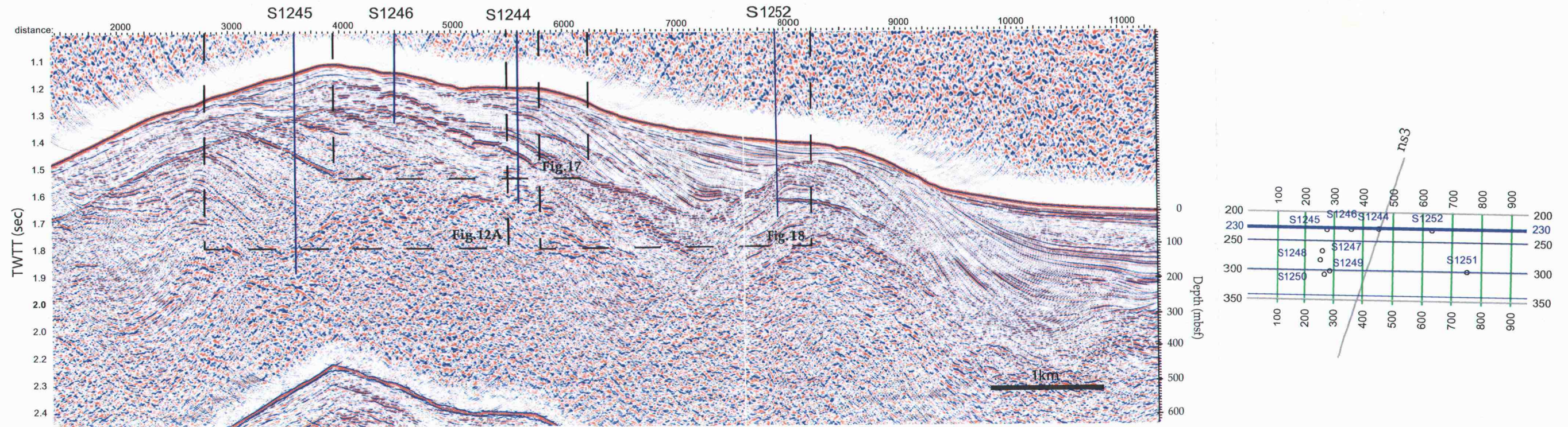


Figure 6A.a) EW line 230

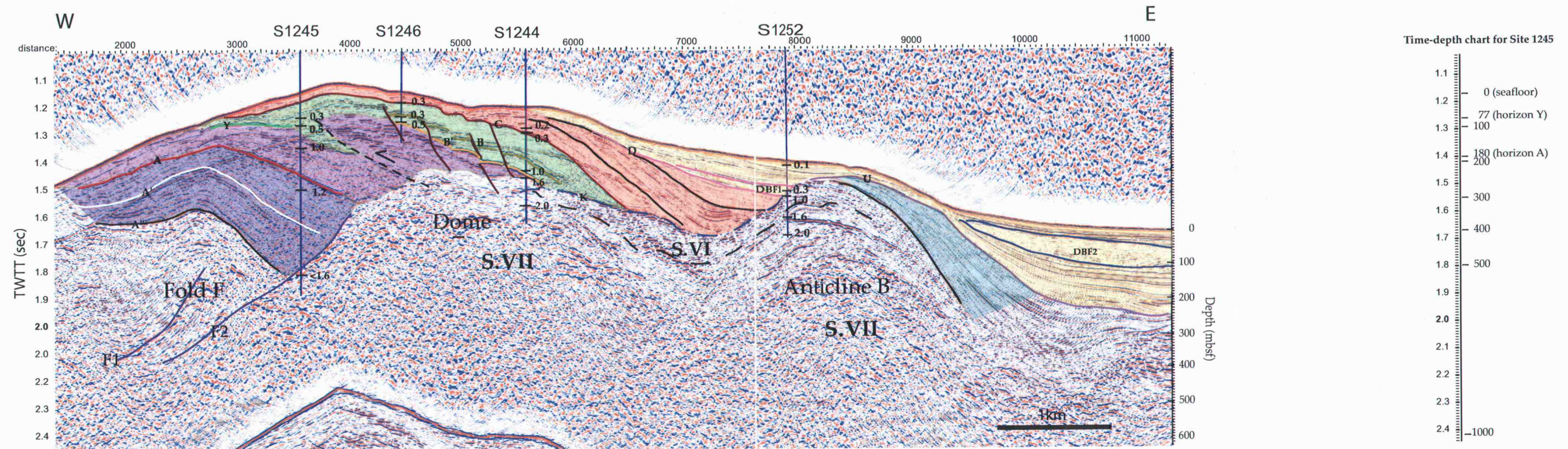


Figure 6A.b) EW line 230

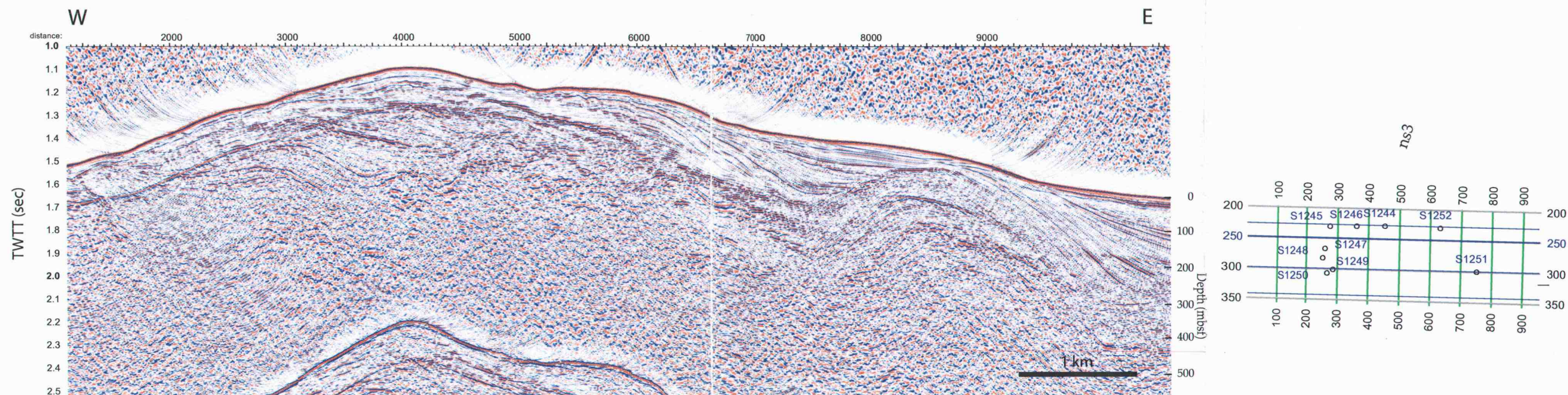


Figure 6B.a) EW line 250

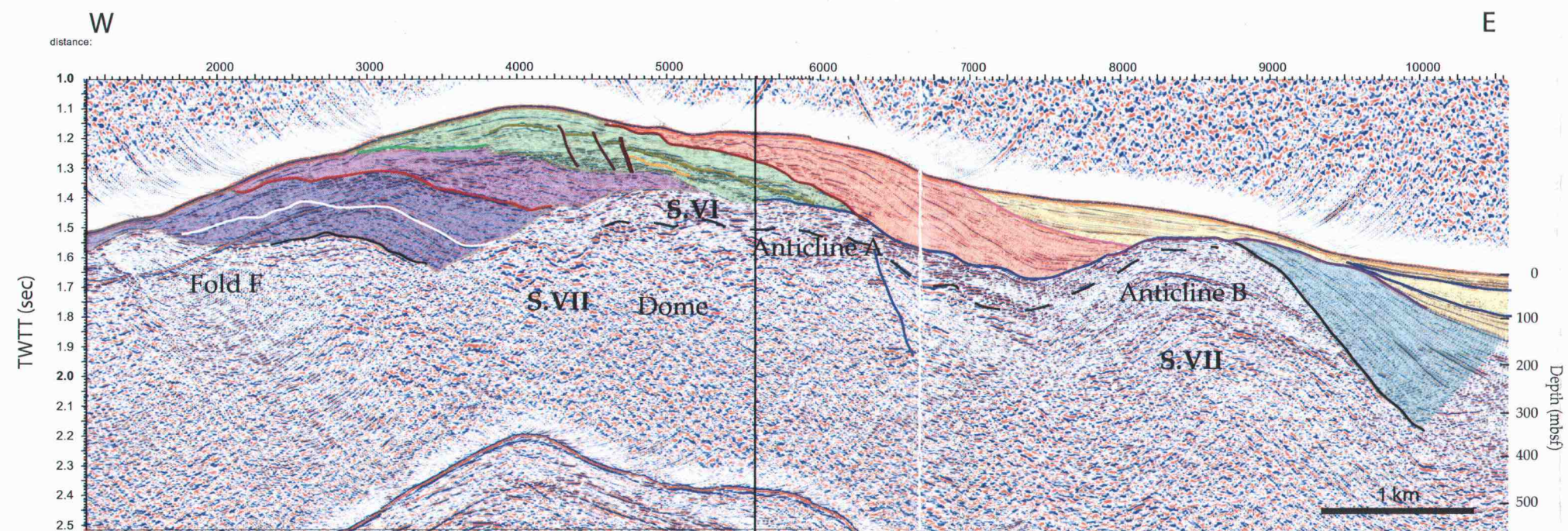


Figure 6B.b) EW line 250

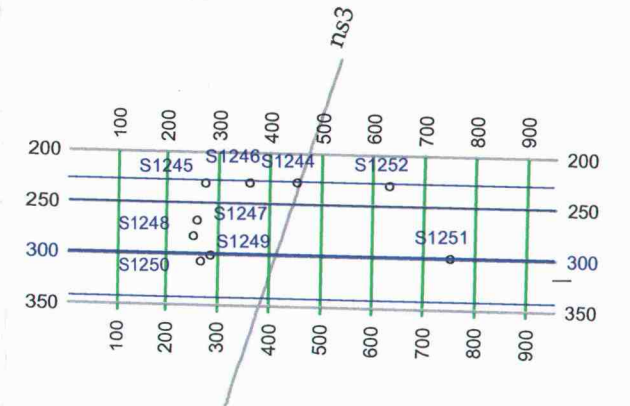
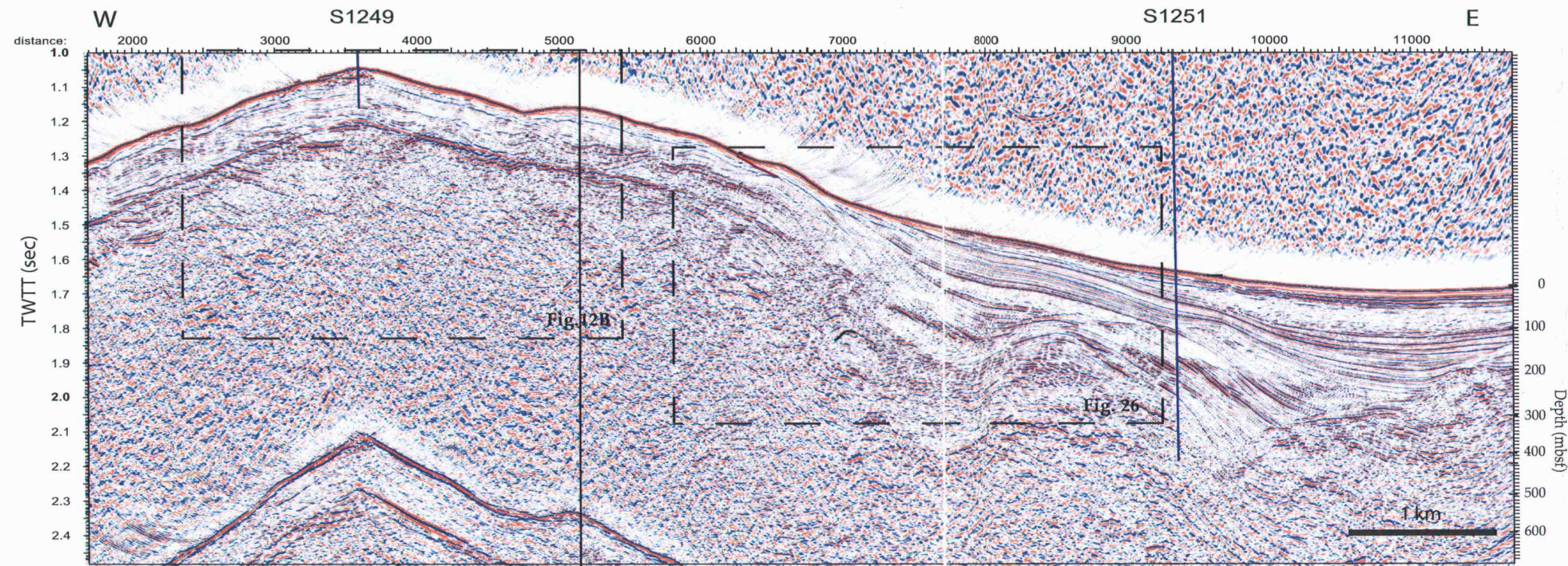


Figure 6C.a) EW line 300

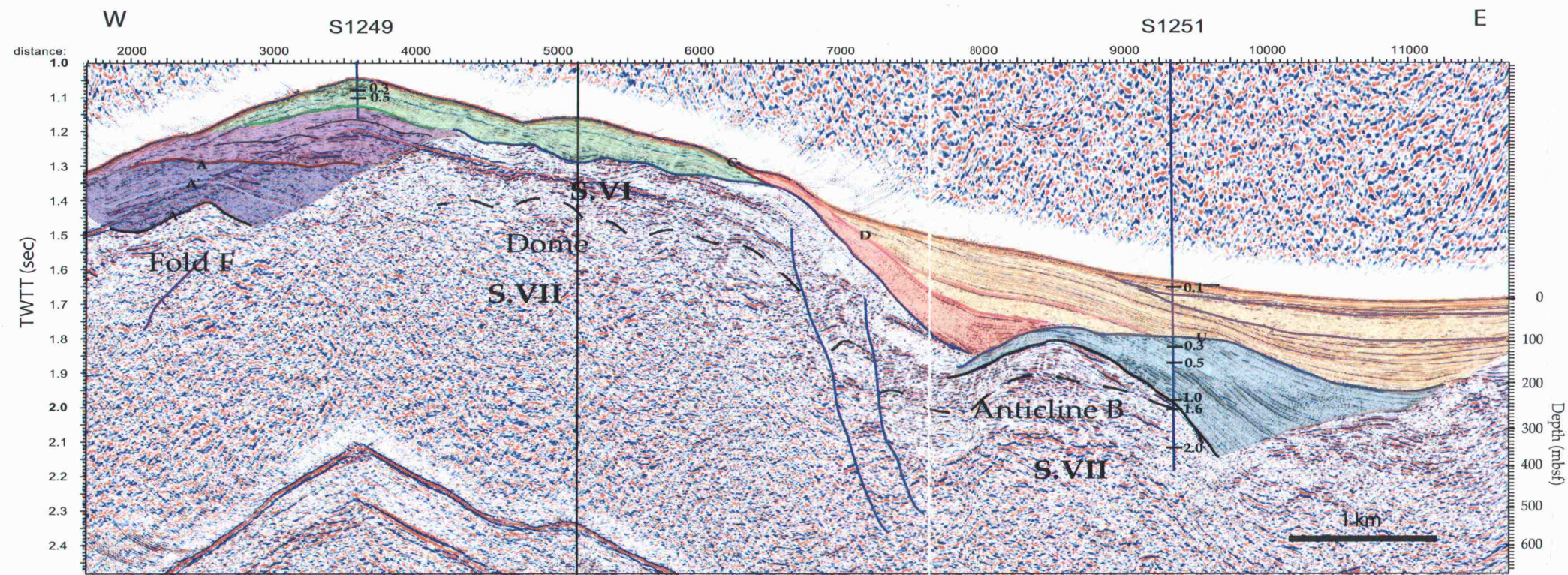


Figure 6C.b) EW line 300

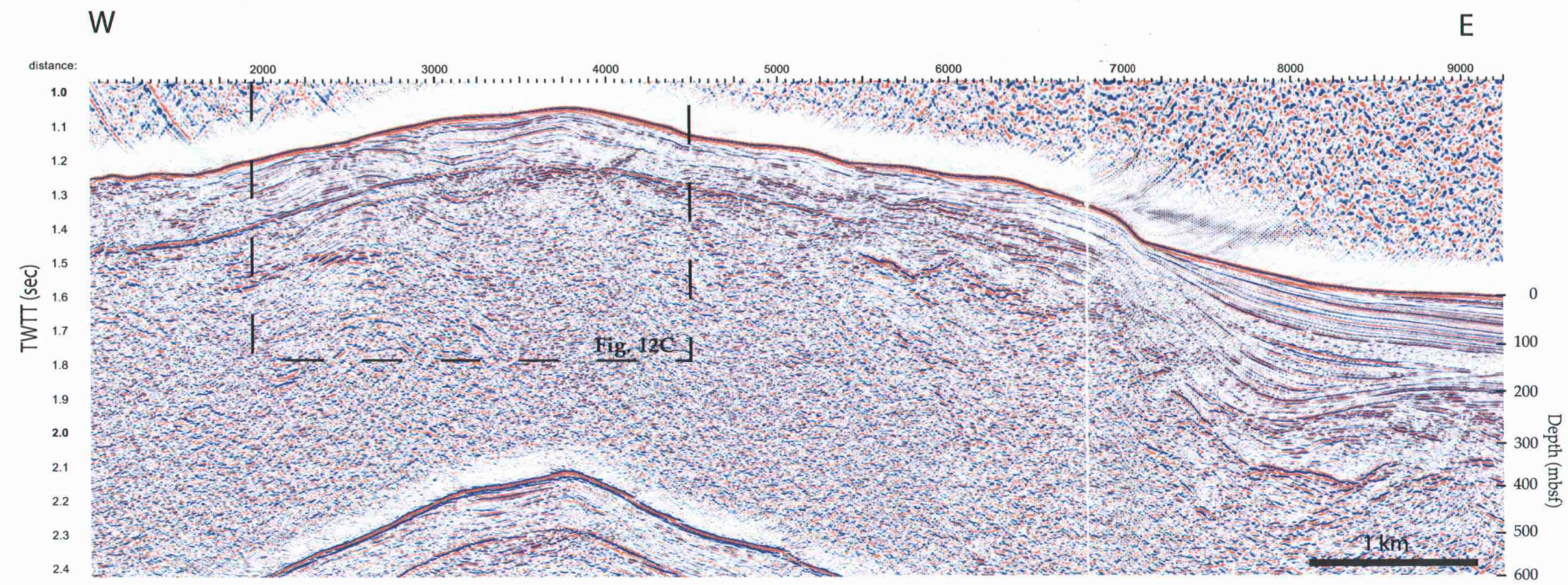


Figure 6D.a) EW line 343

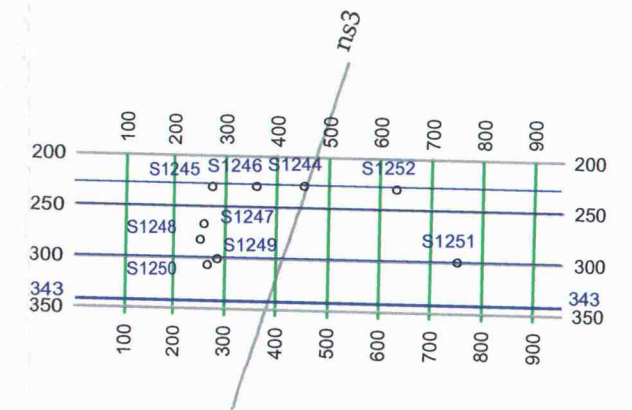
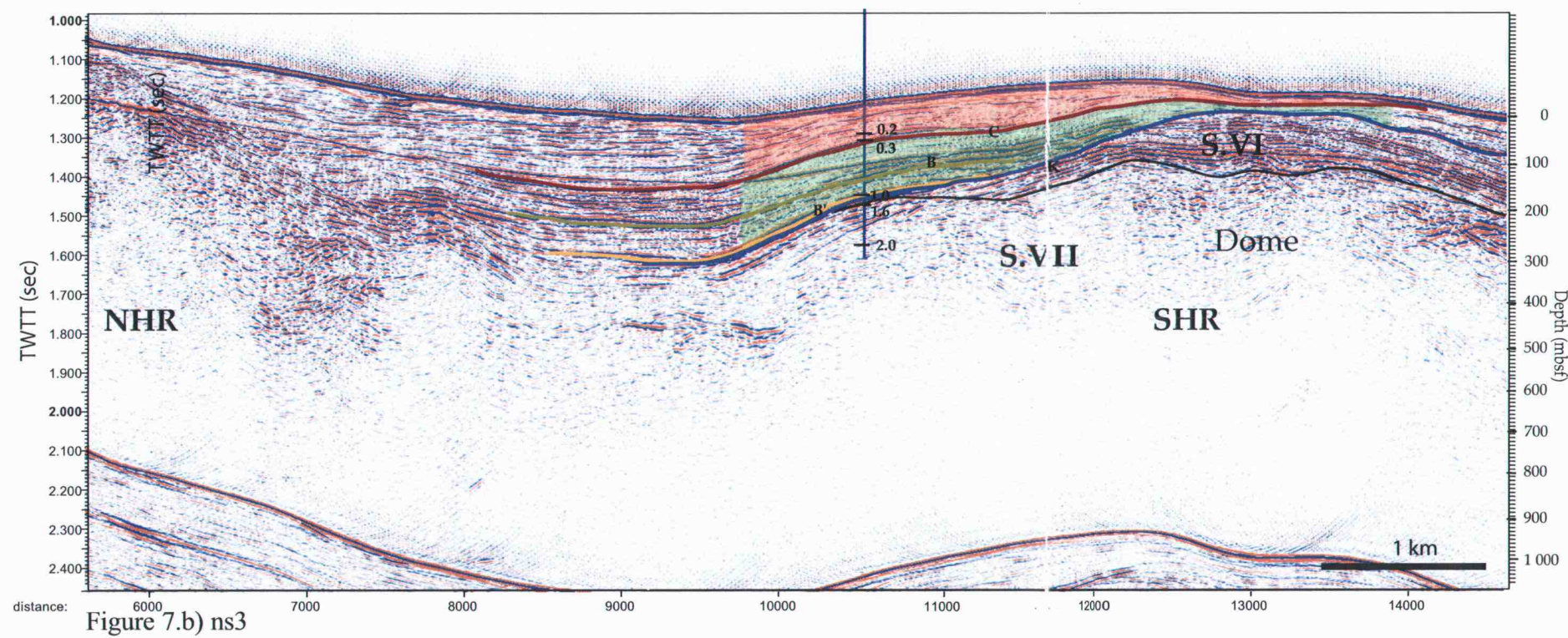
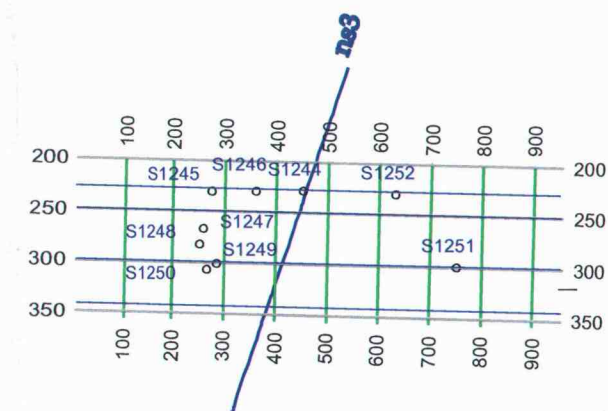
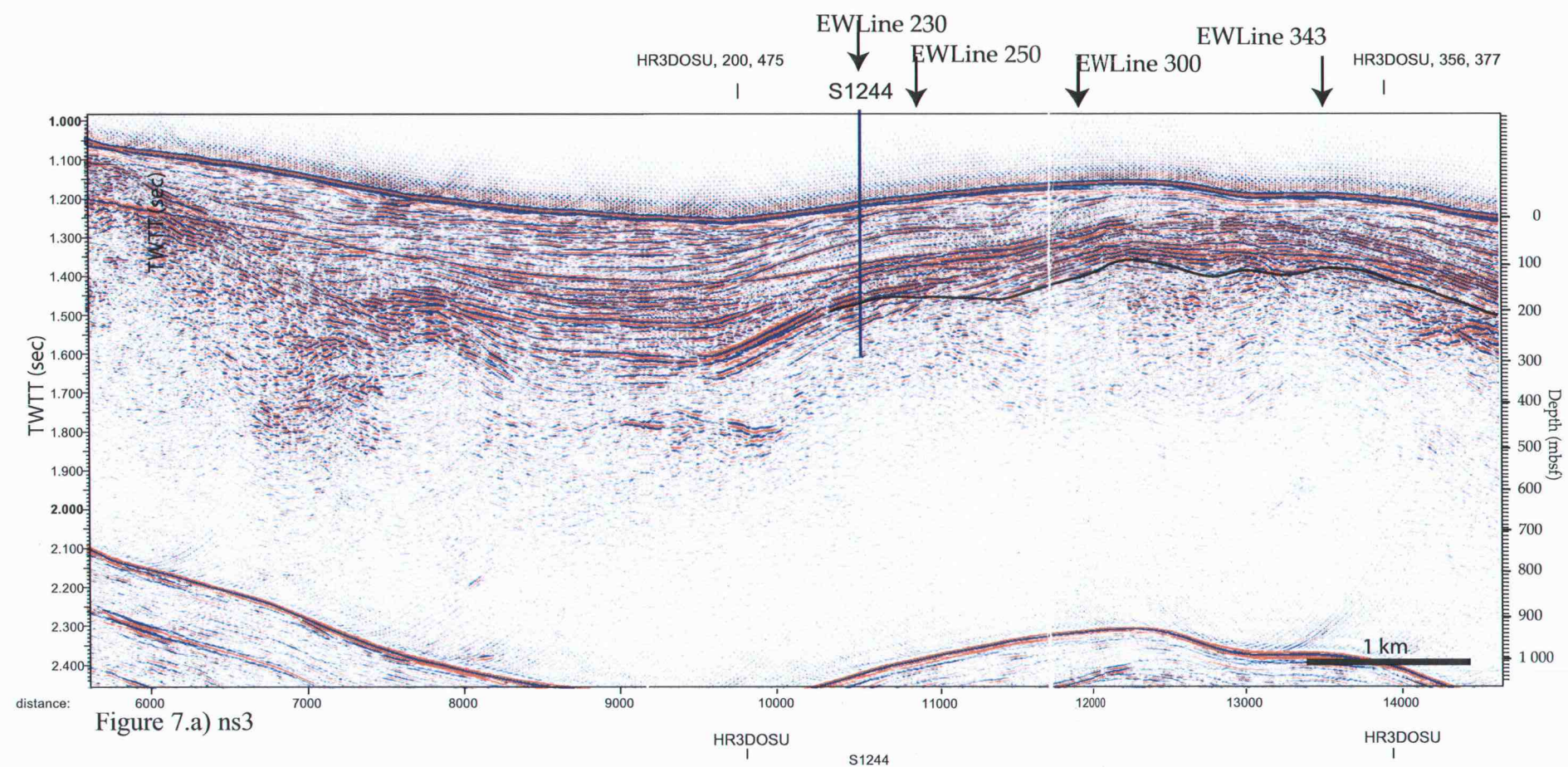


Figure 6D.b) EW line 343

Figure 7: (a) un-interpreted and (b) interpreted version of 2D migrated seismic line ns3. The figure shows the NS view of the features presented on the EW section of Figure 6. It extends across the saddle observed between northern HR (NHR) and southern HR (SHR) on the bathymetry (Fig. 1). The features shown are: The seismic units and the seismic horizons described in seismic sequence stratigraphy chapter 4 (see appendix A for the legend). The ODP sites presented in Figure 4 (blue vertical lines). The ODP biostratigraphic results are marked along the wells (in Ma). They are discussed in the biostratigraphy chapter 5. Finally the structural features inferred from the cross-sections as well as from the depositional history of the sediments. They are presented in more detail in the structural chapter 6. Notice the time-line 1.6 Ma in black, which marks the boundary between S.VI and S.VII). The northern and southern extension of the seismic volume are indicated “HR3DOSU” above the seismic profile and coincide with the end of the coloring on Fig. 7b. The location of the section is shown in the plan view of the seismic volume, upper right corner of the page.



4.3 Descriptions of the seismic units

The seismic stratigraphic units are presented in chronologic order, oldest to youngest, in this section. The description for each unit includes geological setting, lithological results and geometry. The most important units are color-coded on the seismic and geologic cross-sections (see Appendix A).

4.3.1 Unit S.VII (>2 -1.6Ma)

Unit S.VII forms anticline B. Seismically, it is characterized by irregular discontinuous and chaotic reflections, including a few deformed angular unconformities (Fig. 6). Because these angular unconformities are themselves folded, we can conclude that the growth of the anticline occurred during a succession of erosive phases and/or sedimentation pauses separated by sedimentation phases. Correlation of the biostratigraphy results between S1251 and S1244 suggests that S.VII strata are coeval with the deeper stratigraphy cored at S1244 within the main ridge, (see Biostratigraphy chapter). The same age is supported by the low-coherency and chaotic reflections that characterize the seismic facies of both seismic regions.

This interpretation is also supported by the correlation of the lithology results for the different sites (Lithologic unit L.III, S1252 and S1251 in the basin and unit L.III; S1244 on the ridge, Fig. 4, 6.A, 7) (see appendix B for the relation between the lithologic units and the seismic units). Both lithologic units are characterized by a relatively high degree of lithification and both contain glauconites-rich layer interlayered within the strata (Shipboard Scientific Party, Site 1244, 2003). Both lithologic units were interpreted to represent highly deformed sediments of the accretionary complex (Trehu et al., 2003a).

4.3.2 Unit S.VI (>1.6 – 1.0 Ma)

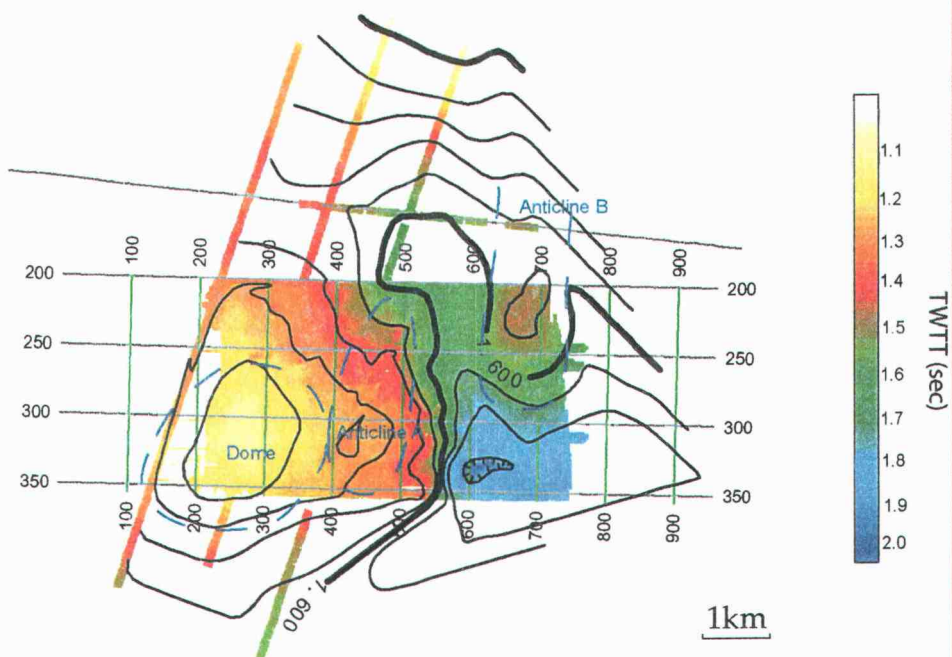
The unit encompasses strata 1.0 Ma and 1.6 Ma in age as inferred from the biostratigraphy results at S1244, S1252 and S1251 (see Biostratigraphy section). The 1.0 Ma time line coincides with the onlap surface K beneath the summit of southern HR (blue on Fig. 6 and 7, Fig. 8A). The strata lay sub-horizontal in the NS. sections (Fig. 7) as well as in the EW direction (Fig. 6). S.VI strata are distinguished from the deeper strata (S.VII) by an increase in coherency and continuity. The wavy to chaotic facies of the unit results from several para-sequences, whose geometry is controlled with small-scale anticlines (400-800m wide). One larger anticline, named anticline A (Fig. 6B, C, D), will be mentioned in the tectonic chapter. Multiple angular unconformities, characterized by a small extension, cross each other and often correspond to the limbs of the anticline features (4000 –6500m, 1.3 – 1.5s on Fig 6B & C). Strata become less coherent beneath these anticlines.

S.VI was not distinguished as single lithologic unit. Seismic interpretation indicates that the coring sites coincide with the pinch-out zones of the unit. Hence, the unit's lithology is known from thin cores sections at S1244 and S1252. It was sampled between 216mbsf and 245mbsf at S1244 and interpreted as upper part of lithologic unit II (described in the Unit S.II section). At S1252 it corresponds to the strata between 114 mbsf and ~150 mbsf. These strata were assigned to lithologic unit III (described in the Unit S.VII section). It fills the space between the S.VII strata and Unit S.II and S.IB (Fig. 7).

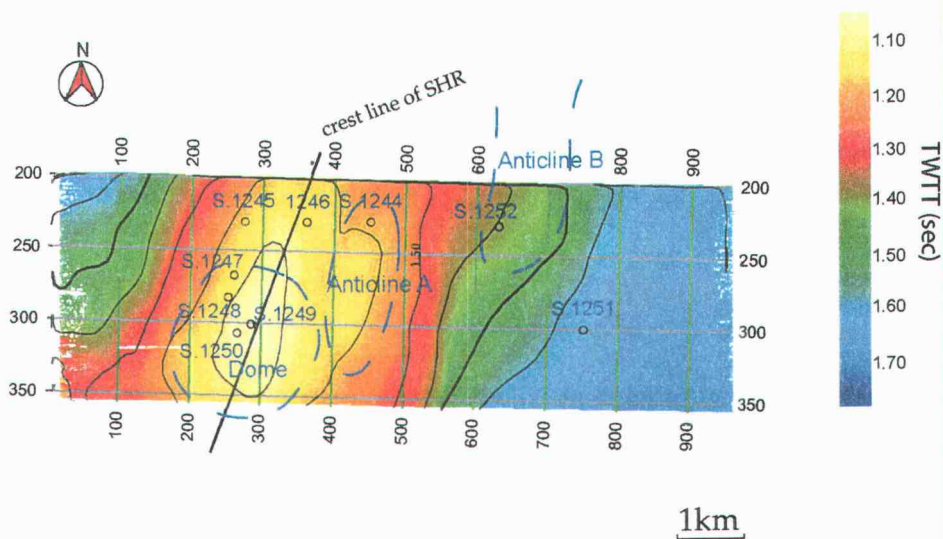
Seismic horizon K (Fig. 6) marks the upper limit of Unit S.VI. K maps an angular unconformity visible on seismic sections, which is defined by the termination of the younger strata lapping onto the lower-coherency facies. A time-map of horizon K (Fig. 8A) reveals the dome-shape of Unit S.VI in the southern

central region of the survey as well as a NNW striking syncline northeast of the dome with 0.5 sec (~387 m) of relief. The Dome is a major structure in the subsurface of the ridge (see Structure chapt.) and is still expressed in the current bathymetry (Fig. 8A). The syncline coincides with the down-throw of fault E. The eastern continuation of the strata could be traced across the fault system E (Fig. 6C & D). They pinch-out to the east onto anticline B (Fig. 6), which indicates the anticline existed prior to the deposition of the unit. Unit S.VI strata lies east of the strata folded by fold F (Fig. 6). To the east, S.III strata lap, onto S.VI strata along the upper extension of F2 (Fig. 12A). The stratigraphic relation between S.IV and S.VI is ambiguous, structural geometry of the strata suggests that the landward vergent thrust fault separates both units. However, based on the biostratigraphy, sediments of the footwall of the fault are older than the sediments of the hanging wall, implying a complex tectonic history (see tectonic model, chapt. 7).

Figure 8: A) Time map of onlap surface K. The deeper structures discussed in the structure chapter are highlighted. B) Bathymetry of southern HR, The deeper structures discussed in the structure chapter are highlighted as well as the crest line of the current summit. Note that the crest line is parallel to the hinge line of the 2nd order fold that deforms S.II strata (Fig.16), which is parallel to the strike of F2 (Fig.11).



A Unconformity K time map; Contour Interval: 0.1 sec



B Bathymetry time map; Contour Interval: 0.1 sec

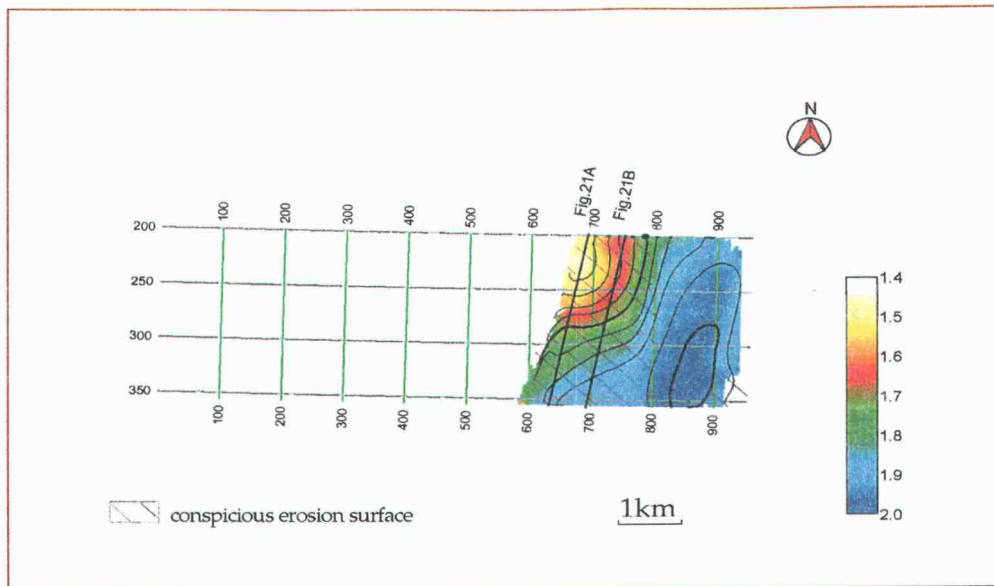


Figure 9 Unconformity U time map and its correlative surface : contour interval 0.05 sec

4.3.3 Unit S.V (1 Ma - 0.3 Ma)

Unit S.V, on the eastern side of anticline B, is distinguished from S.VII by closely-spaced, high amplitude seismic reflections. These are bounded to the top by a conspicuous erosion surface named “U” (Trehu et al., 2003a) (Fig. 4, 6, 9). The unit composes the eastern flank of anticline B but is missing on the western limb of the anticline, instead, S.II and S.IB strata directly onlap onto S.VII (Fig. 6). The strata are divergent, indication of syn-sedimentary growth of the anticline.

The unit’s lithology is distinguished from the units above by its significant decrease in biogenic content (foraminiferas, diatoms, nannofossils) within L.II related with a higher percentage of clastic material (silt size quartz and feldspar grains). It is also characterized by higher frequency of turbidites below the erosion surface U. The erosion event can be mapped over the whole basin in the south and only on top of the anticline in the north (Fig. 9). The unit boundary is extended along the correlative conformable surface.

4.3.4 Unit S.IV (<1.6 Ma - 1.15 Ma) (dark blue)

Unit S.IV built the western flank of southern HR. The growth of the frontal-thrust-fault-related-fold F (see structure chapt. 5) controlled the tectono-sedimentary evolution of S.IV strata (Fig. 6). The fault F1 can be inferred within the deeper stratigraphy (Fig. 6). F2 is a second splay of the fault system that was active more recently because it disrupts younger strata than F1 does. It is possibly responsible for the up-turn of the S.IV strata at their eastern extremities (horizons A (red) and A’ (white) on Fig. 6).

Unit S.IV comprises three depositional sequences separated by three angular unconformities; horizons A’’, A’ and A (Fig. 6, 10). The lower boundary of the

unit is defined along horizon A'' as it corresponds to the deepest distinguishable reflection. To the west, the strata pinch-out at the seafloor on the western flank of the southern HR. The eastern extension of the unit is defined at the termination of coherent reflections against F2 (Fig. 6).

Lithologic evolution of S.IV is controlled by tectonic deformation. The unit comprises three lithologic units, L.V, L.VIA and L.IVB (Fig. 4). Unit L.IVB and L.V strata are nannofossil rich silty claystone, interlayered with thick turbidites, containing wood fragments. Unit L.IVA is composed of nannofossil-rich clay and silty clay. It is marked by an increase with time of biogenic opal (diatoms), and a distinctive ash layer marks its upper boundary (coincident with reflection A). Frequent thick turbidites (from 5 to 20 cm at S1248) distinguish it from L.IVB. The degree of lithification increases to claystone within Unit L.IV. Lithologic units L.V, L.IVA, L.IVB and L.IIIB are distinguished from each other by subtle changes in biogenic content, minor lithology differences and sedimentation rates. Each change coincides with an angular unconformity that defines the three depositional sequences. For this reason, the changes in depositional environment expressed in the lithology are interpreted as the result of the syn-sedimentary tectonic deformation.

Figure 10: Four geologic stages of one seismic section achieved through flattening of three AU, horizons A'' (T1), A' (T2) and A (T3) and current configuration (T4) along a profile of fold F. The horizons are interpreted as paleo-seafloor with the assumption of a sub-horizontal seafloor. Note that Horizon A is dated approximately 1.15 Ma (Shipboard Scientific Party, 2003, Site 1245). Beginning of fold F is inferred from the divergence of the strata. It occurred between the deposition of horizon A' and horizon A, that is approximately 1.15Ma. Parallel bedding among the strata deeper than horizon A' are evidence for a quiescence period prior to the growth of the fold. In addition, the flattening method reveals the activity of a local feature to the west (T1) prior to the deposition of horizon A''. The extension of the feature could be delineated on a time slice; it has an oval shape, approximately 1km in diameter.

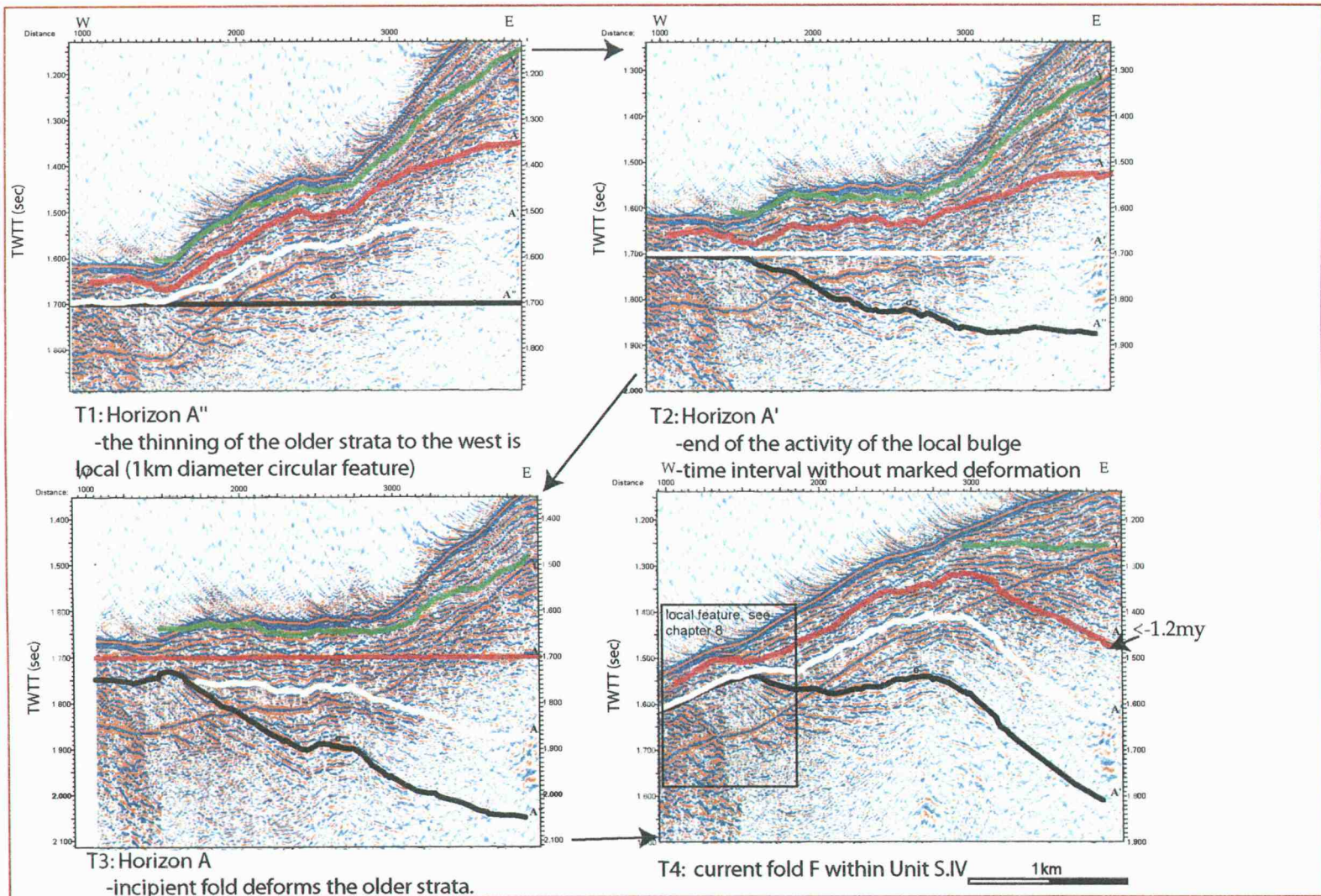
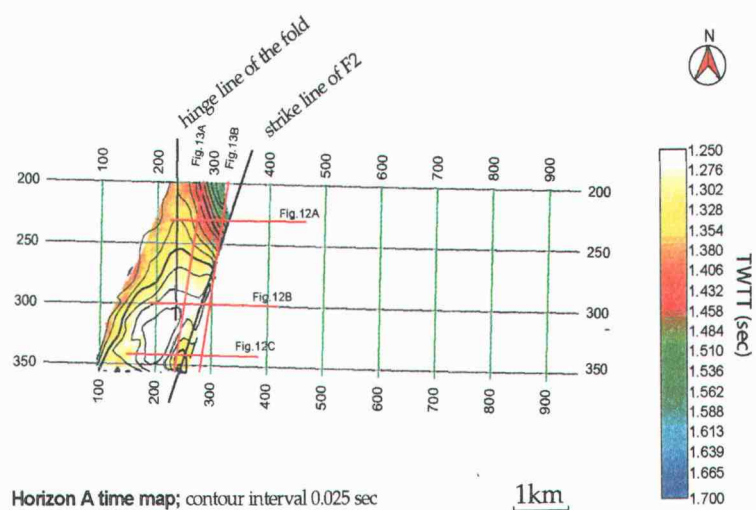
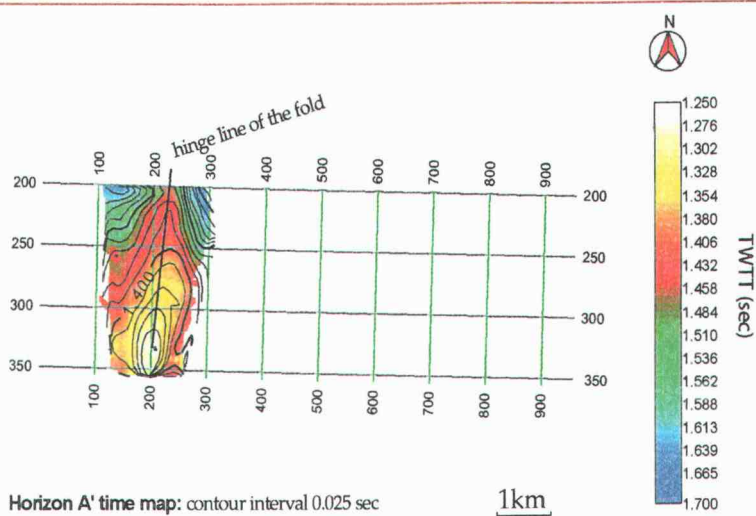


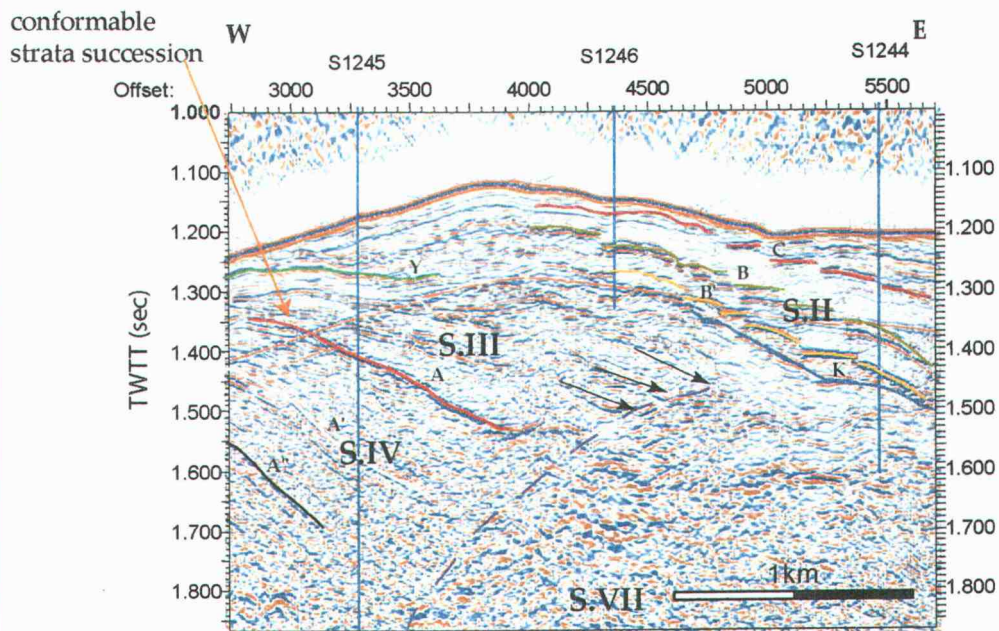
Figure 11: A) Time map maps of horizons A'. The black line indicates the crest line of the fold F as inferred from the contours of horizon A', B) Time map maps of horizon A. The NS. black line indicates the crest line of the fold F as inferred from the contours of Horizon A. The diagonal black line shows the strike of the thrust fault-splay F2. Comparison of F2 with the crestal line of the current southern Hydrate Ridge suggests a correlation between these two structural features. Locations of the sections from Figure 12 & 13 are shown in Red



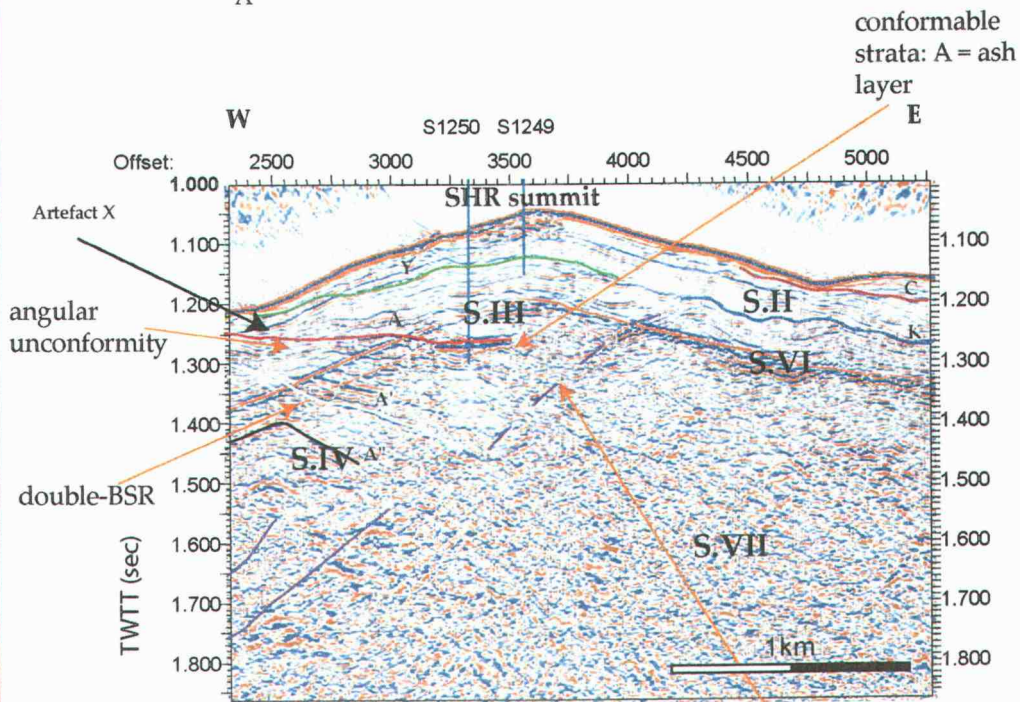
The fold F is a doubly plunging, 2-3km long, NNE striking fold but the seismic volume encompasses only the northern half of it (Fig. 11). No deformation can be inferred on the NS cross-sections partly due to the low coherency of the reflections on these sections. Hence the origin of the plunging of the northern and southern end of the fold could not be analyzed in more detail.

On EW sections, within the eastern limb of the fold, the unit thickness can be observed to increase from the center outward by up to 0.2 sec (~ 160m). In the north, only the eastern limb is observed to be divergent. In the south the western limb also shows divergence of the strata to the east as well as to the west. Divergence of the strata suggest the progressive tilting of the depositional surface, which means the syn-depositional, progressive, steepening of the limb of the fold. In the north, an inherited local active feature masks divergence to the west at the time of deposition, causing the strata to converge to the west (Fig. 10). Timing of the activity of the fold is based on the interpretable internal geometry patterns. In fact, time isopach maps suggest that a tectonic quiescent period existed prior to horizon A' and the incipient folding stage occurred prior to the deposition of ashes at horizon A. This interpretation can be visualized by flattening successively the three horizons A'', A' and A (Fig. 10). The horizons are interpreted as paleo-seafloor-surfaces, which imply they represented a sub-horizontal seafloor at each respective time period. Hence, Figure 10 presents the reconstruction of the geometry of the strata at four different points in time. Prior to horizon A' (Fig.10 T1 and T2) strata are affected by the activity of a local feature mentioned above (1000 – 2000m, 1.5 – 1.65s Fig.10 T1,). The extension of the feature could be delineated on time slices; it has an oval shape, approximately 1km in diameter. The local feature's activity causes the strata to converge against it, which imply syn-depositional uplift until 1.2 Ma. As opposed to the subsequent period T3, no fold F related deformations could be observed on these two time shots. At T3, a small fold deforms the strata, suggesting the incipient phase of the fold F ~1.15

Ma. Geometry at period T4 that is at present time shows the fully developed fold F.



A



B

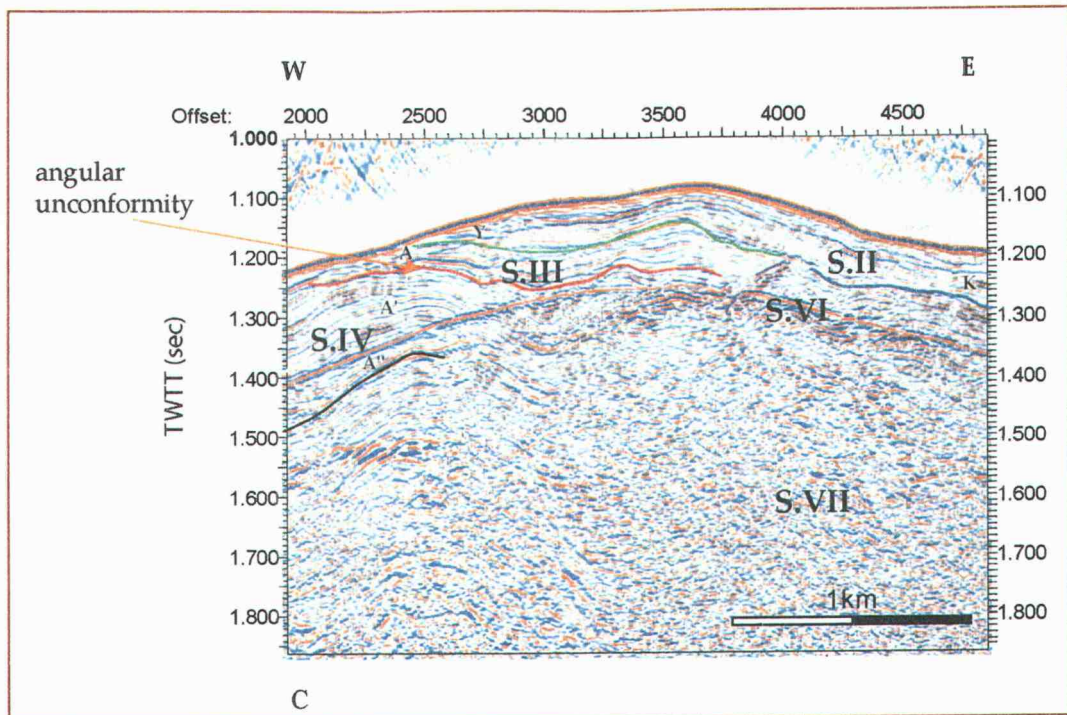


Figure 12: Three EW, showing the structural variations beneath the southern Hydrate Ridge summit from north to south. A) In the north, the eastward continuation of Y (green) and A (red) cannot be clearly traced. Horizon A (red) lay conformable with the surrounding strata. The eastern termination of the strata cannot be distinguished; it is interpreted as terminating against the upper part of F2 (dashed purple). B). In the south: The continuation of A and Y to the east are as ambiguous as in the north but differ markedly. However strata are interpreted to onlap onto A to the west. To the east the reflector A onlaps onto the conspicuous seaward vergent angular unconformity, that is the upper continuation of F2 (dashed purple). (see Figure 11B for locations)

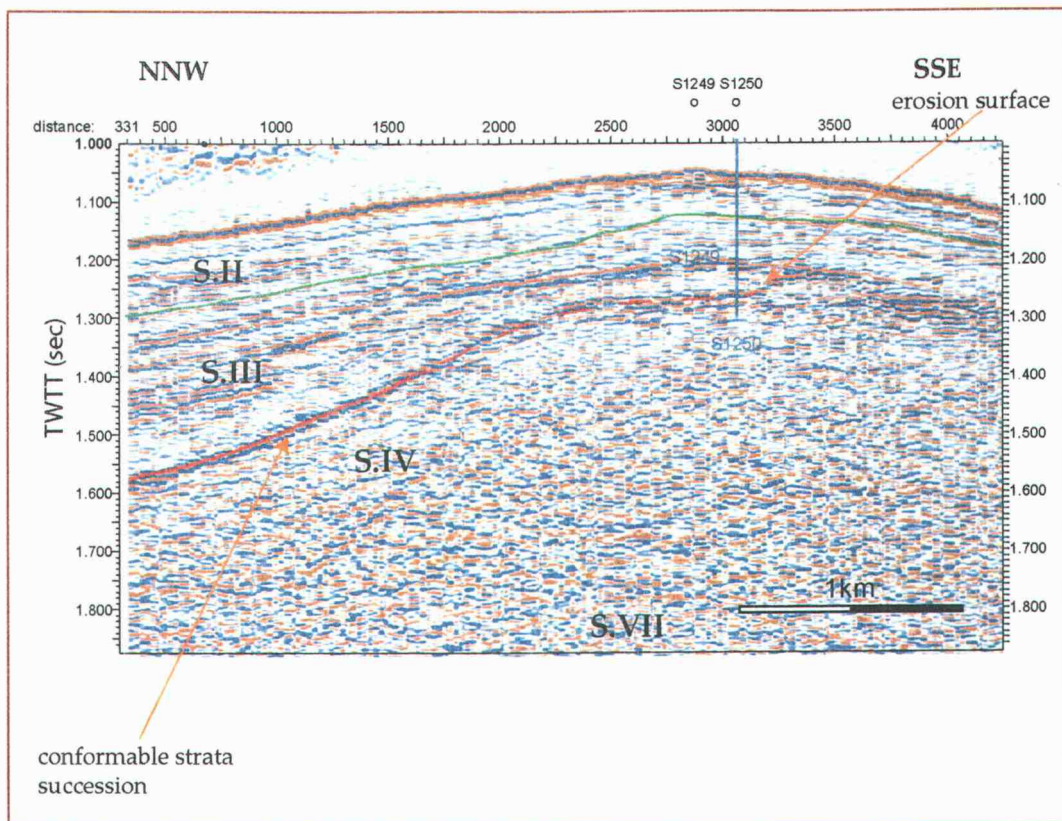


Figure 13: Two NNW, migrated time sections extracted from the seismic volume, parallel to the crest line of fold F. A) To the west: the section crosses the area in which A coincides with the ash layer in the north. The ash layer is interpreted as correlative to an angular unconformity located in the south (Fig. 12). B) To the east: the section runs across the area in which horizon A joins the upper continuation of extension of F2. (see Figure 11B for locations)

Horizon A marks the boundary between units S.IV and S.III. The horizon is characterized by its particularly bright amplitude, “Ten times brighter than the surrounding reflections “ (Trehu et al, 2002) (Fig. 6). It was correlated with an ash-rich sediment layer at sites S1250, S1248 and S1245. Studies from Trehu, Fleming et al. (2003) of horizon A showed that it is a gas conduit that leads free gas from the older lithified region to the gas hydrate stability zone. The gas is focused along horizon A until it reaches a pressure high enough to overcome the lithostatic stress and breaks vertically through the sediment column. From a stratigraphic point of view, this occurs where the ash-rich layer laps onto a paleo-bathymetric-high (Fig. 12, 14). Figures 12 and 14 show horizon A laying conformable to the surrounding layer along the NS transect cored during Leg 204. It is interpreted as the correlative conformity of an angular unconformity lying south and west (Fig. 12 and 13). At S1247, the ash was not observed at Hole 1247B, although the LWD data for Hole 1247A was similar to the data for 1245, 1248 and 1250. This suggests a strong lateral change in the stratigraphic character of horizon A between Holes 1247A and 1247B (Fig. 14). We propose that the two holes at S1247 encompass the angular unconformity (Hole 1247B) just above the onlap-line of the ash-layer (Hole 1247A) (Fig. 14).

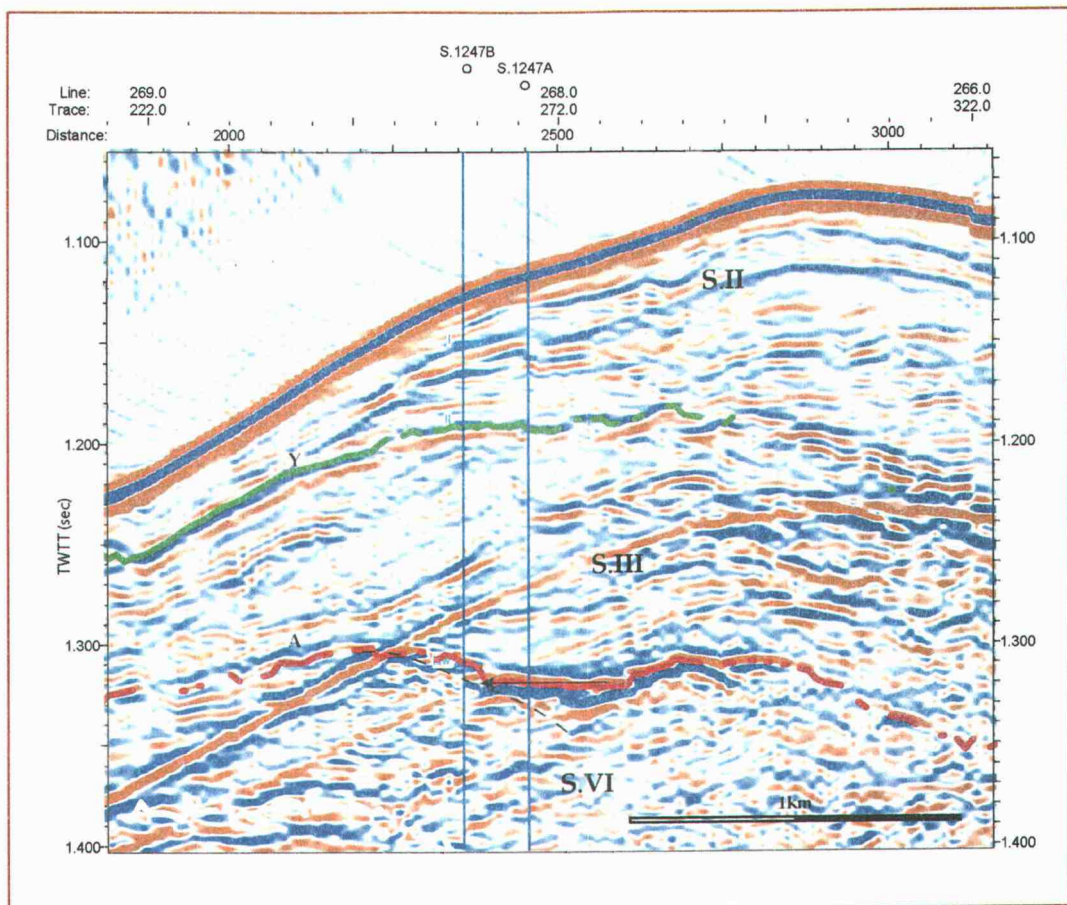


Figure 14: Close-up of migrated-time section of EW line 268, around S1247 area. Shows horizon A (red) and horizon Y (green). Location can be inferred from the line and trace numbers, which correspond to the survey numbers as shown on Fig.1. The black arrow represents the onlap of the ash-layer (horizon A) onto the bathymetric-high (dashed line) as suggested by the stratigraphic model (see text).

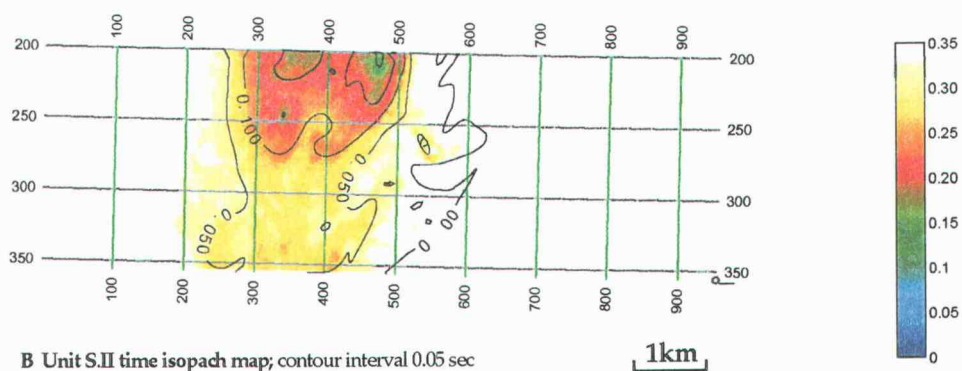
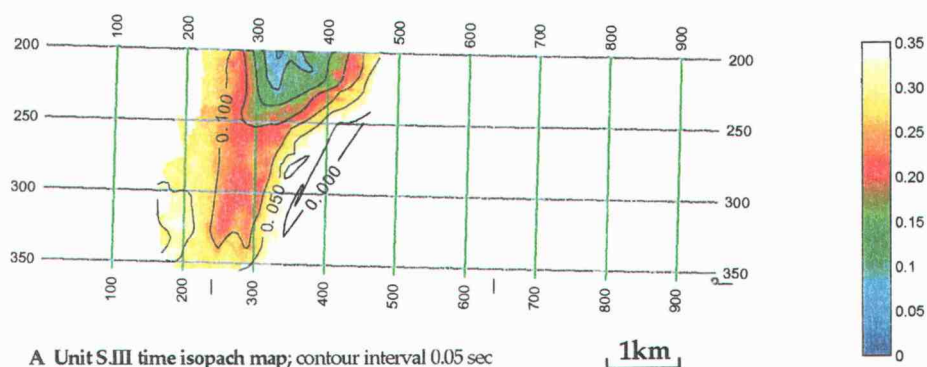
4.3.5 Unit S.III (1.15 Ma - 0.5Ma) (purple)

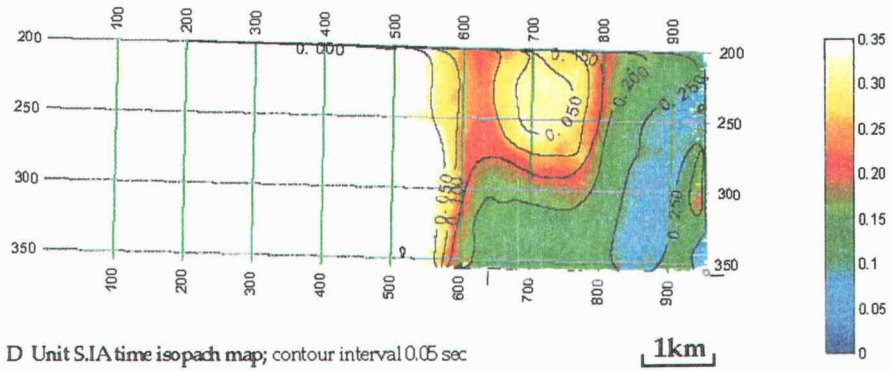
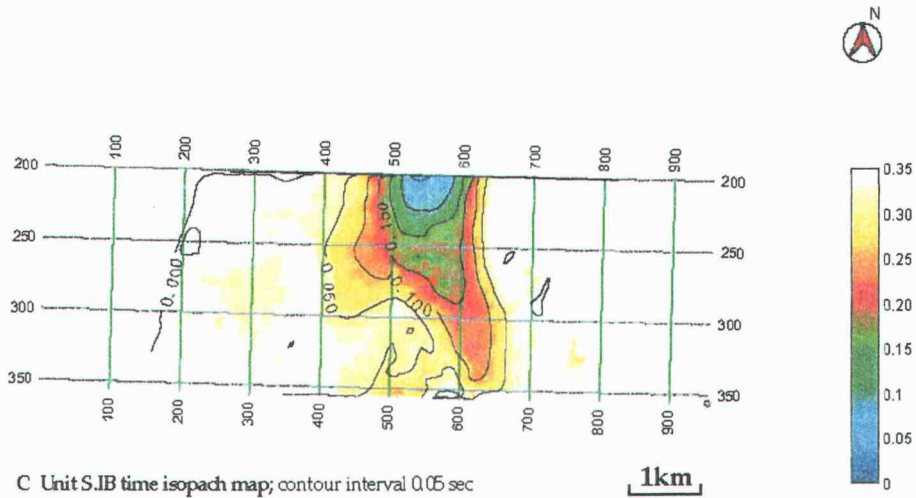
The unit is confined to the western part of the survey. The lower and upper boundaries are defined respectively by seismic horizons A and Y (Fig. 4, 6), which stand-out because of their high amplitude. Unit S.III fills the foreland basin that formed during the growth of fold F (Fig. 6). Comparing the strike and the dip of the plunging fold F and the time isopach map of S.III (Fig. 15A) suggests that S.III filled the accommodation space created between the plunging of the fold to its south and the Dome to its east. The unit is marked by compression deformation, evidenced by small-scale folds (Fig. 12C).

Coring along the north-south transect showed clay and silty clay with high-frequency turbidites and a high concentration of opal. A decrease in calcareous fossils at horizon A distinguishes the lithologic unit L.IIIA from L.IIIB, which correspond to seismic unit S.III from S.IV respectively (Fig. 4, Appendix B). A high sedimentation rate at S1245 (31 cm/ky) compared to ~10 cm/ky within the same unit at the sites further south were computed based on the biostratigraphic results. They suggest a depocenter in the north and a bathymetric high in the south during this time period.

Divergence of the S.III reflections on EW seismic sections, evidence the syn-sedimentary activity of fold F (Fig. 6, 12). On NS sections, the unit thins along the hinge of fold F from 160 m in the north to 128 m in the south (Fig. 15A). This observation supports the interpretation of a depocenter in the north inferred from the sedimentation rate. The upward extension of F2 is interpreted as an onlap surface along which S.III strata lap onto S.VI (Fig. 6, 12, 15A), which implies the existence of the dome (unit S.VI) to the east of the depocenter during the deposition of S.III and an age older than 1.15 Ma (age of S.III lower boundary) for the S.VI strata (Fig.12B).

Figure 15: Time isopach maps of Units S.III, S.II, S.IB, S.IA





4.3.6 Unit S.II (0.5 – 0.3Ma) (green)

Unit S.II is a prominent ridge building unit in the northern part of the seismic volume. Its lower boundary is defined by the termination of eastward dipping reflections against the onlap surface K and its westward dipping reflections against horizon Y (Fig. 6). The unit is prominent in the northern EW sections. It thins rapidly to the south against the dome observed in the central region of the survey (Fig. 7, 15B).

At S1244, lithologic unit L.II is distinguished from the surrounding units by an increase in coarser material and in turbidite frequency. The presence of ash-rich turbidite events suggests a connection between the active slope-basin and the Astoria Fan during the deposition of B'. Reflections B and B' coincide with two lithologic events interpreted as marker horizons that tie S1246 to S1244 (Fig. 4, 16, Appendix B). B' at S1244 is a 60 to <0.1 cm thick volcanic ash-rich horizon at 216 mbsf with 50% glass content. At S1246, two discrete volcanic glass-bearing layers at 88 and 95 mbsf (<1 and <0.1 cm thick respectively) were interpreted as the continuation of B' to the west. Reflection B coincides with multiple turbidites clustered into thick zones at S1244 as well as at S1246, and is parallel to the ash event B'. These two reflections are relatively bright although their respective amplitudes vary considerably (Fig. 6, 7).

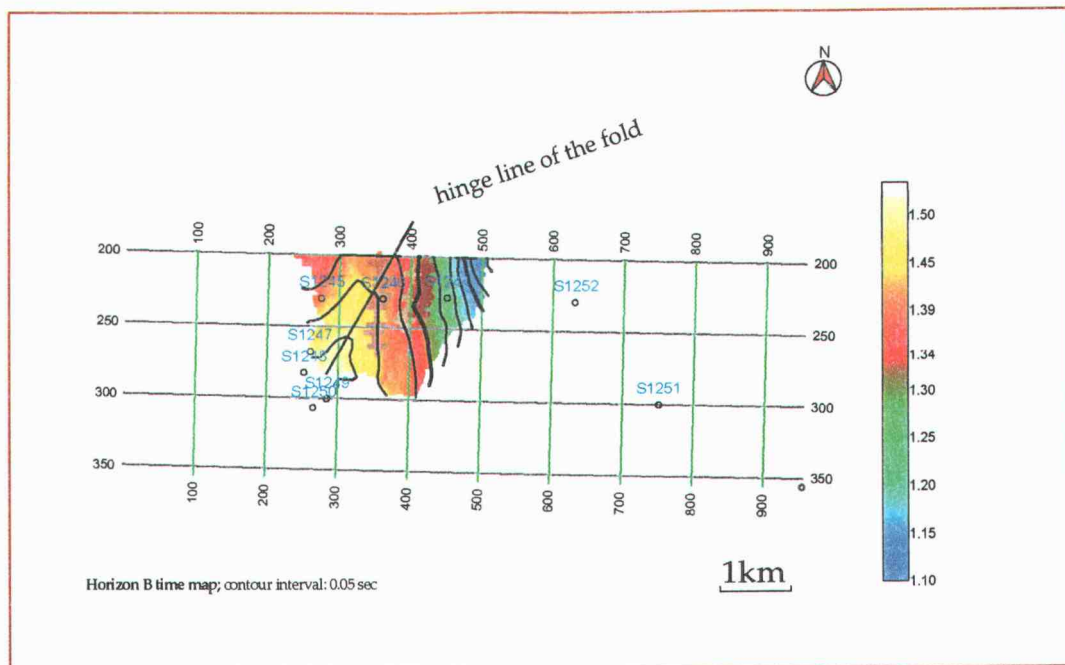


Figure 16: Time map of horizon B, also shown is the strike of the normal-faults that disrupt S.II strata and the hinge line of the 2nd order fold discussed in the text. Profile view of these tectonic structures can be view on Figure 17.

The upper boundary of Unit S.II is defined by Horizon C, which corresponds to a reflection (Fig. 6) that lays parallel to B over its whole extension. Horizon K, is defined by the downlap termination of S.II strata. It is interpreted as corresponding to the floor of the basin-fill sequences units S.II and S.IB. It can be extended to the north across the saddle that separates southern HR from northern Hydrate Ridge summit (Fig. 7). Horizon K joins the angular unconformity U to the east (Fig.6). To the west the horizon K is interpreted until the horizon vanishes in the deformed region between S.III and S.V (Fig.12). Horizon K probably marks a major sedimentation hiatus.

Figure 17 is a close-up from the EW line 230 (Fig. 6A) on S.II. The stepwise decrease in the thickness to the east between horizons B and B' (green and yellow on Fig. 17), which coincides with NS-striking normal faults, is interpreted as an evidence for syn-faulting sedimentation of S.II (Fig. 16, 17). This syn-sedimentary normal faulting is interpreted to have accompanied the folding of the strata observed on the time map of horizon B (Fig. 16). Post-sedimentary bending of the strata is evidenced by a monocline that deforms the eastern part of the strata (Fig. 6, 16). NS sections show the Unit S.II strata are bedded sub-parallel (Fig. 7) but the whole unit is thinning to the south (Fig. 15B) and is up turned in the southern part of the section (Fig. 7). This geometry suggests a reactivation of the Dome, after it was initially buried by unit S.II.

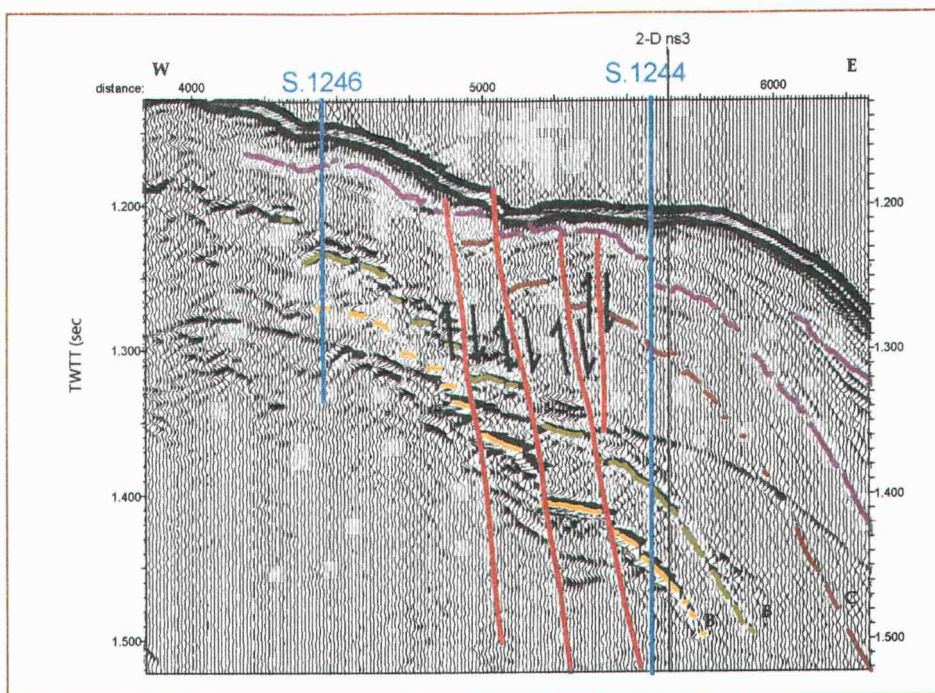


Figure. 17: Close-up of migrated time section of an EW line across S.II. Horizons C (red), B (darkyellow) and B' (yellow) reveal the offset along the normal faults mapped on Figure 16. The discrete decrease in thickness between the stratigraphic horizons toward west suggests syn-sedimentary activity of the faulting. For location see Fig. 6A

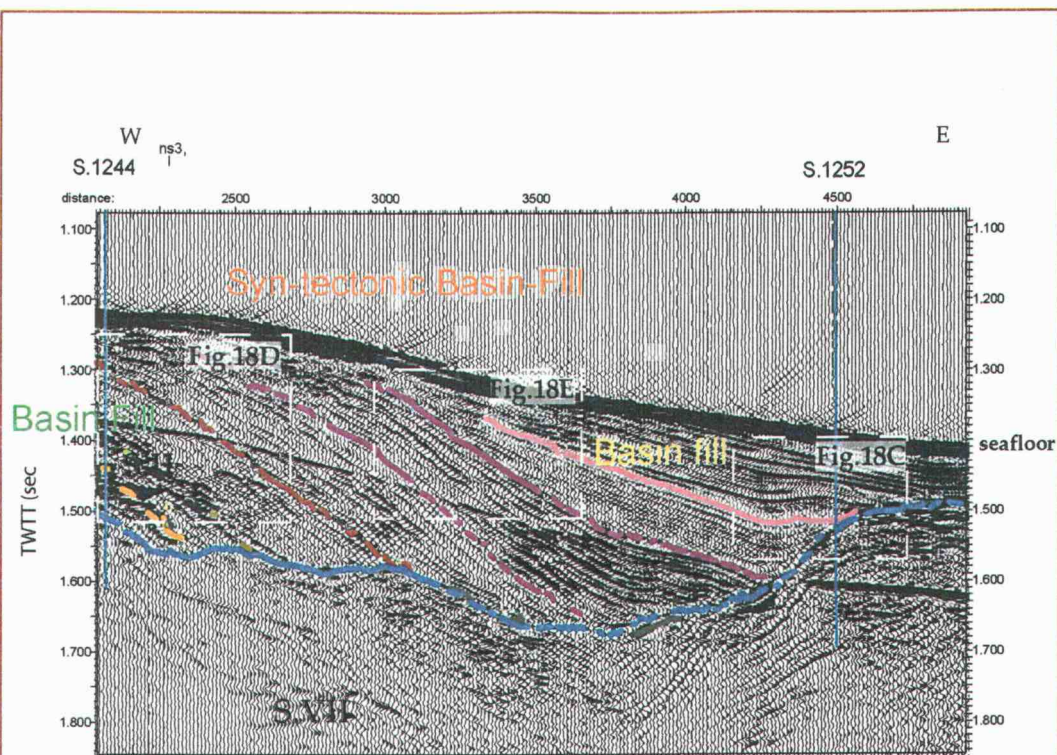
4.3.7 Unit S.IB (0.3 Ma – 0.2 Ma) (orange)

Unit S.IB fills the syncline observed in the time map of angular unconformity K between the Dome in the central region and anticline B (Fig. 8A, 15C). The strata lap onto horizon C to the west (Fig. 6, 18, 19) and onlap to the east onto the buttress unconformity U, which delineates anticline B (Fig. 6). Four depositional sequences compose the unit and are topped by mudflow event DBF.1 that reaches a maximum thickness of 0.07sec (~60 m) (Fig 6, 18). This event marks the upper boundary of Unit S.IB and presents an excellent marker horizon across the survey.

Unit S.IB is not identified as a lithologic unit in the ODP Initial Report (Shipboard Scientific Party, 2003; Sites 1244 and 1246). The core section from 96.5 to 114 mbsf at S1252 (Fig. 4) was attributed to lithologic unit L.II in the ODP Leg 204 results because of the presence of several fining upward events and coarser sediments that distinguish it from L.I, (Shipboard Scientific Party, 2003, Site 1252). But the coeval section at S1244, as mapped on the seismic sections (Fig. 6), is characterized by a dramatic decrease in turbidites (Shipboard Scientific Party, 2003, Site 1244), which distinguishes it from Unit L.II. The strata cored between 0 and 77mbsf at S1244 and between 96.5 and 114 mbsf at S1252 is interpreted as one distinct seismic stratigraphic unit (Fig. 4). On the ridge, S.IB consists of dark greenish gray hemipelagic clay and silty clay with a low total biogenic content (<10%) as determined by smear slide analysis, although diatoms are present throughout. At S1246 the clays are diatom-rich silty clay and nannofossil and diatom-bearing silty clay near the base of the unit. Lithologically, the unit is distinguished from S.II by its low content of turbidites. Two depositional models were proposed for the unit based on the lithology: 1- The unit represents a hemipelagic apron laying unconformably on top of southern HR. 2- The absence of turbidites may also be explained by a decrease in slope failure on top of the ridge as the depositional environment changed from active slope basin to

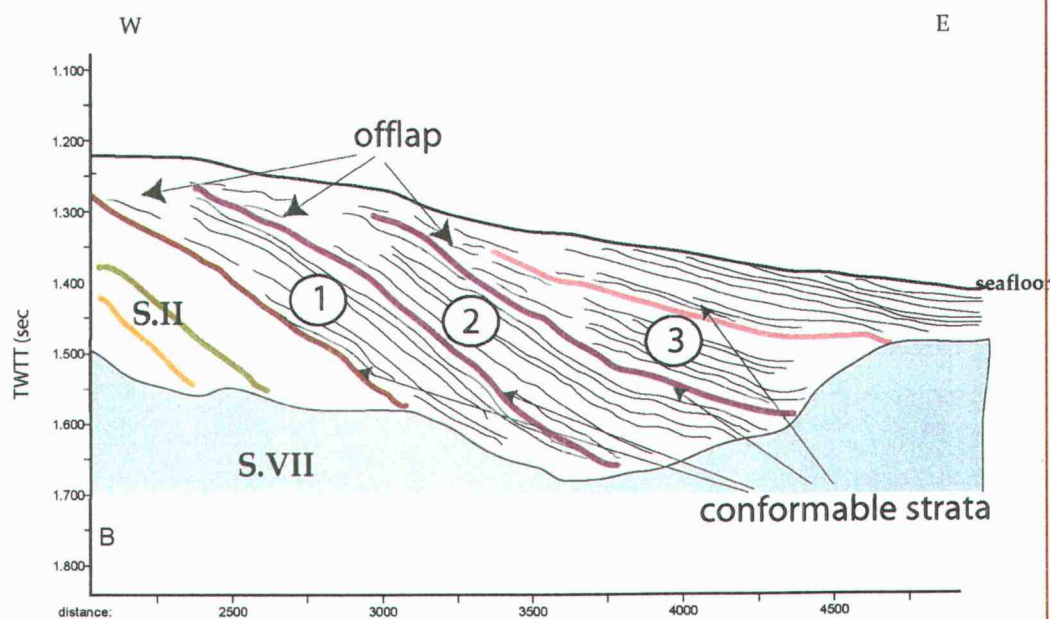
elevated platform due to the uplift (Shipboard Scientific Party, 2003, Site 1246). Low coherency and artifact X (Fig. 18A) on the seismic profile impede the tracing of horizons in the shallow subsurface on top of the main ridge, which limits our understanding of the relation between S.IB and S.II. However in the syncline between the ridge and the basin, lithology of the unit cored at S1252 shows some turbidites and the presence of coarser grains within the minor lithology suggesting the recycled material from older strata, ponded down along the flank of the ridge during its uplift (Fig. 18, 20).

Figure 18: EW section extracted from the 3D seismic volume with AGC A) Close-up from EW line 230 (Fig. 6A) across Unit S.IB. B) Sketch-diagram of the section of Figure 18A. The sequence analysis is presented on Figure 20; location is shown on figure 6A.



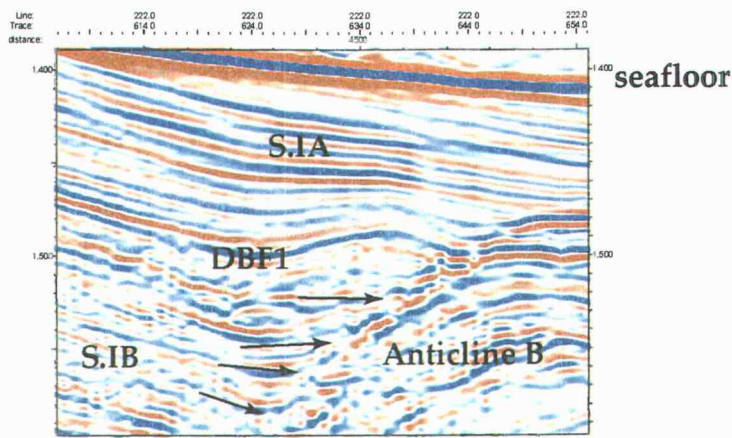
A

Syn-tectonic basin-Fill

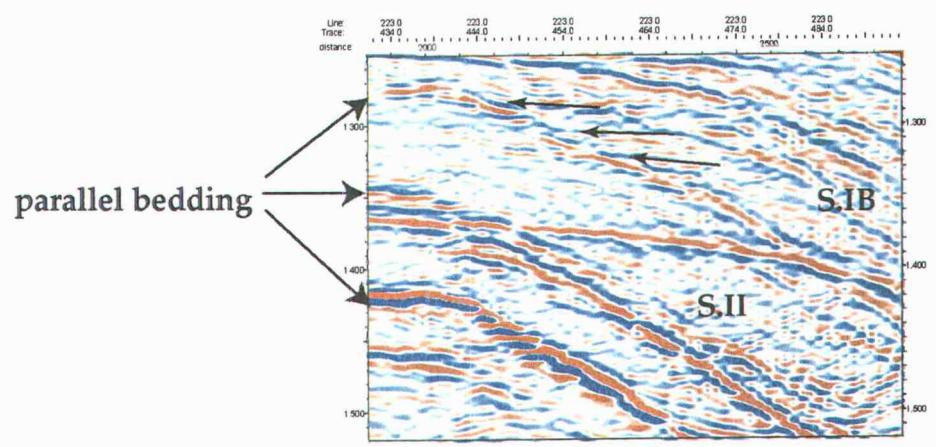


B

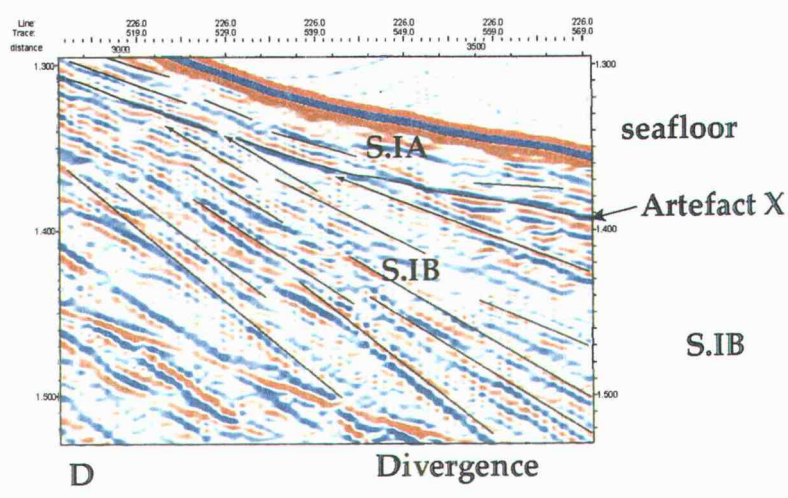
Figure 19: Close-ups from Figure 18A showing examples of sequence boundary details discussed on Figure 5. Black arrows show the onlapping. A) S.IB strata onlap onto anticline B followed in time by the overlap of the anticline by S.IA strata. B) Parallel bedding of S.II strata indicate post-sedimentation bending of the strata. S.IB strata onlap onto the bended S.II strata, indication for post-deformation deposition of the S.IB strata. C) Divergence of the reflections (underline in black on the figure) is evidence for the syn-sedimentary uplift, in this case of the western side of the slope-basin. Reflection X is inferred to be an artifact based on the analysis of the wavelet and its similitude with the seafloor wavelet. However it coincides with a change in dip of the strata. This interpretation imply the termination of the S.IB strata as shown on the figure, suggesting the overlapping of the S.IA strata over the offlapping S.IB strata. (See Fig. 18A for location of Fig19). Depositional sequences are discussed in Figure 20.



A

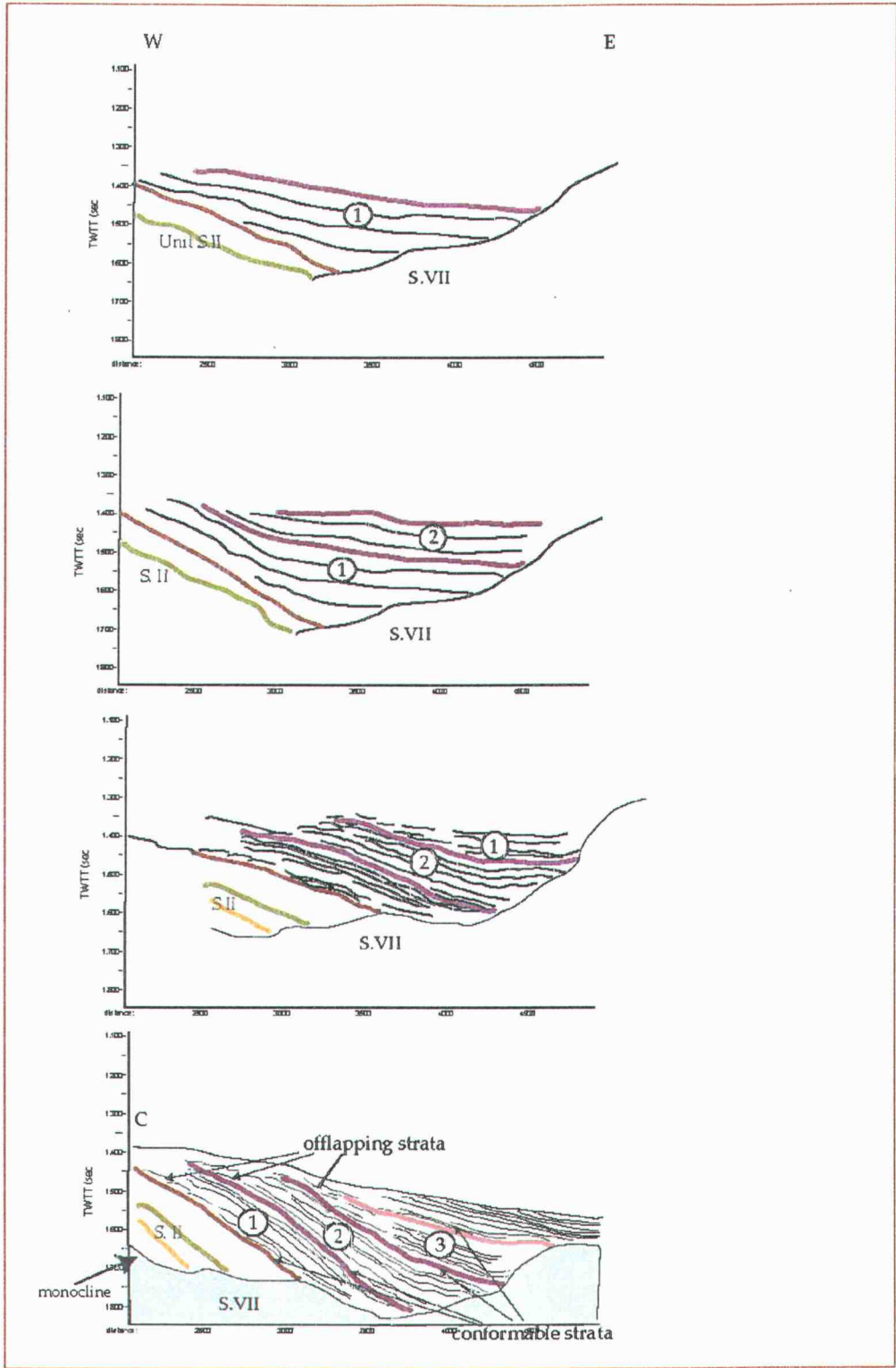


B



D

Figure 20: Sketches showing the deformation of the depositional history of the strata in Fig. 18, S.IB. A) Tilt of the S.II strata forces the migration of the depocenter to the east. The new basin filling creates the new active slope-basin. Offlapping of the strata suggest that, contrary to the deposition of the sequences of Unit S.II, the sediment supply during the deposition of the unit IB strata does not keep-up with the uplift rate. A major uplift event occurred during or at the end of the deposition of sequence #1 material is shed from the resulting high and ponded onto the active slope-basin. Conformable strata to the east show that this basin fill is controlled by the ongoing uplift of its western edge the deformation. B) and C) Continuation of the deformation during the deposition of subsequences #2 and #3. The increase of the dip of the strata with age indicates the progressive migration of the uplift to the east.



The reflections from S.IB are continuous with an increase in dip with time (Fig. 18). The change in dip occurred at discrete interval along each of the angular unconformities (AU) observed (Fig 18, 19). Each AU corresponds to an onlap surface in the upper part (western part) of the group of reflections and its correlative conformity to the east (Fig. 18, 20). They divide the unit into three depositional sequences, each corresponding to one depositional stage as shown on Figure 20. Horizon C represented a low angle tectonic slope-surface after the uplift of the west (Fig. 20A). The uplift probably corresponds to the formation of the monocline observed to deform the strata within S.II (Fig. 6A, 16, 18). The three following stages present similar patterns; strata onlap to the west against a recently uplifted surface. They show a continued ponding of the sediments from the slope into the slope-basin. Each transition between depositional stages 1, 2 and 3 is marked by the uplift of the western part of the depocenter. The strata offlap to the west (Fig. 18, 20), which is in contrast to the S.II strata geometry. Offlapping indicates a decrease in the ratio between sedimentation rate and growth rate that is either a decrease in sedimentation or an increased activity of the ridge.

In summary, sedimentation of S.IB was the result of a gradual degradation of the ridge through continuous slope-failure and/or recycling of the proximal bathymetric highs (fold F, the Dome, anticline B). A minor original dip can be expected prior to the deposition of the unit; however the geometry of these deposition sequences recorded the progressive formation of the monocline that bends the S.II strata.

Deformation patterns observed within Unit S.IB suggest two contrasting stress regimes. 1- The progressively fanning of the strata suggest the relative subsidence of the fold B. 2- The up-turn of the same strata against the buttress unconformity (Fig. 6A) suggests post sedimentary growth of the anticline or simply horizontal

compression. Subsidence through bending caused by horizontal thrust forces may be the answer for this apparent contradiction.

4.3.8 Unit S. IA (0.2 Ma-Holocene)

Unit S.IA represents the youngest seismic stratigraphic unit within the survey. Its lower boundary is defined by the mudflow (DBF1 on Fig. 6 and 17). Strata of Unit S.IA terminate against the angular unconformity U, a prominent erosion surface on top and on the southern flank of anticline B (Shipboard Scientific Party, 2003) (Fig. 6, 9, 21).

Lithologic unit L.I consists of dark greenish gray, diatom-rich to diatom-bearing homogeneous silty clay, locally interbedded with silt to fine sand lenses and mud clast deposits, which are interpreted as turbidites and debris flows, respectively. Unit L.I is divided into four subunits (Sub-units L.IA, L.IB, L.IC, and L.ID Fig. 4) based on the changing abundance of biogenic components and grain size. The uppermost sediments recovered at S1252 contains bands of gray clay and turbidites as observed at S1251. This suggests the continuation of sub-unit L.IA at S1252. Two large-scale lens-shaped sediment packages with chaotic internal reflection patterns and an erosional base (sub-units L.ID and L.IB Fig. 4) are also interbedded within the unit. They are interpreted as two mudflow events (DBF.2 and DBF1 respectively). Reflections of sub-unit L.IA at S1251 are shown onlapping with a small angle on DBF.2 in the seismic cross-sections (Fig. 6A) and they thin to the west (divergence to the east) (Fig. 6). With exception of the internal facies of the two mudflow-deposits, unit S.IA is characterized by continuous, coherent reflections (Fig. 6).

Subunit ID at S1252 corresponds to the older of the two large mudflow deposits, which was not drilled at S1251. The major lithology's mineralogy of Unit L.II is

similar to that of lithostratigraphic Subunit ID (Shipboard Scientific Party, 2003), suggesting a proximal origin for the mudflow. The sediments possibly slumped down the flank of the newly uplifted ridge as the slope failure threshold point was reached. A change in dip within Unit S.IA with time is observed, overlain with upturn of the strata against the main ridge and against anticline B as well as thinning of the same layers against anticline A in the southern part of the main ridge's flank (Fig. 6D). The thinning is less evident to the north (Fig. 6A). We interpret the geometry of the strata as recording the continuation of the compression regime inferred from the seismic stratigraphic analysis of the previous units. The north-south variation of thinning may be related to the presence of anticline A in the south.

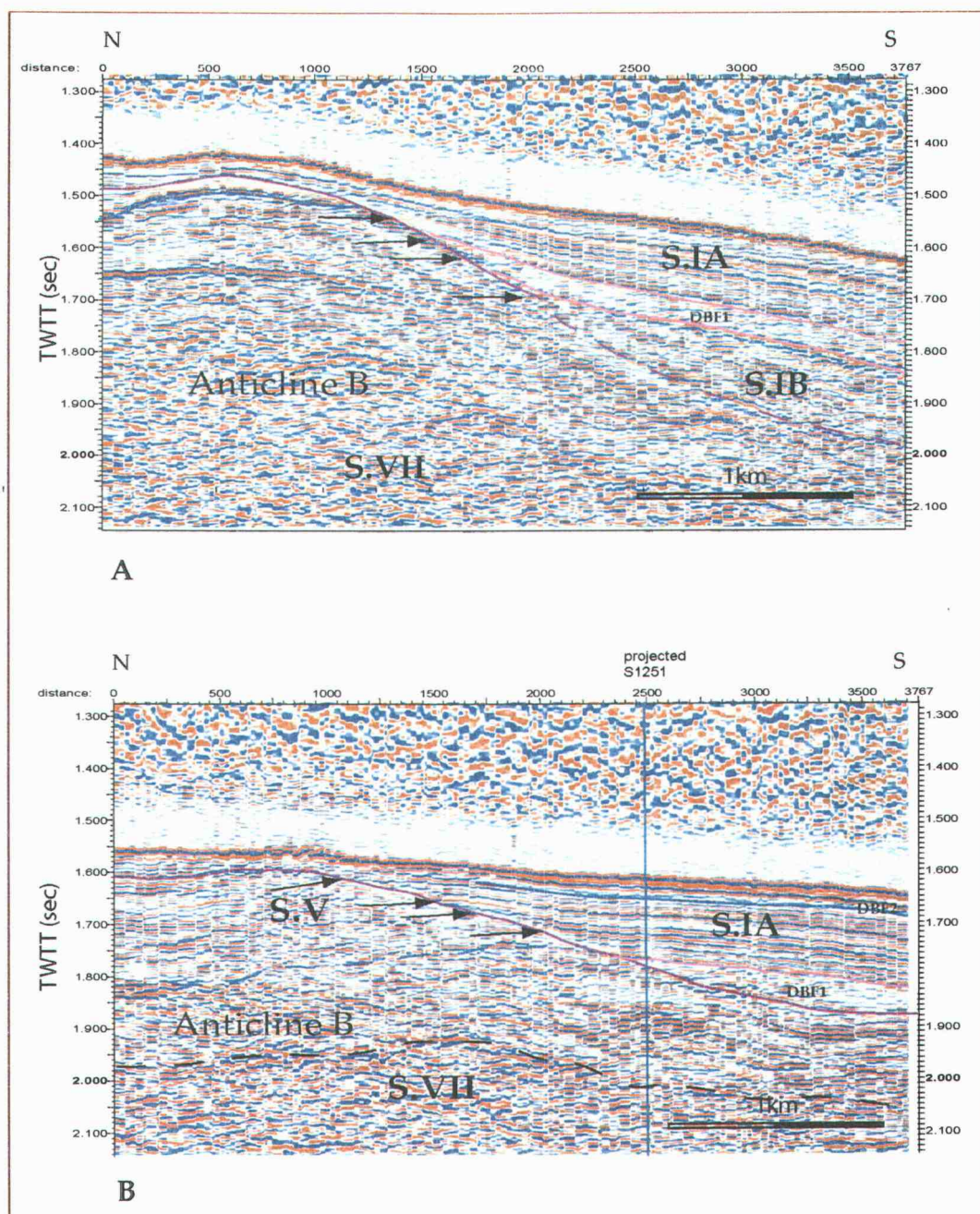


Figure 21: NS section across the eastern basin, extracted from the 3D migrated seismic volume, with AGC A) across the summit of anticline B, B) across the eastern flank of anticline B C) (Location of (A) & (B) are shown on Figure 9).

5. BIOSTRATIGRAPHY

Depositional history of the sedimentary units and evolution of the geological structure can be inferred from the sequence stratigraphic analysis of the seismic data. The ODP biostratigraphic results are a valuable complementary dataset because it provides absolute ages for the sediments and allows timing of the events recorded by these strata. The biostratigraphic ages also help to constrain the time correlation of some the units, for example units S.III and S.II are coeval with S.V, this could not be inferred from the seismic data only. However, confidence in the biostratigraphic ages is dependent on the quality of the bioevents (quantity and quality of the fossils) and on depositional environment (e.g. turbidites). This chapter presents the biostratigraphic ages as shown on Figures 6A & C and discusses the ages of the units described in the previous chapter based on the biostratigraphic results. M. Watanabe confirmed the value of the dates in the deeper stratigraphy at S1244, S.1245 and S.1246, he was less confident on the ages inferred from the shallower fossil events at these same sites (oral and written commun., 2003).

Units S.VII was sampled at the bottom of S1252, S1251 and S1244 and interpreted during the ODP Leg 204 to represent the accreted abyssal plain sediments (Shipboard Scientific Party, 2003). At S1252 and S1251 these strata were assigned to 1.6 Ma and 2 Ma (Fig. 6A & C). Unit S.VII was reached at the bottom of S1244 (Fig. 6A). Two biostratigraphic events suggest an age of 1.6 Ma at 244 mbsf and of 2 Ma at 314 mbsf for these well-lithified claystones.

Unit S.IV was sampled along the NS transect. A fossil event younger than 1.6 Ma was found at S1247. At S1245 biostratigraphic results suggest an age between 1.15 and 1.6 Ma for the whole sequence between seismic horizons A and A'' (Fig.

6). The 343m thick unit at S1245 is coeval with less than 30m at S1251 (Fig. 6C), ~45m at S1252, and ~30 meters at S1244 (Fig. 6A). However, strata of S.VI in the southern part of the survey have not been cored. These are interpreted to be older than S.III and younger than 1.6 Ma. We interpreted the strata of S.VI to be older than S.III based on a conspicuous onlap surface that separates both units locally (Fig. 12A, upper extension of F2). The relation between S.VI strata and S.V strata supports the interpretation. S.V strata are coeval to S.III strata. S.VI built the western flank of anticline B, these strata are clearly older than S.V (Fig. 6A) and hence older than 1.0 Ma (Fig. 6A). The maximum age of S.VI is inferred from the 1.6 time map interpreted on 2D line NS3 (Fig. 7).

Unit S.V was sampled at S1251, the strata were assigned an ages between 0.3Ma and 1.0 Ma old. This age corresponds to the age of S.III and S.II strata. No arguments could be found to divide this seismic unit as are units S.III and S.II.

Ages of the S.III strata are inferred to be between 1.15 and 0.5 Ma from the cores retrieved at the four sites along the NS transect (S1250, S1248, S1247 and S1245). However, Unit S.II at S1244 is assigned an age between 1.0 to 0.5 Ma at S1244. These ages are considered as confident by the micro-paleontologist (M. Watanabe, 2003, oral communication), which restrain the age of S.III strata to between 1.15 and 1.0 Ma. This is also the age of the lower part of S.V strata on the eastern limb of anticline B.

Unit S.II includes the two marker horizons B and B' these were cored at S1244 and S1246. At S1244, the upper 91.13 mbsf (above horizon C on Fig. 6) are dated less than 0.3 Ma based on a diatom event and less than 0.46 Ma old based on the nannofossil found. Because diatoms are common to abundant in the upper 120 mbsf, while nannofossils are barren or of trace abundance in the whole length of the core, and because no seismic evidences for hiatus or erosion can be observed in the 100 mbsf region around S1244 to explain the juxtaposition of these two ages, it

seems likely that reworking of the sediments explains the presence of *P.Lacunosa* (0.46 Ma) at this shallow depth, which is why the 0.5 Ma event was not located on Figure 6A. At S1246, two fossil events suggesting 0.3 Ma old strata are observed, one at 22 mbsf and one at 80 mbsf. It is simple to explain the presence of older fauna at shallow depth by reworking of sediments in particular since the upper sample was taken within a turbidity event. Considering the 0.3 Ma old deeper sample, we infer an age of 0.3 Ma for horizon B. At S1244, a nannofossil middle Pleistocene acme zone (1.0 Ma) can be identified at 200 mbsf with good confidence and be supported by the siliceous fauna. Diatoms and nannofossils found between 230 and 240 mbsf (1.6 Ma in age) are likely to be part of reworked sediments because this interval is noted for a high concentration of turbidites. This leads to the age between 1.0 and 0.3 Ma for Unit S.II. (Fig. 6). Correlation of the ages between S1244 and S1246 suggest a major hiatus between 0.5 and 1.0 Ma followed by a drastic increase in sedimentation rate 0.3 Ma. This leads to an age of 1.0 Ma for horizon B' while horizon B is 0.3 Ma old. The lower boundary of unit S.II was merged with the 1.0 Ma time line that is parallel to B'. Western extension of seismic reflections above horizon B' are onlapping onto horizon Y to the west, which, considering the ages inferred above, imply 1.0 to 0.5 Ma old strata onlapping onto a 0.5 Ma old surface (horizon Y). In addition extension to the east of the 1.0 Ma event cored at S1245 and the geometry of Horizon B' (also 1.0 Ma) suggest the duplexing of the S.III strata (Fig. 6A). We propose a seaward vergent thrust fault that disrupts S.III strata causing their duplexing between S1245 and S1246, under the southern HR summit (Fig. 6A). This 2nd order thrust accommodated the shortening during the uplift of the central region (see structure section).

Two fossil events date Unit S.IB older than 0.3 Ma at S1252, but these were found within the mudflow DBF1 and hence are likely to come from the recycled sediments. Instead seismic stratigraphic correlation with S1244 suggest an age of

0.3 Ma and younger for Unit S.IB and younger than 0.2 Ma for Unit SIA. Within the basin, a change in color within the clay similar to the one found at S1251 and S1252 is regionally identified throughout the central Cascadia margin and is typically interpreted as the transition from Pleistocene to Holocene sedimentation (1.1 Ka) (Shipboard Scientific Party, 2003).

6. STRUCTURAL GEOLOGY

6.1 Regional structures

Regional structures surrounding Hydrate Ridge (HR) are largely controlled by the subduction style and rate of the Juan de Fuca Plate beneath the North America plate. The Astoria fan does not only supply most of the sediments composing HR today, it also plays a major role in the structural geometries of the region. The high sedimentation rates within the fan lower the friction at the decollement, which is responsible for the dual thrusting regime observed along the deformation front of Oregon and Washington (MacKay et al, 1992, Mac Kay, 1995). Hydrate Ridge is located landward from the southern end of the fan which is why it is located at the transition zone between the two different thrusting regimes (Fig. 2).

The frontal thrust-faults are offset by left-lateral strike-slip faulting on the Oregon continental margin (Goldfinger et al., 1996). These strike-slip faults accommodate the oblique component of the Cascadia subduction zone (Fig. 1). Two of these left-lateral strike-slip faults, Daisy Bank Fault and Alvin Canyon Fault bound Hydrate Ridge to the north and to the south, respectively (Goldfinger et al., 1996). They may cause HR to act as an independent block rotating clockwise between the two strike-slip faults (J. Johnson, oral commun., 2003).

6.2 Structures on southern Hydrate Ridge

The bathymetry of southern HR is controlled by deep subsurface structures identified in the seismic sections (Fig. 8). While these structures were mentioned in the description of seismic units sections, we present their major features in this chapter. Further analysis on the nature of the strain expressed by these features

will be discussed in the tectonic evolution chapter in conjunction with the restored cross-sections presented on Figures 22 and 23. The southern summit of the ridge coincides with a dome-shaped feature that affects unit S.VI best seen on the time map of horizon K (Fig. 8A). Two buried elongated bathymetric elevation, named anticlines A and B (Fig. 8B) are also still an expression on the bathymetry. Anticline A corresponds to a secondary bulge on the eastern flank of the dome, anticline B corresponds to a complex fold buried in the adjacent basin (Fig. 6A). The crestal line of the current ridge coincides with the hinge line of a secondary fold that deforms younger slope-basin sediments (S.II). Further west, a NS-striking fold can be mapped, buried under the western flank of the ridge, which we call fold F (Fig. 6, 11). Stratigraphic and structural analysis of younger slope-basin sediments provides insight on the most recent activities and evolution of these deeper features. The structural features are present in order of their formation time.

6.2.1 Anticline B

Anticline B (Fig. 6, 8) is interpreted as a buried thrust related fold, formed at the deformation front east of the fold F. Internal facies are chaotic and indicate a high degree of tectonic activity. Anticline B is a prominent buried anticline on the northern EW sections (Fig. 6A, B), but vanishes to the south (Fig. 6C, D). Progressive fanning of the strata on the eastern side of the feature suggests that the major growth period of the feature occurred during the deposition of S.V (1.0 to 0.3 Ma). However, the geometry of the angular unconformities within S.VII suggests that the fold formed prior to 2 Ma (see Fig. 6, 22). This old age is also supported by the geometry of S.VI strata (1.6 - 1.0 Ma), which pinch-out against the anticline B.

Anticline B is bounded by a sharp buttress unconformity U (Trehu et al., 2003a) (Fig. 6, 9, 21). The slope-basin strata downlap onto the feature, providing evidence

that anticline B represented a bathymetric high at least 0.2 Ma ago (minimum age of Unit S.IB). The progressive tilt and bending of Unit S.II, and S.IB strata and onlap of these onto the flanks of anticline B suggest progressive subsidence of the feature relative to the main ridge and eventual burying by Unit S.IA since ~0.2 Ma. The configuration of Unit S.IA strata also suggests activity of the anticline in the same period of time. This may be explained by the ongoing EW compression regime inferred from the multiple tectonic events throughout the history of the ridge.

6.2.2 Dome

Mid to late Pleistocene slope-basin strata onlap onto a dome-shaped feature, which is delineated by horizon K (Fig. 8A). Anticline A is a bulge on the eastern flank of the Dome. Its distinct NS elongated summit can best be seen on a time map of horizon K (Fig. 8A). The shapes of the Dome and of anticline A control the extension to the east of S.III strata (Fig. 15A), of S.II (Fig. 15B) and of S.IB (Fig. 15C). Both the Dome and the anticline A are defined by the onlapping of the overlaying strata against the paleo-relief. Extension of Unit S.IB in particular follows the shape of anticline A (Fig. 8 & 15C). But the existence of the relief between 1.15 and 1.0 Ma as presented on Fig. 22 is inferred from the pinching-out of S.III strata to the east. This interpretation is supported by the restored cross section of EW line 300, on which anticline A was interpreted as a relief based on the termination of the S.II strata and on the folded shape of the reflections that build the anticline (Fig. 6C; 6000 – 7500 m, 1.34 – 1.9 sec). The Dome's formation occurred prior to 1.0 Ma (age of S.III). Deeper strata are too deformed to reconstruct the evolution of the dome itself.

6.2.3 Fold F

The most prominent fault-related-fold (fold F) deforms Unit S.IV and controls the geometry of S.III strata in the western region of the survey (Fig. 6). The fold is a NNE striking, doubly plunging fold. The seismic survey encompass only its northern half, which is plunging by ~3 degrees.

The interpretation of the fold as a thrust-fault-related fold is based on: 1-The reconstruction of the fold's evolution inferred from the geometry of the strata, which suggests a thrust fold in the hanging wall and the foreland basin in the footwall of fault F1. This model explains the depocenter forming east of the fold. 2-The similarities between the tectonic structures observed at southern HR and their similarities with the imbricated trust faults studied by Flueh et al. (1998) on the accretionary prism offshore Washington. 3-The tectonic setting of southern HR; imbricated thrust faults are one of the mechanisms common on accretionary prism to accommodate the shortening concomitant to the subduction (Seely et al, 1974).

Two splays F1 and F2 of the deeper-rooted thrust fault system could be mapped. F1 was inferred from the small interlimb angle of fold F (Fig. 6). F2 is a conspicuous termination surface is good to map in the deeper stratigraphy in the north (Fig. 6A) and in the lower stratigraphy in the south (Fig. 12). It is interpreted as a thrust fault based on its geometry and its position relative to fold F. It disrupts younger strata than does F1 suggesting more recent activity than F1. However, no offset could be clearly defined neither from the seismic data despite its conspicuous seismic image nor from the biostratigraphy (see Biostratigraphy chapt.). No significant changes in velocity between S1244 and S1245 were measured that could account for distortion of the profiles due to velocity effects.

6.2.4 Syn- and post deformation recorded within S.II strata; uplift of southern HR

Contours on the time map of horizon B (Fig. 16) show an anticline plunging to the NNE. The fold is slightly asymmetrical, with the northeast limb dipping more steeply than the western limb. Note that the hinge line of the fold corresponds to the current summit of southern HR (Fig. 8A & 16), but more important it also parallels the strike of F2 (Fig. 11), which suggests a correlation between the more recent activities of fold F and the folding of S.II strata. The eastern limb of the fold is more prominent and is disrupted by NS-striking normal faults (Fig. 6A, 16). Discrete stepwise thickening of the interval between the stratigraphic horizon B, B' and C along the faults were interpreted as evidence for growth strata which imply syn-sedimentary faulting (Fig. 17). The NS striking normal accompanied the folding, which is interpreted as a fault-bend folds that formed concomitant to a seaward vergent reverse fault. The thrust fault is inferred from the duplexing of S.III strata (Biostratigraphy chapt.).

The S.II strata are also deformed by a post-sedimentary monocline. (Fig. 6A & B, 16), which partly affected S.IB strata. The monocline maybe a drape fold that is the surface expression of a buried seaward vergent normal fault that accommodate the subsidence of the basin relative to the ridge. Alternatively it may be the surface expression of a blind landward vergent reverse fault, not mapable because of the low coherency within Unit S.VI.

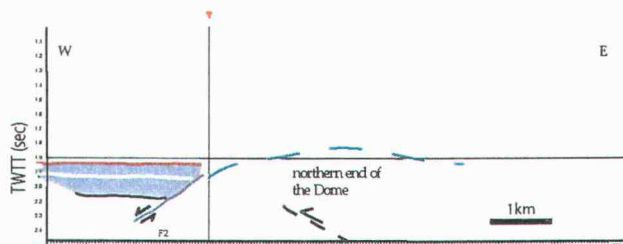
6.2.7 Fault system E

The normal fault system E accommodates the subsidence of the eastern basin relative to the southern HR. Two fault-splays are shown on Figures 6C and D, they strike NS. The offsets of the faults average around 0.2 sec and sum up to a total

offset of 0.5 sec (~387 m) that disrupts S.VI strata in the southern part of the survey. The offset decreases to zero to the north. This NS variation correlates with the uplift style of the ridge. In the south, early-Pleistocene strata are being uplifted a few hundreds of meters (387 m) over just about 1km horizontally along the faults E. While north of southern HR culmination, the younger strata are not disrupted (Fig. 18A), They geometry suggest syn-deformation sedimentation gradually compensating the tilt of the slope (Fig.20). The uplift is inferred to have occurred most recently, that is during the deposition of S.IB, less than 0.3 Ma. These strata were not disrupted by the faults, which is explained by syn-faulting sedimentation filling the offset.

Figure 22: Sequence of structural evolutionary cross-sections of EW line 230 (Fig. 6A). The section is located in the north of the survey; it runs across the young slope basin deposits. Retro-deformation of the strata to their original geometry was achieved using rule of constant length and surface and the help of vertical and horizontal pine lines as reference (marked by a black lines and red nail).

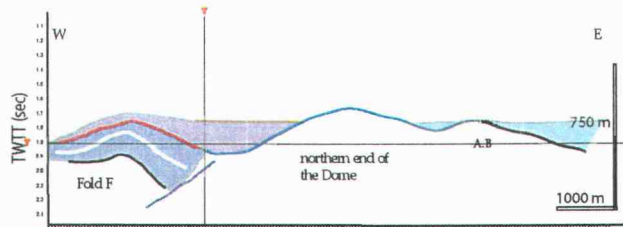
Before 1.6 Ma



Tectonic Model:

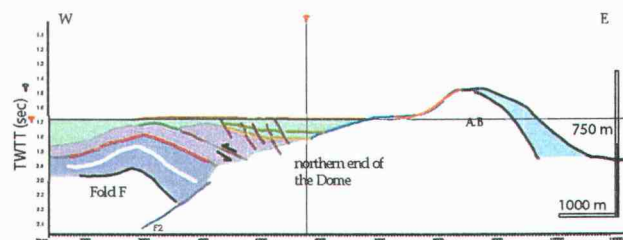
- Uplift of the dome as the surface expression of seaward vergent faulting at the deformation front. The uplift causes the relative subsidence of the strata west of the dome along normal fault F2.

Depositional setting for horizon B' = 1.0 Ma



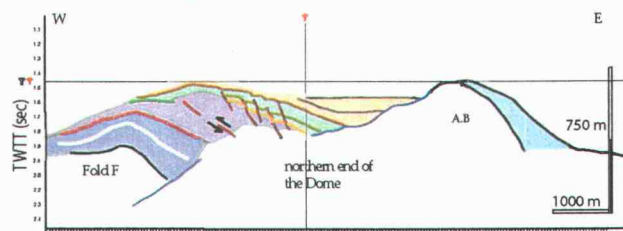
- Incipient accretion; compression intensified at the deformation front causing the formation of the landward-vergent thrust-faults-related folds A.B and F.

Depositional setting for horizon C = 0.3 Ma



- Shortening and uplift of the current ridge. Incipient phase of a 2nd order seaward vergent fault disrupting S.III strata
- Growth of A.B. A.A is present in the south as a bulge, on the eastern flank of the Dome, which get buried by S.II.

Depositional setting for horizon D = 0.2 Ma



- Relative subsidence of the eastern basin causes burying of A.B. The relative subsidence is accommodated in the south, by normal fault system E, that disrupt the deeper stratigraphy.
- Formation of the current ridge crest. Normal faulting within S.II accompanied the active 2nd order seaward vergent fault within S.III

Present time

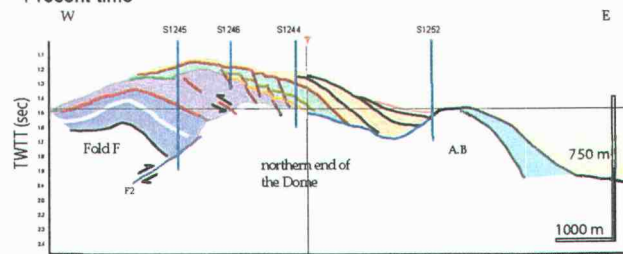


Figure 23: Sequence of structural evolutionary cross-sections of EW line 300 (Fig. 6A). The section crosses the summit of southern HR, which encompasses the Dome and the shallowest region of fold F. Both restored cross sections, EW230 and 300 were chosen to cross as many ODP sites as possible in order to have a maximal time constrain for the reconstruction. Retro-deformation of the strata to their original geometry was achieved using rule of constant length and surface and the help of vertical and horizontal pine lines as reference (marked by a black lines and red nail). (anticline A = A.A; anticline B = A.B).

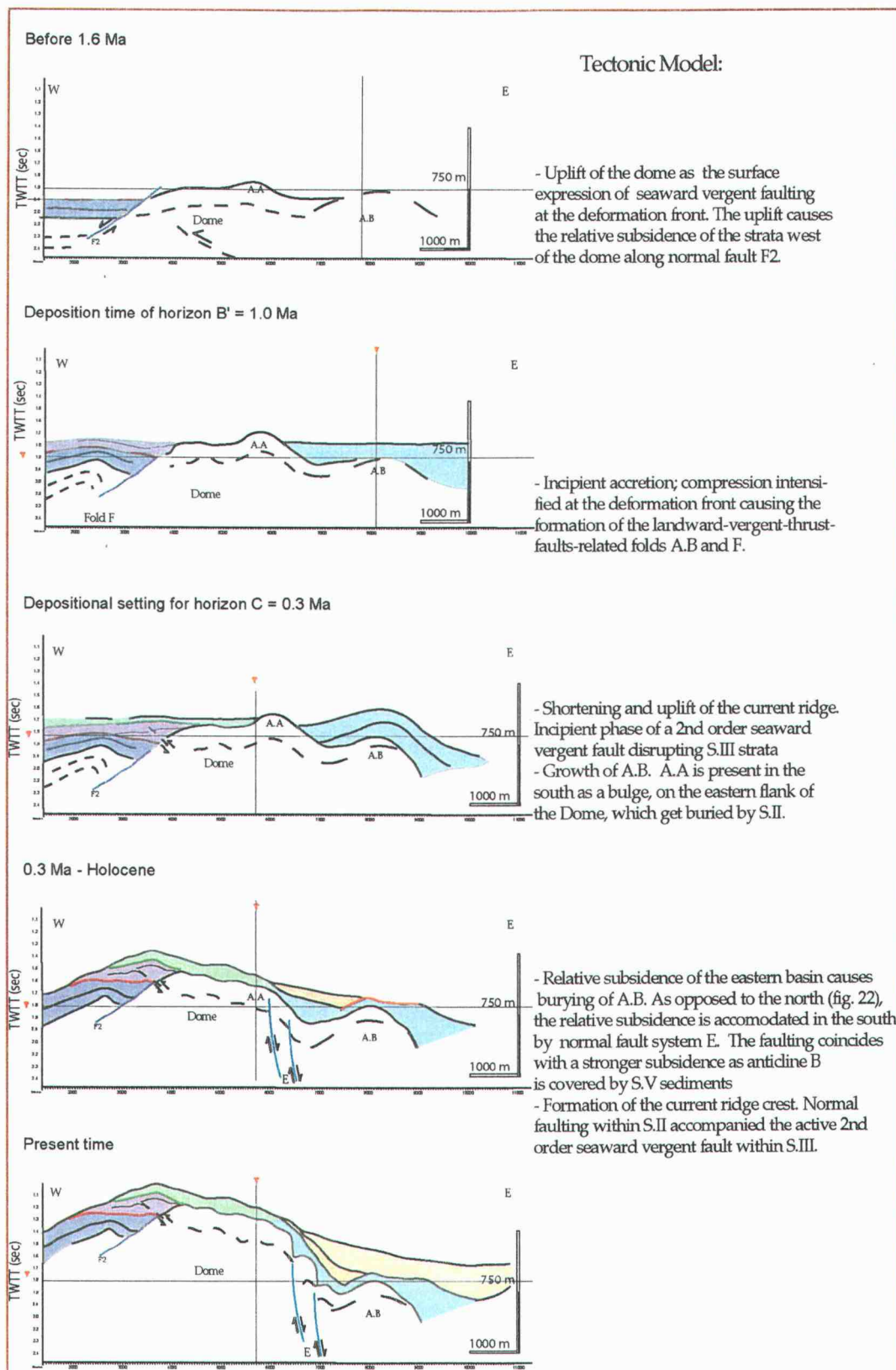
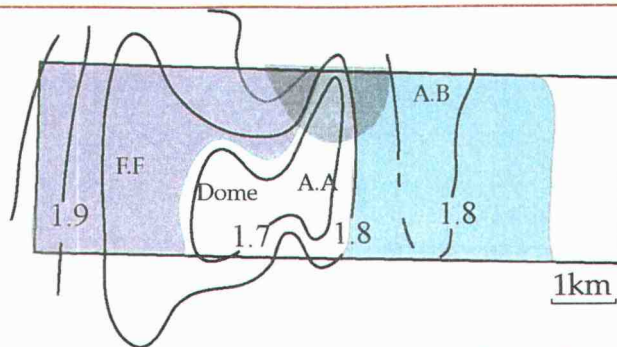
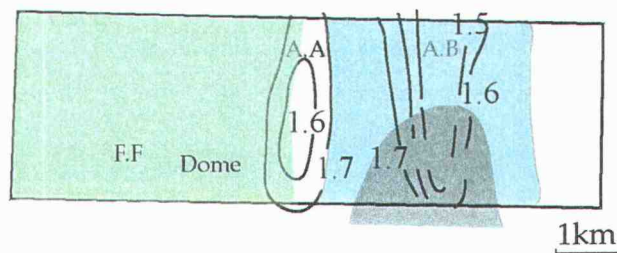


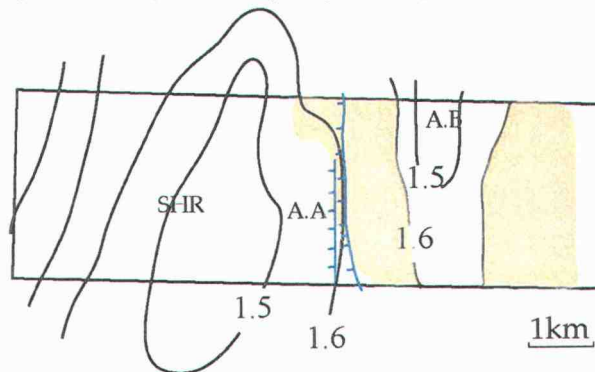
Figure 24: Four successive paleo-bathymetric maps constructed based on the structural evolutionary sections presented on Figure 22 and 23. Bathymetric highs and lows of the maps can be inferred from the named structural features: fold F (F.F); the Dome; anticline A (A.A); anticline B (A.B), southern HR (SHR). The colors represent the depocenters for each unit. Gray shaded areas corresponds to two speculated slope-failure-events-surfaces discussed in chapter 7. (See appendix A for the legend).



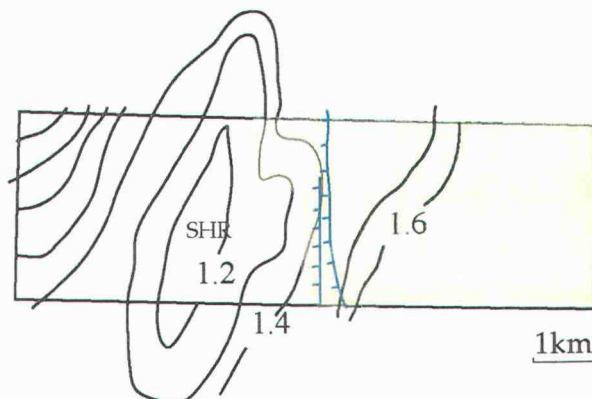
A S.III (1.15 - 1.0 Ma) Paleo-bathymetry time map; Contour Interval: 0.1 sec



B S.II (1.0 - 0.3 Ma) Paleo-bathymetry time map; Contour Interval: 0.1 sec



C S.IB (0.3 - 0.2 Ma) Paleo-bathymetry time map; Contour Interval: 0.1 sec



D S.IA (0.2 Ma - Holocene) Bathymetry time map; Contour Interval: 0.1 sec

7. TECTONIC HISTORY OF SOUTHERN HYDRATE RIDGE

The depositional and structural history presented in this section results from the compilation of the seismic sequence stratigraphy, the ODP biostratigraphy and the structural observations presented in the previous chapters. The results were summarized and completed into a time-series of cross-sections (Fig. 22 and 23). Structural restoration of southern HR was achieved by sequential removal of the effects of deformation. Initially the horizon to be flattened was backstripped and the remaining strata modified for the effects of post-sedimentary deformations. Fault displacements were removed and then folding deformation was removed by unfolding the particular horizon to horizontal. Because the goal was to obtain a first step approximation of the evolution of southern HR, plane strain could be assumed, allowing application of the constant bed length and the constant area rules. Some unit boundaries had to be approximated for they are poorly constrained by the data. Horizontal original bedding was assumed. We also interpreted the absence of deposition sequences as evidence for paleo-bathymetric highs that either impeded the deposition or caused slope failure events. The construction of the structural evolutionary cross-sections was performed on two EW present-day sections: EW line 230 (Fig. 22) and EW line 300 (Fig. 23). These sections cut across most of the ODP sites and hence contain a maximum of the absolute time constraint. EW line 230 represents the northern part of the survey area where the slope-basins S.III, S.II and S.IB are prominent and provide detailed information on the late-Pleistocene geology. EW line 300 presents a profile across the shallowest part of fold F and across the Dome. It includes Unit S.VI and VII and provides better resolution for the tectonic reconstruction of the early-Pleistocene events. Comparison of both sections illustrates the important NS stratigraphic variations within the survey area.

7.1 Early Pleistocene; 1.6 - 1.15 Ma

Early Pleistocene sediments cored at southern HR correspond to deep-sea Astoria fan abyssal plain sediments (see Geological setting) accreted onto the accretionary complex offshore Oregon (Units S.VII, S.VI, S.V, S.IV see Appendix C). High syn- or post-sedimentary deformation appears to have destroyed most of the original structures of these strata (S.VII). The oldest deformation event clearly recorded by the strata is within unit S.IV and is the growth of the thrust-related-fold F (Fig. 6, 11). Evolution of fold F started in the time between the deposition of horizons A' and A, which, based on the biostratigraphy, corresponds to 1.15 Ma (Fig. 10). The folding most likely occurred at the deposition front. The hinge line of fold F strikes NS, suggesting an EW strain, which supports the model (Fig. 11). Strata coeval to S.IV are not cored at S1244 (Fig. 6A, 7). But unit S.VI was assigned to between 1.6 and 1.0 Ma based on seismic interpretation shown on Figures 7 and 12. These early-Pleistocene strata pinch-out against anticline B (Fig. 6C, 23), which implies that anticline B formed a relief prior to 1.6 Ma, prior to fold F. This interpretation is supported by angular unconformities interpreted as suggesting tectonic activity of anticline B more than 1.6 Ma, prior or during the early Pleistocene. In addition, thick series of glauconite-rich sand layers, retrieved at S1252 and S1251 within S.VII suggest a relatively long period of quiescence (Leeder, 1999) expected, for example on top of an anticline and support the model of anticline A being older than fold F.

The dome is a dome-shaped feature observed on the time map of horizon K (Fig. 8A). Its origin is not resolvable; it would require among others a better resolution of the deeper stratigraphy. Timing of the formation of the feature is little constrained. Wavy to chaotic seismic facies of S.VI suggest the strata were subject to intense syn- and/or post-deposition deformations prior to 1.0 Ma but they do not provide any information on the type of deformation (Fig. 6, 7). Joel Johnson

(2003, oral commun.) proposes the dome to be the remnant of a seaward-vergent-thrust related fold preceding the landward-vergent-thrust-related fold F. This model would explain the presence of early Pleistocene to Pliocene strata in the footwall of the younger (1.2 Ma) fold F (Fig. 6A). However, uplift of the region during the middle Pleistocene is recorded in the upturn of the S.II strata that are onlapping onto the dome (Fig. 7).

7.2 early to middle Pleistocene; 1.15 – 0.3 Ma

Fault-bend fold F was active during the deposition of Unit S.III. This is evidenced by the divergence of the strata on the flanks of the fold (Fig. 6). S.III strata were interpreted as onlapping onto the upper extension of F2 (Fig. 12). Hence three paleo-bathymetric-highs can be inferred to have controlled the extension of S.III strata; fold F to the west (Fig. 6), the Dome to the south (Fig. 8A) and anticline A to the east (Fig. 22 and 23). A similar relief (same highs) controlled the extension of unit S.II (Fig. 15B). (Fig. 22 and 23). Anticline A is located on EW lines from Figure 6, and is mapped on Figure 8 as a secondary bulge on the eastern flank of the Dome. But this paleo-high was strongly deformed and disrupted during the uplift of the current southern HR and is barely recognizable today. Sequential retro-deformation of the structure was achieved by looking at the termination of S.III (Fig.12) and S.II (Fig. 6A) against it (Fig. 22, 1.0 and 0.3 Ma). It is a secondary bulge on the eastern flank of the Dome and appears as a bathymetric high between 1.0 and 0.3 Ma on the structural restored cross sections of EW line 300 (Fig. 23) and EW line 230 (Fig. 22). The sediments of S.III and S.II are very similar to abyssal plain sediments in their lithologic composition and grain size and frequent turbidity deposits were observed within the strata. Because of the tectonic setting, decoupled from the Astoria fan, these sediments must be recycled abyssal plain sediments. In other words, they were shed from the top of the anticlines, which newly formed concomitant to the

ongoing accretion of the abyssal plain sediments. This material was then ponded into the adjacent slope basin, in this case the basin constrained by fold F, the Dome and anticline A (Fig. 24 1.0, note that at the end of deposition of S.II strata, fold F was covered and did not appear as a bathymetric high anymore, Fig. 24, 0.3 Ma).

The onlapping of S.III strata onto F2 (Fig. 12A) imply an older age than 1.0 Ma for S.VI strata and the absence of strata coeval to S.III deposits in the central region of the survey. This is accounted for by the presence of anticline A in the restoration of the original geometries as discussed in the section above (Fig. 22 and 23). However, based on the biostratigraphic ages, S.V strata in the current basin on the eastern flank of anticline B are coeval to S.III and S.II. These strata are divergent as the result of the syn-sedimentary activity of anticline B. Unit S.V strata lay unconformable onto S.VII strata with a very small angle (Fig. 6) suggesting a relatively low relief of anticline B 1.0 Ma. This implies that the major uplift of anticline B occurred during deposition of S.V, between 1.0 and 0.3 Ma (Fig. 22 and 23).

Today, the western flank of anticline B consists of S.VI (1.6 to 1.0 Ma) (Fig. 6C, D). The absence of S.V-coeval strata on the western side of anticline B suggests either a continuous high between anticline A and anticline B that did not provide any accommodation space for sediment deposition in this region or an erosion event as proposed on Figure 22 and 24, between 1.0 and 0.3 Ma (red line Fig. 22, 0.3 Ma, gray shade on Fig. 24). The occurrence of a slope failure during the middle Pleistocene along horizon K on the northern flank of the Dome/anticline A would also explain the sudden truncation of S.VI strata to the north as observed on 2D line NS3 (Fig. 7).

Unit S.II shows a migration to the east of the depocenter relative to Unit S.III. As discussed above, the unit's extension is still controlled by fold F, the Dome and

anticline A (Fig. 22 and 23). The eastward migration of the depocenter is due to the uplift of its western edge. In the mean time, a 2nd order fold (1km wide) which strikes NNE, strictly parallel to F2 (Fig. 11) deforms the S.II strata beneath the current crest of southern HR (Fig. 16). A seaward-vergent thrust fault is inferred from the fold and the duplexing of the S.III strata inferred from the biostratigraphy (see Biostratigraphy chapter) (Fig. 22 and 23). The thrusting and folding is accompanied by syn-sedimentary normal faulting beneath the crest (Fig. 16, 17), which provides a time constrain for the deformations to the middle Pleistocene (deposition period of S.II). The strike of the fold is parallel to the strike of the fault F2. F2 appears as the younger of the two blind splay of thrust fault system F (see Structure chapter, Fig. 12). This correlation suggests that the deformations observed within S.II are related to the thrust system F. It also suggest a clockwise rotation of the maximal strain axes from EW (Hinge line of fold F, Fig. 11A) to WNW Hinge line of the fold within the slope-basin strata S.II, Fig. 16)

S.V strata are truncated at the erosion surface U (Fig. 21A & B). The strata are assigned to less than 0.3 Ma based on the biostratigraphic results at S1251 (Fig. 6C), which hence is the maximum age for the erosion event U. Unconformity U can be mapped on the seismic sections in the southern flank of anticline B (Fig. 9). The erosion event capped the anticline between traces 600 and 800 (Fig. 6, 9). Because the north erosion surface is currently dipping to the south, and there is no indication for a tilt of the strata to the south, we suggest that the event U correspond to a slope failure along the southern flank of anticline B that truncated S.V strata (Fig. 23, 24). This event possibly occurred during the culmination of the uplift of anticline B, which we infer to have grown between 1.0 and 0.3 Ma from geometry of unit S.V (see red line in Fig. 22 and 23 and gray shade on Fig. 24).

In summary, early to middle Pleistocene strata S.III and S.II correspond to a period of intense tectonic activity. They recorded the growth of both thrust

anticlines; fold F and anticline B (Fig. 22 & 23). Two gravity driven slope failure events were inferred to have occurred at the culmination times of the uplift of anticline A and of anticline B respectively (Fig. 24). Additionally, the depositional patterns of the strata were influenced by a bathymetric high in the southern part of the survey (Fig. 15, 24). At that time, the current southern HR was not formed yet. Unit's S.VII, VI, IV strata are interpreted as abyssal plain sediments (Appendix B, see Seismic Sequence Stratigraphy chapter). Unit S.III and S.II lithology is very similar to the one from abyssal plain deposits, but the depositional setting of the S.III and S.II was decoupled from the Astoria fan source as discussed above (Fig. 22 and 23). Hence, the deposits consist of recycled abyssal plain sediments coming from the surrounding bathymetric highs.

7.3 Middle Pleistocene - 0.3 - 0.2 Ma

Unit S.IB strata recorded the uplift of the current southern HR during the middle to late Pleistocene (Fig 18, 19 and 20). Bending of the S.II strata accommodated the uplift of the current ridge, which formed a monocline (Fig. 6, 22, 0.2 Ma). In the south, offsets along splays of fault system E can be observed disrupting the deeper stratigraphy (S.VI strata) in the transition zone between the ridge and the basin to accommodate the uplift (blue on Fig. 6C & D, Fig. 23). Offlapping of the S.IB strata (Fig. 18) shows an increase in uplift rate versus sedimentation rate (Fig. 5), which coincide with the uplift period of the current ridge to the west of the unit S.IB. Within the same strata, the increased importance of the pelagic sediments with time is observed (appendix B). This is interpreted as the result of the decoupling of the slope-basins from the Astoria Fan concomitant to the accretion and the progressive mixing of pelagic components out of the water column. The decoupling was already inferred from the geometry of units S.III and S.II (see paragraph above).

7.4 Late Pleistocene –Holocene - 0.2-present

Onlap-geometry of the S.IA strata (Fig. 6) implies that the anticline B represented a bathymetric high prior to the deposition of the unit. Anticline B represented a prominent bathymetric high within the current adjacent basin in two separate depocenters until very recently (less than 0.3 Ma), before being buried by S.IA sequences (Fig. 6, 24D). Increase in dip of the layers with time and the two mudflow deposits (DBF1 and DBF2 on Fig. 4, 6 and appendix B), as well as the thinning of the beds against the flanks of the main anticline, are evidences for the ongoing relative subsidence of the basin during the deposition of S.IA, probably corresponding to the continuation of the uplift of the current ridge recorded within S.IB strata (see section above). In addition, contemporaneous thinning and upturn of the strata against anticline B suggest ongoing of the compression recorded in the older deposits of the region.

7.5 Summary

The succession of deformation events, as reconstructed for the early Pleistocene strata at southern HR (units S.VII, S.VI, S.V, S.IV) begins with thrusting and folding of Astoria deep-sea fan deposits at the deformation front as the strata were accreted to the accretionary complex. The Dome is speculated to result from a seaward-vergent thrust fault. It probably preceded anticline B and the landward-vergent-thrust-bend fold; fold F. Even so, anticline B started forming prior to fold F, the major activity period of both anticlines occurred between 1.2 and 0.3 Ma. In other words, the anticlines grew continuously as accretion was going on. Early to middle Pleistocene strata (units S.III, S.V and S.II) consists of recycled abyssal plain sediments shed from the bathymetric-highs and ponded into the depocenters. The depocenters are the slope-basins that resulted from the folding of the abyssal plain strata into several anticlines mentioned just above. Compression of the strata

was still ongoing; during the sedimentation within the slope-basins a seaward vergent thrust disrupted and folded the slope-basins to accommodate the shortening. The hinge line of the fold and the strike of the older, landward thrust fault suggest a connection between fold F and the fold deforming the slope-basin sediments. Middle to late Pleistocene strata (unit S.IB and S.IA) record the beginning of the uplift of what is today southern HR. The relative uplift is accommodated by normal-faulting in the south, but upturn of the younger most slope-basin strata against the ridge suggest the continuation of the EW compression regime. The gradual increase in pelagic content with time within the younger slope-basin sediments corresponds to the decoupling of the depocenters from the Astoria fan and the increased importance of pelagic sedimentation on top of the accretionary complex.

8 IMPACT OF THE STRATIGRAPHY ON GAS HYDRATES AND FLUID FLOW

8.1 Effects of tectonic uplift on gas hydrates

Gas hydrates probably initially formed at the deformation front when abyssal plain sediments began to be uplifted because the decrease in pressure associated with tectonic uplift of the sediments caused a decrease in the solubility of methane dissolved within the pore fluid. The gas hydrates may have begun to form as early as 1.6 Ma within anticline B and/or within the Dome. Later formation of fold F (1.2 Ma) may have induced formation of gas hydrate in the western part of the survey as well.

As the uplift continued (between 1.2 Ma and today), so did the associated decrease in solubility, increasing the available quantities of methane. Worldwide, gas hydrates are commonly found at water depths more than 300 – 500m. In such water depths, the base of the gas hydrate stability zone (GHSZ) seems to be located hundreds of meters below the seafloor (Kastner, 2001). If gas hydrates formed in the early Pleistocene within the sequences studied in this thesis, as hypothesized above, then they were probably laying at hundreds of meters below the seafloor. During tectonic uplift, as the water depth decreased, the gas hydrate stability field migrated upward in the sediment column because of the decrease in pressure caused by the uplift (Pecher et al. 2001) (Fig. 25). Upward migration of the hydrate stability field was additionally enhanced on the northern flank of southern HR summit and in the eastern basin by the sedimentation, which induces the upward movement of the isotherms (Fig. 25). Thus, we can infer an upward migration of the BHSZ within the sediment column, from a few hundred meters below the seafloor to approximately 100 m beneath the seafloor where it is

observed today. Upward migration of the GHSZ within the sediment column was accompanied by the decomposition of hydrates at the base of the gas hydrate zone. The methane thus released probably migrated upward to be recycled at the base of the GHSZ. The processes described above are enhanced by upward migration of fluids that accommodates dewatering of the prism. The gas hydrate system act as a semi-permeable cap that, to some extent, impedes upward migration of the free gas, causing it to pool at the base of the hydrate bearing layers (Pecher et al. 2001).

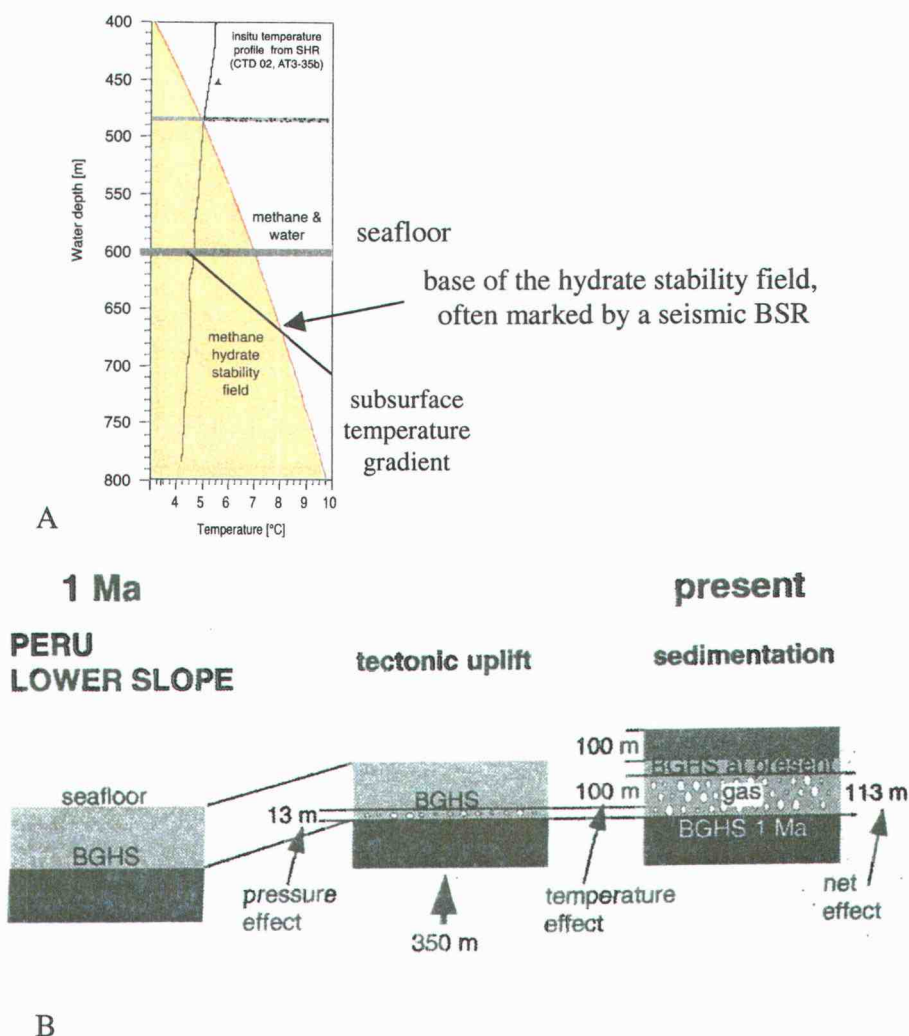


Figure 25: A) Phase diagram for methane – water (red curve) as a function of temperature and pressure (and equivalent depth). Also shown is the base of the hydrate stability field for the water depth and temperature gradient for southern HR summit. Note that the position of hydrate stability field is affected by water temperature, uplift, subsidence, fluid flow, salinity, etc. B) Uplift tectonism and BSRs, after von Huene and Pecher [1999]. Uplift on the Peru lower slope causes an upward movement of the base of the GHSZ with respect to the sediments column because the associated pressure decrease moves GHSZ towards lower temperatures (‘pressure effect’). Sedimentation causes an upward movement of isotherms and hence the base of the GHSZ (‘temperature effect’). An upward movement of the base of the GHSZ in the sediment column is predicted to lead to dissociation of gas hydrates and generation of free gas at the base of the GHSZ causing BSRs. (out of Pecher et al., 2001)

8.2 Double-BSR as a relict of the tectonic uplift

The Bottom Simulating Reflector (BSR) is a strong, conspicuous reflection commonly interpreted as marking the base of the GHSZ. In several parts of the 3D survey, a second reflection B is observed approximately parallel to and underlying the BSR. It is most apparent beneath the western flank of southern HR (Fig. 12B). The deeper reflection appears discontinuous beneath the ridge in regions where the BSR crosses the deeper stratigraphy of Unit S.VI (left marked feature on Fig. 26, distance: 5500m - 6500m). The amplitude of this event is much lower than that of the BSR, which is strong and continuous. The origin of the deeper BSR is speculative, possibly a magnetic relict of the ancient base of the GSHZ (Musgrave et al., 2003). A deeper paleo-BSR implies the uplift of the base of the gas hydrate system as inferred from the tectonic history of the southern HR. The uplift occurred 0.2 Ma and hence can explain the upward movement of the base of the GHSZ within recent geologic time, as required by the model of Musgrave et al. (2003).

A double BSR can also be observed in the syncline between anticline B and the ridge (Fig. 26. distance: 7300m – 8100m). Here the deeper of the two reflections is much brighter and shingled in character. The expected depth of the base of the GHSZ at 1099 m water depth, assuming 3°C seafloor temperature and a geotherm of 0.055°C /m as indicated by Leg 204 data (Trehu et al, 2003b) is 189 mbsf which was found to correspond accurately to the upper, faint BSR (Fig. 26). We speculate that the deeper of the two reflections corresponds to an ancient zone of highly concentrated gas hydrates close to the ancient base of the GHSZ, similar to the one inferred today at S1251, based on the chlorinity and temperature anomaly (Trehu et al., in press). As the base of the GHSZ moved upward due to the uplift and the sediment accumulation, this gas hydrate layer decomposed, leaving a zone rich in free gas, which is recorded in the seismic volume as a bright shingled BSR

~30m beneath the actual base of the GHSZ. Low permeability of the slope basin sediments may have impeded the upward movement of the free gas. If this scenario is true, the accumulation of free gas beneath the GHSZ may cause a significant slope failure hazard, for free gas weakens the sediment layers and is related to shale mobilization observed in mud volcano studies (Dillon et al., 2001). This type of scenario could potentially have played a role in the two gravity-driven slope failure events inferred to have happened between 1.0 and 0.3 Ma (in red on Fig. 22 and 23).

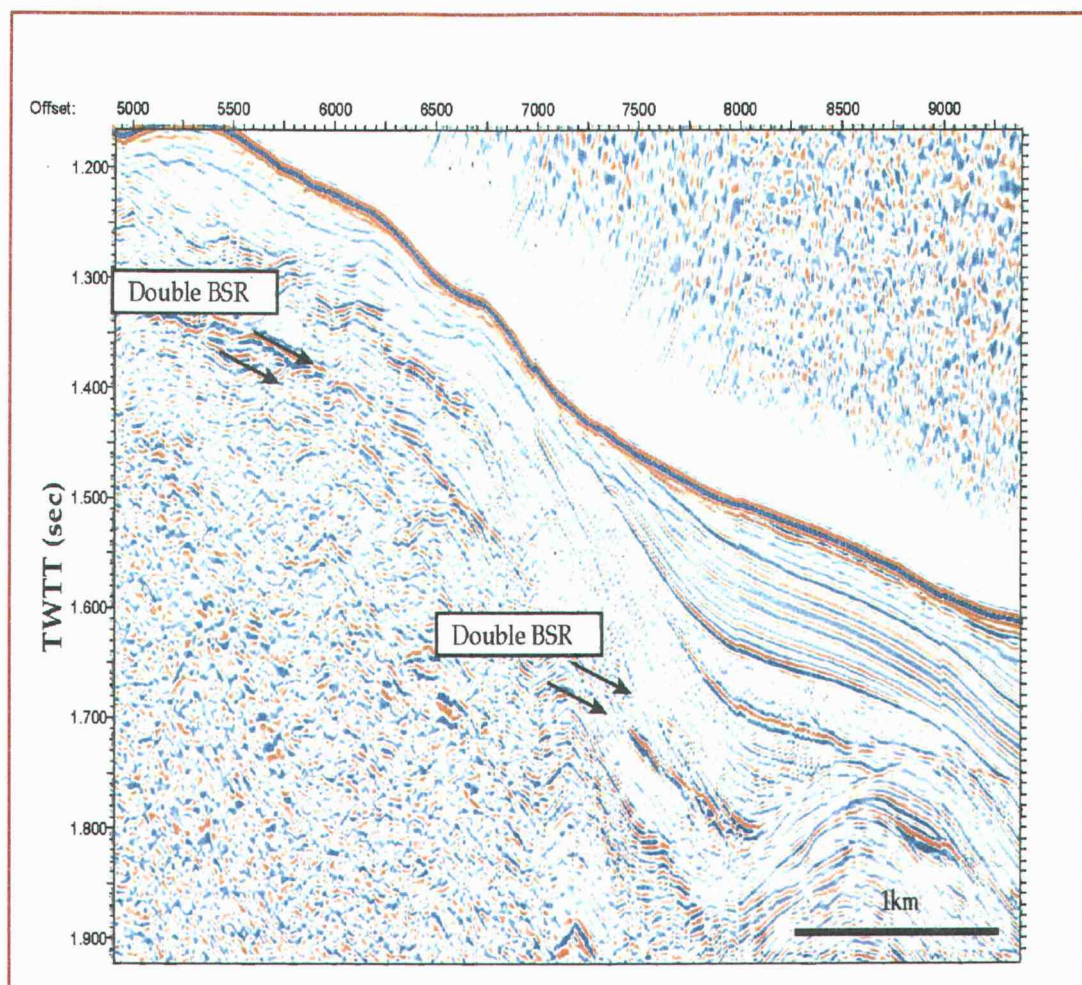


Figure 26: EW section from the 3D migrated seismic volume showing two aspects of the double BSR discuss in the text (see Fig. 6C for location).

8.3 Gas hydrate distribution and faulting

An overall higher concentration of gas hydrates at S1244 and S1246 relative to the other sites is probably due to the presence of normal faulting within Unit S.II (Trehu et al., in press). The faults provide pathways for the free gas into the GHSZ, across the strata that appear to be otherwise impermeable (see paragraph above and conclusion of section 8.5) (Rowe & Gettrust, 1993). The new pathways across the gas hydrate stability zone, allowed removal of the free gas from beneath the gas hydrate occurrence zone possibly lowering the slope failure hazard. The unit's sediment layers differ from each other in their grain sizes (Shipboard Scientific Party, 2003; sites 1244 and 1246). This is imaged in the seismic data by the highly variable amplitudes observed within the unit. The pervasive offsets of these strata lead to a patchwork of host-lithologies more or less suited for gas hydrate formation, which was found to be very sensitive to the grain size of the host-sediments (Weinberger et al., 2003). This may explain the highly heterogeneous distribution of gas hydrates as indicated by discrepancies in gas hydrate concentration between boreholes at the same site (Trehu et al., in press).

8.4 Stratigraphy of horizon A

Horizon A is an anomalously bright reflection in the western part of the survey. It was correlated with an ash-rich sediment layer at sites S1250, S1248 and S1245. However, the ash was not observed at Hole 1247B, although the LWD data for Hole 1247A was similar to the data for 1245, 1248 and 1250. This suggests a strong lateral change in the stratigraphic character of horizon A between Holes 1247A and 1247B (Fig. 14). Further seismic stratigraphic analysis of the seismic horizon reveals its dual stratigraphic origin as the ash-rich layer corresponds to the correlative surface east- and northward of an angular unconformity, which delineates a bathymetric high; (fold F in Fig.12, 13 and 14). This stratigraphic

horizon channels free gas in a zone of otherwise impermeable strata (S.IV, S.III) (see section 8.5 BSR amplitude) to the gas hydrate stability zone (Trehu, Fleming et al., 2003). Underneath the summit of southern HR the gas pressure at the top of horizon A was computed to be close to lithostatic pressure (Trehu, Fleming et al., 2003), which allows the gas to break its way through the sedimentary column into the seafloor. The region of vertical gas migration coincides with the region in which the BSR and the onlapping line of the ash-layer onto the bathymetric high join each other (white line on Fig.27). The transition from focused fluid flow along horizon A to diffuse vertical fluid flow seems to occur where the ash-rich layer laps onto the paleo-bathymetric high.

8.5 Relation between BSR amplitude anomalies and stratigraphy

The BSR is a conspicuous reflection with negative amplitude through most of the 3D survey. Its amplitude, however, varies greatly. Figure 27 shows the variation in amplitude along the BSR overlain by the boundaries between the stratigraphic units hosting the BSR. It shows four distinct zones of amplitude anomalies. In the central-north region, the anomaly corresponds to the interference between the BSR and the anomalously bright reflections B and B' (Fig. 6, 17). Hence this zone probably does not correspond to a real change in gas hydrate content beneath the BSR. The three other zones occur within Units S.VII and S.VI.

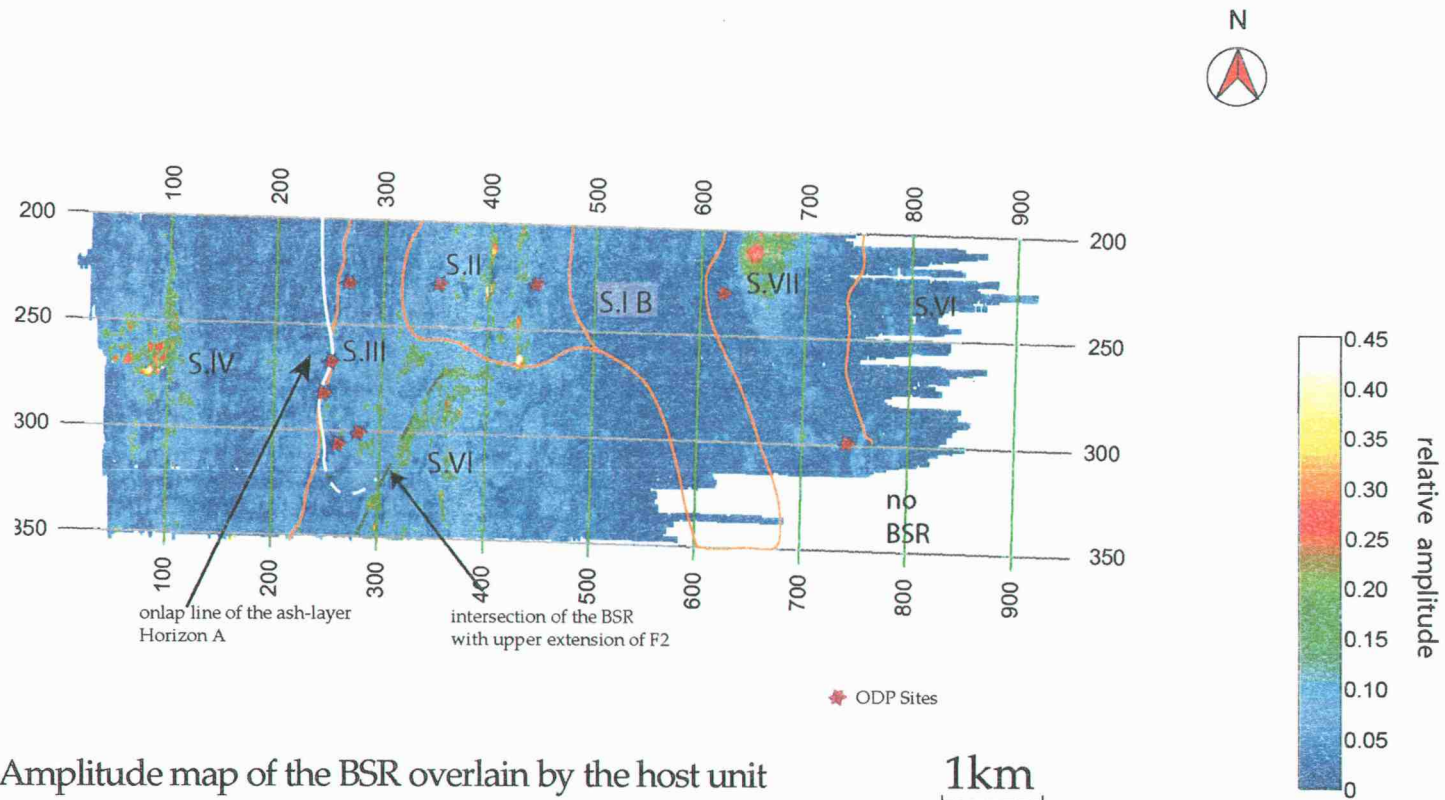
The most outstanding bright circle lies at the intersection between trace 680 and line 220, where the BSR is beneath anticline B and lies in S.VII strata of Pliocene and early Pleistocene age.

The second bright spot within the survey corresponds to the region in which the BSR lies within S.VI strata. This anomaly is of greater extent and contains amplitude variations that form rounded and linear patterns (Fig. 27). The geometry of the amplitude anomaly is due to interference effects between the BSR and

bright reflections. It reveals a stratigraphic organization of the sediments as seen on seismic-cross-sections. (see the upper extension of F2 on Fig. 12, an angular unconformity characterized by a zone of particularly bright reflections right underneath it. The intersection between the BSR and the upper extension of F2 is dashed green on the Fig. 27)

The third bright zone on the map corresponds to a local anticlinal feature that deforms S.VII strata and formed a bulge on of the seafloor 1.6 Ma (Fig. 10, T1). Again, the brighter BSR amplitude coincides with the oval zone in which S.VII sediments host the BSR because of the uplift of older strata. ODP Leg 204 geochemical results suggest that mixing of fluids occurs within S.VI and S.VII (Shipboard Scientific Party, 2003, summary), which implies a relatively high permeability within the relatively lithified accreted sediments compared to the younger slope-basin sediments. Additionally, these older strata, are characterized by high amplitude relative to the younger strata suggesting the accumulation of free gas in this zone. We speculate that the BSR amplitude anomalies are the result of an increase of free gas below the younger slope-basin sediments, which confirm the low permeability of these strata. This has an important impact on the fluid distribution and supply of methane to the GHSZ.

Figure 27: Amplitude map of the BSR overlain by the stratigraphy hosting the BSR. The orange lines delineate the different host-units. The black dashed line marks the approximate onlap line of the ash-rich-layer onto the bathymetric high. The orange mesh shows the approximate zone of diffused gas leaving horizon A.



9.CONCLUSION

Sequence stratigraphic interpretation of a seismic volume encompassing southern Hydrate Ridge allows the reconstruction of the sedimentary environment and tectonic evolution of the ridge during the Pleistocene. The subsurface of southern HR consists of accreted, folded, early Pleistocene abyssal plain sediments, which form three uplifted structures; fold F, anticline B and the Dome. These anticlines were leveled out and buried by slope-sediments during the middle to late Pleistocene. The middle to late Pleistocene sediments are likely recycled abyssal plain sediments shed from the lower slope bathymetric highs present during their deposition. They show an overall increase in their pelagic content and a decrease in turbidity beds with time. These slope-basin sediments have recorded a history of horizontal shortening due to the accretion. Three major tectonic episodes have been identified from stratigraphy and seismic sequence analysis:

- 1 – Folding at the deformation front occurred 1.2 Ma.
- 2 – Compressional period, which corresponds to the progressive uplift of the abyssal plain sediments onto the accretionary complex between 1.2 – 0.3 Ma.
- 3 – Formation of the modern ridge and of the eastern basin less than 0.3 Ma. The formation of the eastern basin suggests an extensional phase in the eastern part of the survey.

The tectonic model for the evolution of southern HR is presented in chapter 7 and illustrated in Figures 22 and 23. Although the origin of the dome cannot be inferred from the 3-D seismic data, Johnson et al. (in preparation, 2004) suggest it represents the southern continuation of a seaward-vergent thrust anticline, as observed on regional seismic lines to the north. Although west of Hydrate Ridge the modern deformation frontal thrust is seaward vergent, a brief period of landward vergence (evidenced by fold F) occurred during early Pleistocene (1.2 Ma) time. The possible cause of landward vergence on this portion of the margin

has been attributed to high basal pore fluid pressure initiated by the rapid deposition of the Astoria fan during the Pleistocene (Seely, 1977). The change in vergence direction with time observed here (seaward vergent dome to landward vergent fold F to modern seaward vergence at the deformation front) is consistent with a regional tectonic model proposed by Johnson et al. (in preparation, 2004) which suggests a relationship between the evolution and southern extent of the Astoria Fan sediments and the vergence change of accretionary wedge thrust faults in this portion of the margin with time.

Sequence analysis of southern HR provides examples of how geology controls fluid conduits. One example is horizon A, a coarse-grained, ash-rich layer that focuses free gas towards the summit. Another is a series of normal-faults that disrupt the middle Pleistocene slope-basin sediments and result in heterogeneous gas hydrate distribution. In general, comparison of the stratigraphy with the BSR amplitude anomalies shows a strong relation between the distribution of free gas beneath the BSR and the BSR-hosting stratigraphy. It also confirms the low permeability of the middle Pleistocene to Holocene slope-basin sediments that cap Hydrate Ridge.

Tectonic uplift also affects gas hydrate distribution. Uplift of gas hydrate-bearing sediments leads to the upward movement of the base of gas hydrate stability zone (GHSZ). We hypothesize a localized, bright double BSR beneath the eastern flank of southern HR results from a layer of hydrate concentration that was stranded beneath the GHSZ as the GHSZ became shallower. This would result in accumulation of free gas along the paleo-BSR. If this model is correct, it could have significant consequences for the slope stability.

BIBLIOGRAPHY

- Arsenault M. A., Trehu, A. M., Bangs, N. and Nakamura, Y., 2001, P-wave tomography of Hydrate Ridge, Oregon Continental Margin [abs.], *EOS Transactions, American Geophysical Union*, v. 82, 604
- Bohrmann G., Greinert, J., Suess, E., Torres, M., 1998, Authigenic carbonates from the Cascadia subduction zone and their relation to gas hydrate stability, *Geology*, v. 26, no. 7 p. 647-650
- Burbanks, W. D., Verges, J., 1994, Reconstruction of topography and related depositional systems during active thrusting, *Journal of Geophysical Research*, v. 99, n. B10, p. 20 281–20 297
- Dillon W. P., Nealon, J. W., Taylor, M. H., Lee, M. W., Drury, R. M., Anton, C. H., 2001, Seafloor Collapse and Methane Venting Associated with Gas Hydrate on the Blake Ridge – Causes and Implications to Seafloor Stability and Methane Release. in Paul, C. K. and Dillon W. P. (eds.), *Natural gas hydrates: Occurrence, Distribution, and Detection*, American Geophysical Union, Geophysical Monograph Series, v.124, p. 211 – 233.
- Flueh, E. R., Fisher, M. A., Bialas, J., Childs, J. R., Klaeschen, D., Kukowski, N., Parsons, T., Scholl, D. W., Ten Brink, U., Trehu, A. M., Vidal, N., 1998, New seismic images of the Cascadia subduction zone from cruise SO108-ORWELL. *Tectonophysics*, v. 293, p. 69-84.
- Goldfinger, C., Kulm, L. D., Yeats, R. S., Appelgate, B., MacKay, M., Cochrane, G. R., 1996, Active strike-slip faulting and folding of the Cascadia plate boundary and forearc in the central and northern Oregon, in Rogers, A. M., Walsh, T. J., Kockelman, W. J., and Priest, G. (eds), *Assessing and Reducing Earthquake Hazards in the Pacific Northwest*, U.S. Geological Survey Professional Paper, 1560 p. 223-256.
- Grevenmeyer, I., Rosenberger, A., Villinger, H., 2000, Natural gas hydrates on the continental slope off Pakistan: constraints from seismic techniques, *Geophys. J. Int.*, v.140, p.295–310
- Johnson J. E., Goldfinger, C., Suess, E., 2003, Geophysical constraints on the surface distribution of authigenic carbonates across the Hydrate Ridge region, Cascadia margin, *Marine Geology*, v.202 p.79 - 120

Kastner, M., 2001, Gas Hydrates in convergent Margins: Formation Occurrence, Geochemistry and Global significance, *in* Paul, C. K. and Dillon W. P. (eds.), *Natural gas hydrates: Occurrence, Distribution, and Detection*, American Geophysical Union, Geophysical Monograph Series, v.124 p. 67-86

Kulm, L. D., and Fowler, G. A., 1974, Oregon Continental Margin Structure and Stratigraphy: A Test of the Imbricated Thrust Model, *in* Burck, C. A. and Drake, C. L. (eds.), *The Geology of Continental Margins*, New York, Springer Verlag, p.261-284.

Kvenvolden, K. A., 1993, Gas Hydrates, geological perspective and global change, *Rev. Geophys.*, v. 25, p. 231 –250

Kvenvolden, K.A., and Lorenson, T.D., 2001. The global occurrence of natural gas hydrate, *in* Paul, C. K. and Dillon W. P. (eds.), *Natural gas hydrates: Occurrence, Distribution, and Detection*, American Geophysical Union, Geophysical Monograph Series, v.124,p. 3 - 18.

Leeder, M.R., 1999, *Sedimentology and Sedimentary Basins: from Turbulence to Tectonics*, Oxford (Blackwell Science)

MacKay M. E., Moore, G. F., Cochrane, G. R., Moore, C. J., Kulm, L. D., 1992, Landward vergence and oblique structural trends in the Oregon margin accretionary prism: Implication and effect on fluid flow, *Earth and Planetary Science Letters*, v.109, p.477-491

MacKay, M. E., 1995, Structural variation and landward vergence at the toe of the Oregon accretionary prism, *Tectonics*, v. 14, no. 5, p. 1309-1320

McNeill, L. C., Goldfinger, C., Kulm, L.D., Yeats, R. S., 2000, Tectonics of the Neogene Cascadia forearc basin: Investigations of a deformed late Miocene unconformity, *Geo. Soc. Am. Bull.*, v. 112, no. 8; p 1209-1224

Mann, D., Kukowski N., 1999, Numerical modeling of focused fluid flow in the Cascadia accretionary wedge, *Journal of Geodynamics*, v. 27, p. 359-372

Mitchum, R. M., 1977, Glossary of terms Used in the Seismic Stratigraphic, *in* Payton, C. E. (ed.), *Seismic Stratigraphy – applications to hydrocarbon exploration*, Am. Assoc. Petroleum Geologist Mem. 26, Part 11, p 205-212.

Musgrave, R.J., Hollamby, J. A., 2003, Migration of the base of the Hydrate Zone Tracked by Rock Magnetism [abs.], *EOS Transactions, American Geophysical Union*, v. 84, (46), Fall Meet. Suppl.

Nelson, H., 1976, Late Pleistocene and Holocene depositional trends, processes, and history of Astoria deep-sea fan, northeast Pacific, *Marine Geology*, v.20, p.129-173.

Pecher, I., Kukowski, N., Ranero, C., von Huene, R., 2001, Gas Hydrates along the Peru and Middle America Trench Systems in Paul, C. K. and Dillon W. P. (eds.), *Natural gas hydrates: Occurrence, Distribution, and Detection*, American Geophysical Union, Geophysical Monograph Series, v.124 p.257-271.

Rowe, M. M., Gettrust, J. F., 1993, Faulted structure of the bottom simulating reflector on the Black Ridge, western North Atlantic, *Geology*, v. 21, no. 9, p. 833-836

Seely D. R., Vail, P.R., Walton, G.G., 1974, Trench Slope Model, in Burck, C. A. and Drake, C. L. (eds.), *The Geology of Continental Margins*, New York, Springer Verlag, p.249-260.

Shipboard Scientific Party, 1994, SITE 892 in Westbrook, G.K., Carson, B., Musgrave, R., J., et al., *Proc. ODP, Init. Repts.*, 146, Pt. 1, College Station, TX, (Ocean Drilling Program), p.301-378

Shipboard Scientific Party, 2003, Site 1244. in Tréhu, A.M, Bohrmann, G., Rack, F.R., Torres, M.E., et al., *Proc. ODP, Init. Repts.*, 204, 1-132 [CD-ROM]. Available from: Ocean Drilling Program, Texas A&M University, College Station TX 77845-9547, USA.

Shipboard Scientific Party, 2003, Site 1245. in Tréhu, A.M, Bohrmann, G., Rack, F.R., Torres, M.E., et al., *Proc. ODP, Init. Repts.*, 204, 1-132 [CD-ROM]. Available from: Ocean Drilling Program, Texas A&M University, College Station TX 77845-9547, USA.

Shipboard Scientific Party, 2003, Site 1246. in Tréhu, A.M, Bohrmann, G., Rack, F.R., Torres, M.E., et al., *Proc. ODP, Init. Repts.*, 204, 1-132 [CD-ROM]. Available from: Ocean Drilling Program, Texas A&M University, College Station TX 77845-9547, USA.

Snively, P. D., Jr., 1987, Tertiary geologic framework, neotectonics, and petroleum potential of the Oregon-Washington continental margin, in Scholl,

D.W., et al., (eds.), *Geology and resource potential of the continental margin of western North America and adjacent ocean basins-Beaufort Sea to Baja California*, Houston, Texas, Circum Pacific Council for Energy and Mineral Resources, p.305-335.(R)

Suess, E., Torres, M. E., Bohrmann, G., Collier, R.W., Rickert, D., Goldfinger, C., Linke, P., Heuser, A., Sahling, H., Heeschen, K., Jung, C., Nakamura, K., Greinert, J., Pfannkuche, O., Trehu, A., Klinkhammer, G., Whiticar, M. J., Eisenhauer, A., Teichert, B., Elvert, M., 2000, Sea floor Methane Hydrates at Hydrate Ridge, Cascadia Margin, in Paul, C. K. and Dillon W. P. (eds.), *Natural gas hydrates: Occurrence, Distribution, and Detection*, American Geophysical Union, Geophysical Monograph Series, v.124 p. 87-98

Suess, 2002, The evolution of an idea; from avoiding gas hydrates to actively drilling for them, JOIDE journal, spe. issue, v. 28, no. 1, p. 45 - 50

Taylor, M. H., Dillon, W. P., Pecher, I. A., 2000, Trapping and migration of methane associated with the gas hydrate stability zone at the Black Ridge Diapir; new insights from seismic data, *Marine Geology*, v.164, no. 1-2, p.79-89

Torres, M. E., McManus, J., Hammond, D. E., de Angelis, M. A., Heeschen, K. U., Colbert, S. L., Tryon, M. D., Brown, K. M., Suess, E., 2002, Fluid and chemical fluxes in and out of sediments hosting methane hydrate deposits on Hydrate Ridge, OR, I: Hydrological provinces, *Earth and Planetary Science Letters*, v.201, no.3-4 p.525-540

Trehu A. M., Torres, M., Moore, G. F., Suess, E., Bohrmann, G., 1999, Temporal and spatial evolution of a gas hydrate-bearing accretionary ridge on the Oregon continental margin, *Geology*, v.27, no.10, p.939-942.

Trehu, A., Bangs, N., 2001, 3-D seismic imaging of an active margin hydrate hydrate system, Oregon continental margin, report of cruise TTN112, *Oregon State University Data Report 182, ref.2001-2*, Corvallis, Oregon.

Trehu, A. M., Bangs N. L., Arsenault M. A., Bohrmann G., Goldfinger C., Johnson J. E., Nakamura Y., Torres M., 2002, Complex Subsurface Plumbing Beneath Southern Hydrate Ridge, Oregon Continental Margin, from High-resolution 3D Seismic Reflection and OBS Data. *Proceedings of the fourth International Conference on Gas Hydrates*, Yokoma Japan. May 19-23

Trehu, A. M., Flemings, P., Shipboard Scientific Party, 2003, Lithostatic Gas Pressures and Venting at Southern Hydrate Ridge [abs.], *EOS Transactions, American Geophysical Union*, v. 82, (46), Fall Meet. Suppl.

Tréhu, A.M., Bohrmann, G., Rack, F.R., Torres, M.E., et al., 2003a. Proc. ODP, Init. Repts., 204 [CD-ROM]. Available from: Ocean Drilling Program, Texas A&M University, College Station TX 77845-9547, USA.

Trehu, A.M., Dillard III, E., Huckmeyer, J., Schroeder, D. and Leg 204 Shipboard Scientific Party, 2003b, In situ temperature and thermal conductivity beneath Southern Hydrate Ridge-results from Leg 204, EGS-AGU-EUG Joint Assembly, Nice, France, April 2003.

Trehu, A. M., Stakes D. S., Bartlett C. D., Chevallier J., Duncan R. A., Goffredi S. K., Potter S., Salamy K. A., 2003c, Seismic and seafloor evidence for free gas, gas hydrates, and fluid seeps on the transform margin offshore Cape Mendocino, *J. Geophys. Res.*, v. 108, B5, p. EPM 11-1 – 11-19

Tréhu, A.M., Bohrmann, G., Rack, F., Collett, T., Goldberg, D., Long, P.E., Milkov, A.V., Riedel, M., Schultheiss, P., Torres, M. E., et al., In press, Three-dimensional distribution of gas hydrate beneath southern Hydrate Ridge: constraints from ODP Leg 204, *Earth and Planetary Science Letters*,.

Tryon, M.D., Brown, K.M, Torres, M.E., 2002, Fluid and chemical flux in and out of sediments hosting methane hydrate deposits on Hydrate Ridge, OR; II, Hydrological processes, *Earth and Planetary Science Letters*, v.201, no. 3-4 p.541-557 (R)






Weinberger, J.L., K.M. Brown, P.E. Long, M. Riedel, and Leg 204 Scientific Party, Why hydrates are where they are at Hydrate Ridge: The story from infrared images [abs.], 2003, *EOS, Transactions, American Geophysical Union*, v. 84 (46) Fall Meet. Suppl.,

Westbrook, G. K., 1994, Growth of the accretionary wedges off Vancouver Island and Oregon, in Westbrook, G.K., Carson, B., Musgrave, R., J., et al., *Proc. ODP, Init. Repts.*, 146, Pt. 1, College Station, TX, (Ocean Drilling Program), p.381-388












APPENDICES

APPENDIX A: LEGEND




This Legend apply to all figures included to this thesis.

UNITS		S.unit IV		S.unit VI
		S.unit III		
		S.unit II		
		S.unit IB		
		S.unit IA		

2.0 biostratigraphic age

HORIZONS	Horizon A	
	Horizon B	
	Horizon B'	
	Horizon Y	
	Horizon C	
	Horizon A'	
	Horizon A''	
	Angular Unconformity K	
	Angular Unconformity U	
	Massflow DBF1	
	Massflow DBF2	

WELLS	S1245
	

FAULTS	Fault system F	Fault system G	Fault system E
			

APPENDIX B: Correlation between seismic and lithology results at Site 1244

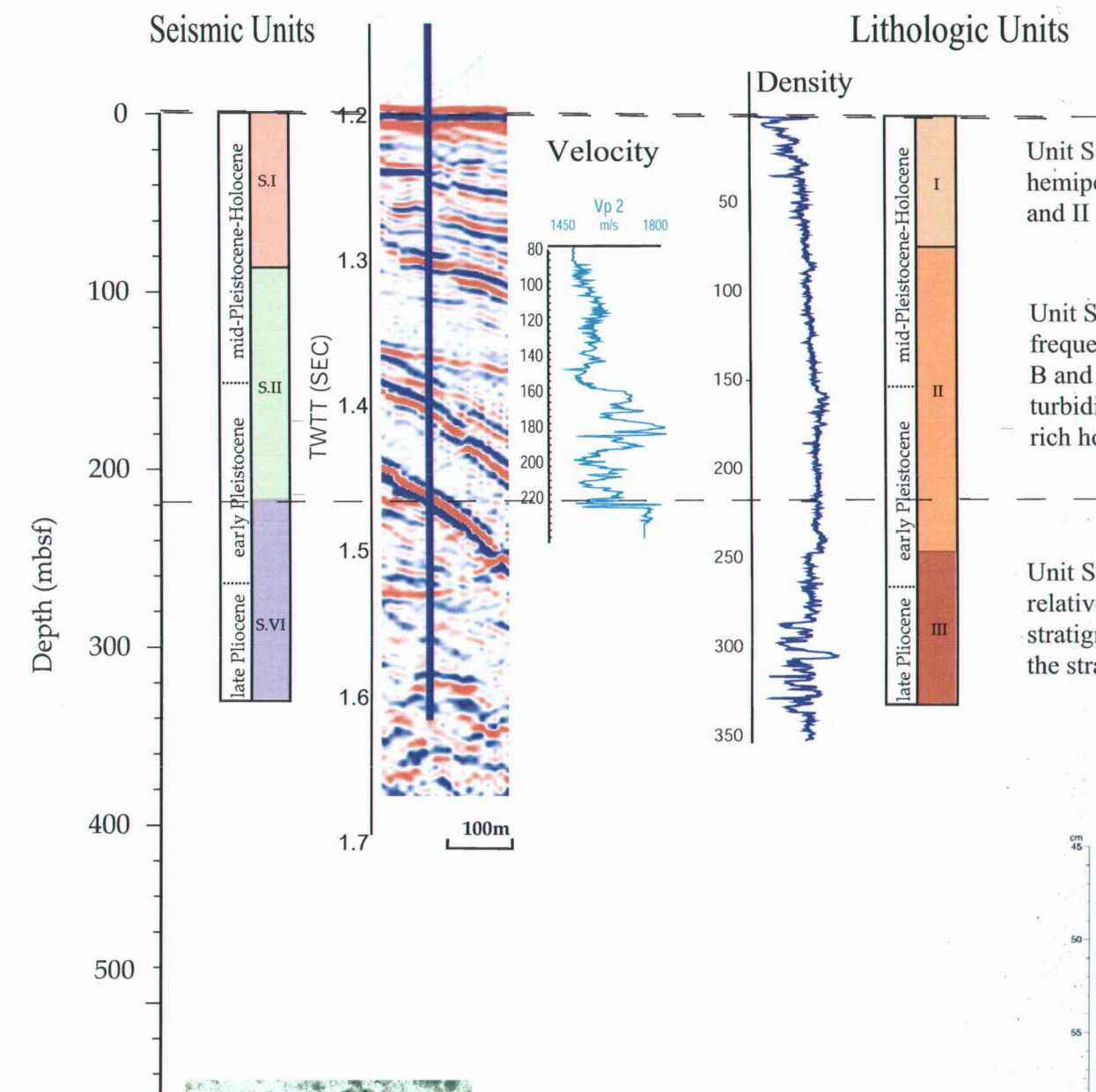


Photo. A. Close-up photograph of claystone, typical of lithostratigraphic Subunit I (interval 204-1244c-002h-06, 99-110cm).



Unit S.IB = L.I at S1244 and along the NS transect. In the ridge region, the unit consists of dark greenish gray hemipelagic clay and silty clay with a low total biogenic content (<10%). The major difference between Unit I and II is in the frequency and thickness of turbidites. Unit I has a few thin turbidites (see Photo. A).

Unit S.II = Unit L.II, Unit II has slightly thicker and more frequent turbidites (see photo. B and C). Two reflections B and B' mark this unit, they coincide with multiple turbidites clustered and to thick zones and volcanic ash-rich horizon respectively (Photo. D), which tie S1246 to S1244.

Unit S.VII = Unit L.III at S1244. Coring at S1244 revealed a relatively high degree of lithification for the deeper stratigraphy and the presence of glauconites within the strata (Photo. E).

Photo.B. Close-up photograph of a turbidite from lithostratigraphic Unit II (interval 204-1244C-010H-5, 59-74 cm).



Photo.C. Close-up photograph of a turbidite from lithostratigraphic Unit II (interval 204-1244C-13H-4, 40-80 cm). The sand layer at 54 cm marks the base of the turbidite. Above this coarse base, the sediment grades to the silty clay of the turbidite tail. Below the base of the turbidite, the sediment is highly bioturbated. These characteristics are common to most of the turbidites found throughout lithostratigraphic Unit II.

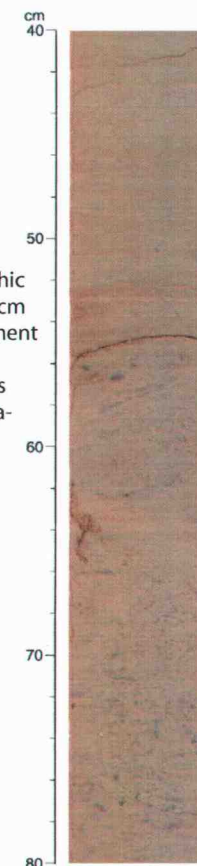


Photo.D. Close-up photograph of ash layer (Horizon B') in lithostratigraphic Unit II (interval 204-1244C-27X-1, 45-70 cm). The base of the ash is present at 61 cm. This horizon extends to the top of the section but is not seen in the previous core because of poor recovery.

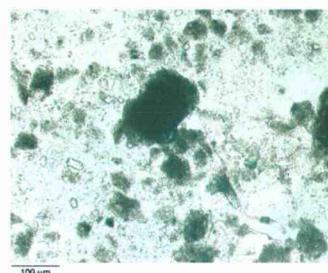
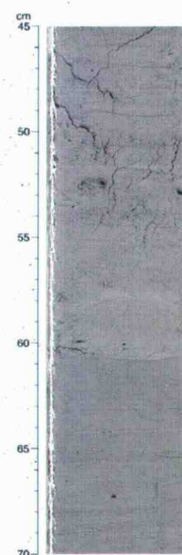


Photo.E. Photomicrograph of glauconite from lithostratigraphic Unit III (Sample 204-1244C-36X-3, 98 cm).

APPENDIX B: Correlation between seismic and lithology results at Site 1245

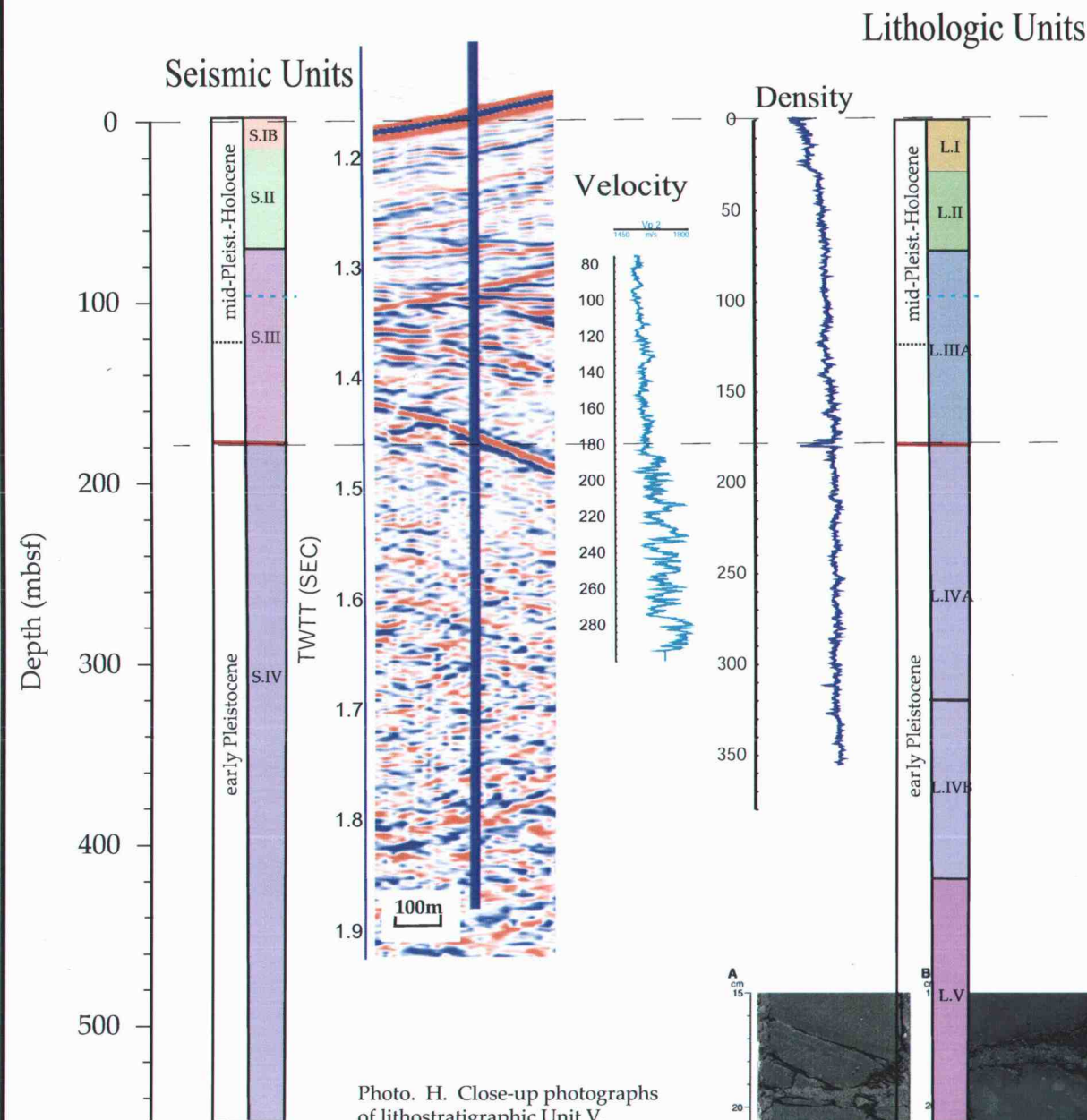


Photo. H. Close-up photographs of lithostratigraphic Unit V. A. A thick turbidite (interval 204-1245B-51X-3, 15-30 cm [~448.45 mbsf]). Notice the visible foraminifers near the coarse base of the turbidite, the parallel laminations, and the cross bedding. B. Mud clasts within the conglomerate of Unit V (interval 204-1245B-53X-4, 15-27 cm [~468.48 mbsf]).

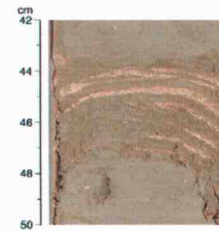
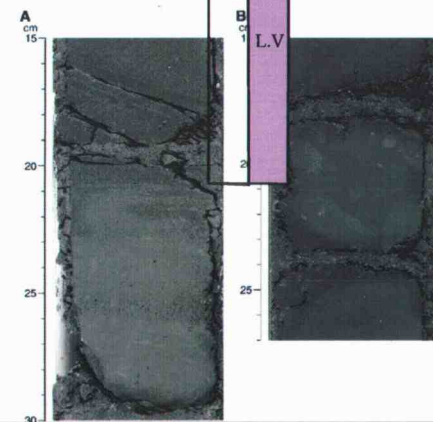


Photo. A. Close-up photograph of a turbidite in lithostratigraphic Unit II (interval 204-1245B-8H-7, 42-50 cm [75.79 mbsf]).

Unit S.IB = L.II at S1252 and L.III at S.1244. In the ridge region, the unit consists of dark greenish gray hemipelagic clay and silty clay with a low total biogenic content (<10%).

Unit S.II = L.II at S12 is distinguished from the surrounding units by an increase in coarser material and in turbidite frequency (Photo. A).

Unit S.III = L.IIIA along the NS transect. It consists of clay and silty clay with high-frequency turbidites and a high concentration of opal, it shows a decrease in calcareous fossils at horizon A, which distinguishes Unit L.IIIA from Unit L.IIIB, that is S.III from S.IV respectively. Horizon A coincides with a ash-rich sediment layer (Photo. B and C).

Photo. C. Close-up photograph of volcanic glass-rich sediment and ash sequences in lithostratigraphic subunit IIIA. A. Volcanic glass-rich sediment and ash sequence (interval 204-1245B-21X-2, 84-103 cm [~178 mbsf]). B. Graded volcanic glass-rich sand (interval 204-1245B-21X-3, 104-113 cm [~180 mbsf]). C. Volcanic glass-rich sediment and ash sequence (interval 204-1245B-21X-4, 13-59 cm [~181 mbsf]).

Unit S.IV = L.IIIB + L.IV + L.V along the NS transect. Sediments consist of nannofossil rich silty claystones, interlayered with thick turbidites, containing wood fragments. Unit L.IVA is composed of nannofossil-rich clay and silty clay. It is marked by an increase with time of biogenic opal (diatoms) (Photo. D). The frequent turbidites (from 5 to 20 cm thick at S1248) distinguish it from L.IVb (photo. E). The degree of lithification increases to claystone within Unit L.IV.

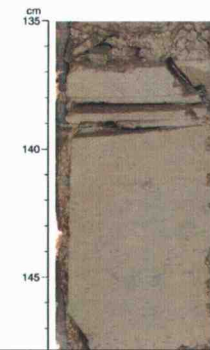
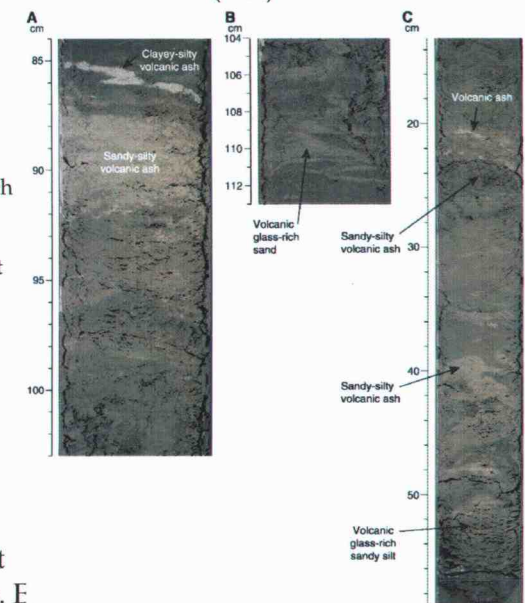


Photo. E. Close-up photograph of claystone with abundant bioturbation below a turbidite with planar laminations from lithostratigraphic Subunit IVb (interval 204-1245B-37X-1, 135-148 cm [~321 mbsf]).

Photo. D. Close-up photograph of nannofossil-rich claystone with abundant bioturbation, typical of lithostratigraphic Subunit IVA (interval 204-1245B-34X-5, 63-74 cm [299.80 mbsf]).



Photo. B. Photomicrograph of sand-sized volcanic glass within the Horizon A volcanic glass-rich sediment and ash sequence in lithostratigraphic Subunit IIIA (Sample 204-1245B-21X-4, 36 cm [180.86 mbsf]) (200x).



APPENDIX B: Correlation between seismic and lithology results at Site 1251

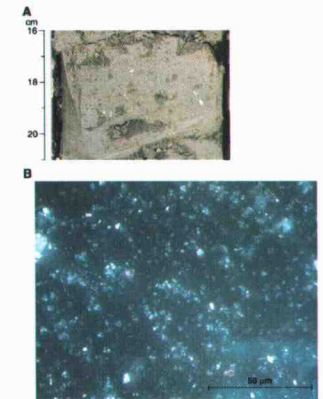
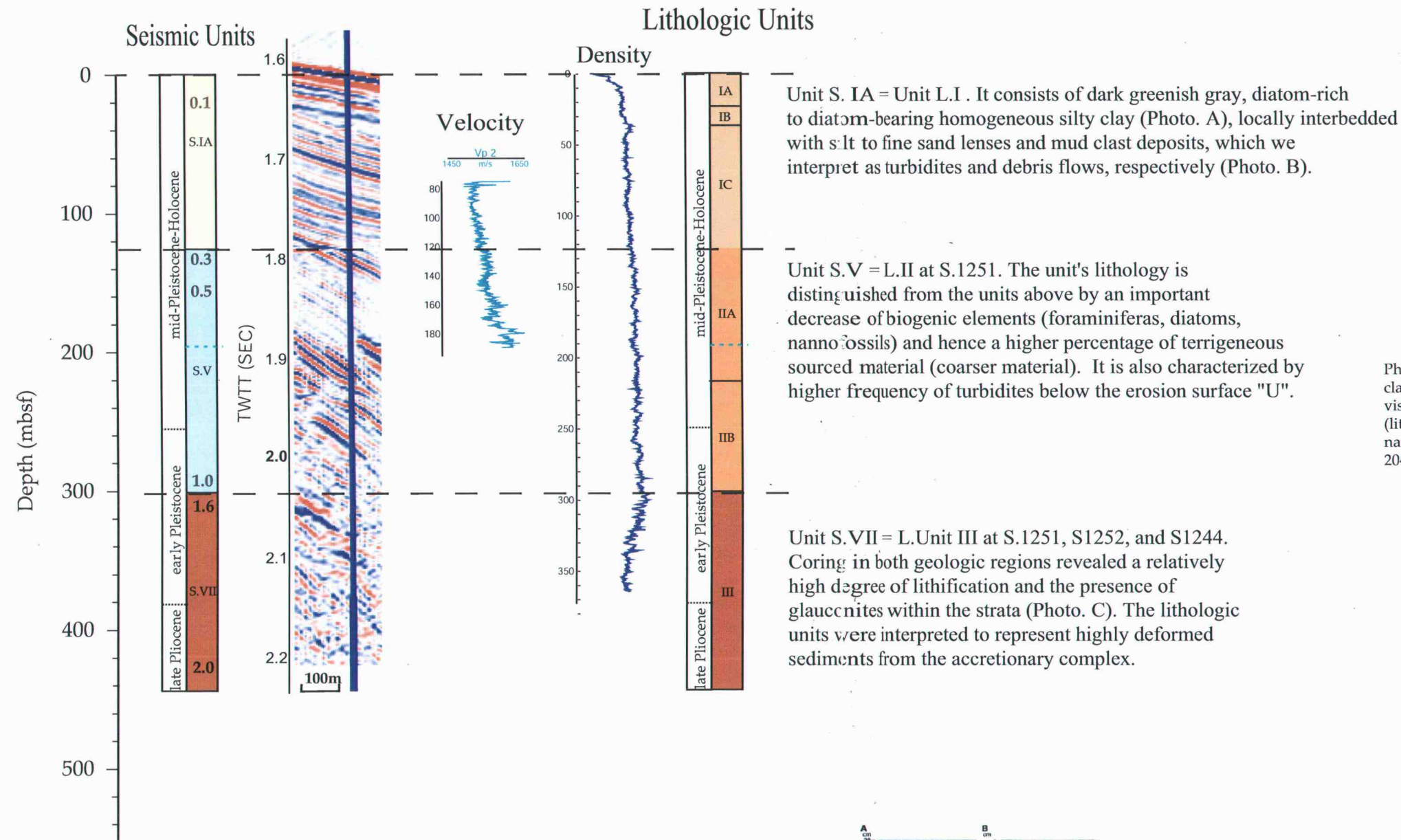


Photo. A. Close-up photograph of foraminifer-rich clay (interval 204-1251B-36X-CC, 16-21 cm) showing visible foraminifer tests (small light-colored specks) (lithostratigraphic Subunit IIB). B. Photomicrograph of nannofossil-rich foraminifer-bearing clay (100x) (Sample 204-1251B-28X-CC, 44 cm) (lithostratigraphic Subunit IB).

Photo. C. Glauconite-rich clay occurrence (interval 204-1251B-37X-1, 28-37 cm) (lithostratigraphic Unit III). B. Close-up photograph of carbonate nodule (interval 204-1251B-52X-1, 128-140 cm) (lithostratigraphic Unit III). C. Photomicrograph of diatom-rich clay (20x) (interval 204-1251B-42X-2, 50 cm) (lithostratigraphic Unit III).

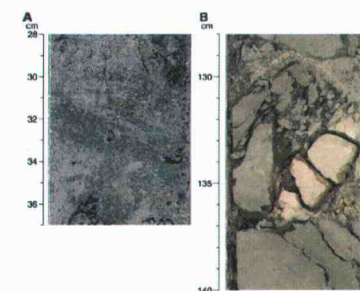
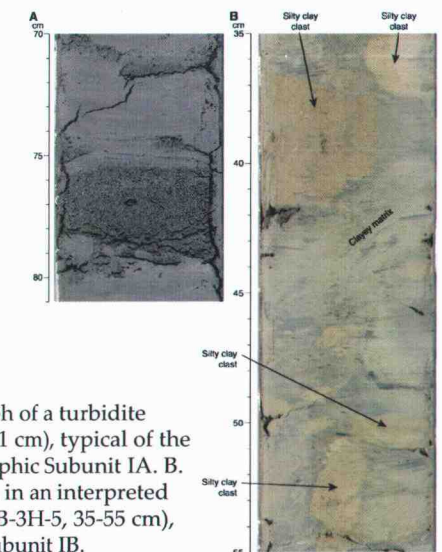

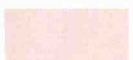





Photo. B. Close-up photograph of a turbidite (interval 204-1251C-2X-4, 70-81 cm), typical of the lower portion of lithostratigraphic Subunit IA. B. Core photograph of soft clasts in an interpreted debris flow (interval 204-1251B-3H-5, 35-55 cm), typical of lithostratigraphic Subunit IB.



APPENDIX C: List of the seismic Units

Seismic Unit	Observations shown on Fig.4, 5 & 6	Pre-existing relief	Syn-sedimentary deformation	Post-sedimentary deformation	Inferred Age (my) Site for absolute age
S.IA 	- Basin-fill onlap against the ridge (Fig.6) - Fanning to the east and up-turn along the bathymetric highs (the main ridge, anticline B) - progressive burying of the anticline B (Fig.6, 15D)	- Southern Hydrate Ridge -Relative subsidence of the basin -Uplift of the ridge	- Uplift of the ridge		0.2 – present (S1251, S1252)
S.IB 	- Basin-fill constrained in the north (Fig.5, 15C) - Fanning to the east (Fig.6), - >16 ° dip (Fig.6A) - Buttrressing against anticline B (Fig.6A&B)	- Bathymetric-high in the south	- Uplift of the ridge - Compression regime	- Uplift of the ridge	0.3 – 0.2 (S1244)
S.II 	- Basin-fill sequences, the strata onlap onto the dome (Fig.7, 15B) and onto S.III upper boundary - Monocline (Fig.6A&B) - Small-scale folding (Fig.3E) - Normal faulting (Fig.6A, 3E)	- Bathymetric-high in the south to the west and to the east	- Migration of the depocenter to the east - Folding of the strata - Extension on top of the fold	- Uplift of the ridge (<0.3mybp –present)	1.0 – 0.3 (S1244)
S.III 	- Sequences constrained in the north (Fig.15A) and onlap onto S.VI (Fig.6B&C) - Divergence to the east (Fig.6) - Smale-scale folding (Fig.12)	- Fold F to the west - Bathymetric-high in the south to the west and to the east	- Activity of Fold F	- Duplexing of the strata	1.15 – 1.0 (S1245, S1247, S1248)
S.IV 	Abyssal Plain sediments (Fig.2) - Divergency to the east in the younger strata (Fig.46)	- Incipient phase of Fold F			1.6 – 1.15 (S1245)
S.V	- Fanning strata to the east (Fig.6)				1.0 – 0.3 (S1251)
S.VI	Sub-horizontal wavy structures (~400m wide) (Fig.6C&D)		Growth of Anticline B		1.6 – 1.0
S.VII	Abyssal Plain sediments (Fig.4) deformed angular unconformities (Fig.6)		Activity of Anticline B	Activity of Anticline B	1.6 - >2.0 (S1251)